GROUND ICE CONTENT AND GEOCHEMISTRY OF ACTIVE LAYER AND PERMAFROST IN NORTHWESTERN ARCTIC CANADA

Marielle Fontaine

A Thesis Submitted to the
Faculty of Graduate and Postdoctoral Studies
in Partial Fulfillment of the Requirements
for the Master of Science Degree in Geography

University of Ottawa
Department of Geography

ABSTRACT

This study aimed to contribute to baseline knowledge of permafrost geochemistry within the uppermost 3-4 m of permafrost at 8 sites on the Peel Plateau and east of the Mackenzie Delta, NWT (67-68^{o}N). The following variables were measured: gravimetric water content (GWC), pore water conductivity (PWC), leachate conductivity (LC), dissolved ions by ICP-AES (i.e. Ca, SO_4, Mg, Fe, K, Na, Mn, Cl), organic carbon content (calculated by linear regression from organic matter content), as well as inorganic carbon content (obtained from loss on ignition analysis). PWC was positively correlated to GWC and values were generally at least 5 times less than LC values, likely underestimating total dissolved solutes using the former method. LC increased with depth to reach maximum values below the paleo thaw unconformity (>10 mS/cm). Carbon content typically remained low throughout the cores with the exception of samples associated to the shallow-rooted vegetation cover at the ground surface. Results showed that the active layer, relict active layer and the permafrost below the thaw unconformity can be divided into three statistically significant layers. PCA results indicated some spatial patterns with increasing LC values at greater depth, suggesting that layer geochemical profiles reflect varying degrees of soil chemical weathering processes since the early Holocene.

RÉSUMÉ

Cette étude de base visait à contribuer aux connaissances biogéochimiques du pergélisol jusqu'à une profondeur de 3-4 m du pergélisol à huit sites sur le plateau Peel et à l'est du delta du Mackenzie, T.N.-O. (67-68^{o}N). Les variables suivantes ont été mesurées: teneur en eau gravimétrique (GWC), conductivité des eaux interstitielles (PWC), conductivité des eaux de lixiviat (LC), ions dissous par ICP-AES (Ca, SO_4, Mg, Fe, K, Na, Mn, Cl), teneur en carbone organique (calculée à partir d'une régression linéaire de la matière organique), ainsi que la teneur en carbone inorganique (obtenue à partir d'une analyse de perte au feu). PWC était positivement corrélée à la GWC et les valeurs étaient généralement 5 fois moins que celles de LC, probablement sous-estimant les ions dissous en utilisant cette première méthode. LC généralement augmentait avec la profondeur pour atteindre des valeurs maximales en-dessous la discordance de dégel (> 10 ms/cm). La teneur en carbone était généralement faible dans les carottes à l'exception des échantillons associés à la végétation à la surface du sol. Les résultats ont démontré que la couche active, la couche active relique et le pergélisol sous la discordance de dégel peuvent être divisés en trois couches statistiquement significatives. Les résultats d'une analyse des composantes principales ont démontré des tendances spatiales avec des valeurs croissantes de LC en profondeur, ce qui suggère que les profils géochimiques des couches reflètent des degrés variables des processus d'érosion chimique du sol depuis le début de l'Holocène.

ACKNOWLEDGEMENTS

This research project was funded by an NSERC Discovery Grant, the NWT Cumulative Impact Monitoring Program, the Northern Scientific Training Program, the Association of Canadian Universities for Northern Studies and the W. Garfield Weston Award for Northern Research. I gratefully acknowledge their support.

I extend a warm thank you to S. Kokelj, T. Goss, R. Way, F. Oliva, P. Bonnaventure, and to my committee members, A.G. Lewkowicz and K. Gajewski, for their comments and insight. I owe my sincere thanks to C. Lapalme, B. Main, D. Lacelle, A. Brooker, A. Forest, C. Paquette, and our guide, J. Wilson, who provided invaluable field assistance over the course of the 2013 and 2014 field seasons. To say that I owe you for making you core in the rain… chip away at permafrost with an axe for hours to dislodge our beloved CRREL corer at the most "fragrant" of sites… or shovel a meter-deep active layer on Inuvik's hottest day in August… would be a gross understatement. I thank the "field pack" for never complaining, for never giving up and, if anything, for always finding a way to share some laughs despite the miserable conditions. Thank you – I will miss our many stops at NorthMart, the fish-n-chip school bus, and the ice cream parlour after a hard day's work covered head-to-toe in mud.

To A. Lapp, M. Grinter, B. Lauriol, I.D. Clark – I will always remember my first field season and the picturesque landscapes at Tombstone, YT. Thank you for showing me the ropes. I have been blessed with great colleagues for both field seasons. You have all taught me how much more productive and enjoyable field "work" can be when you are able to rely on, and trust your fellow team members. I can only hope to find such synergy within my future workplaces.

Thank you to all the beautiful souls I came across in Fort McPherson, Tsiigetchic, Inuvik, at the Aurora Research Institute (particularly Bessie who was always oh, so helpful), and during my travels along the Dempster.

To W. Abdi, P. Middlestead, and P. Wickham at the G.G. Hatch Laboratory and to P. Zhang, and N. De Silva at the Geochemistry Laboratory – Thank you for your insight, and your meticulous yet expeditious work.

To M. Taylor – For being the Woodstock to my Snoopy, and for helping to crush and weigh those never-ending sediment samples. Not the most pleasant task, but your efforts did not go unnoticed. Thank you – you are the best!

To Mr. Goss – I cannot express how much I appreciate your willingness to dedicate your time and effort (voluntarily!) to help a "stranger" in need over statistical e-mail exchanges. Your insight and guidance have been instrumental in my success. I am forever grateful. Thank you.

This work would not have been possible without the help of my supervisor, Dr. D. Lacelle. For taking me on as a graduate student. For being a continuous source of understanding, encouragement and belief in me over the last three years. For bringing me up North and giving me the opportunity to discover a new landscape – beautiful beyond my imagination. (I now share your obsession with the Arctic!). For regularly presenting all of us with, and allowing us to

pursue opportunities that would further our skills and career development (not to mention overall wild and once-in-a-lifetime experiences – e.g. Svalbard!). For pushing me beyond my (perceived) limits. For being available for discussion – whether scientific or not. And for sharing your valuable knowledge and lessons. Thank you. I am glad I can call you a friend, and not just a supervisor.

To the Basement Bitties – You have made my time spent in the dungeon brighter than I could ever imagine. Thank you for the laughs, the heart-to-hearts, the delusional moments, the sing-alongs, the dance-a-thons, the R frustrations followed by the R happy dances, in addition to the "riveting and enlightening" permafrost and statistical analysis discussions (because that is what I am supposed to say, right?!).

To my parents, G, and all of my loved ones both far and wide (special mention to J&RL) – For nurturing my desire to learn and to play in the mud since I was a wee little girl with pigtails. For giving me the drive to pursue whatever big dreams I had. For listening – but really – allowing me to bore you with, and being open to discussions of my results (I will pretend as though I did not notice your eyes glazing over...). For being my unrelenting cheerleaders and a source of endless support. For witnessing and living all the ebb and flows over the years right alongside me. And most importantly, for being the beacons guiding me back to shore...

I made it! With YOU, I made it.
Words could not possibly express...
Thank you.

Now... World, here I come.

TABLE OF CONTENTS

LIST OF FIGURES

LIST OF TABLES

LIST OF ACRONYMS

ACIA	Arctic Climate Impact Assessment
ALT	Active layer thickness
CALM	Circumpolar Active Layer Monitoring
CRREL	Cold Regions Research and Engineering Laboratory
DEM	Digital elevation model
EDA	Exploratory data analysis
GWC	Gravimetric water content
HTM	Holocene Thermal Maximum
ICP-AES	Inductively coupled plasma atomic emission spectroscopy
IPCC	Intergovernmental Panel on Climate Change
IPY	International Polar Year
LC	Leachate conductivity
LIS	Laurentide Ice Sheet
MAAT	Mean annual air temperature
PCA	Principal component analysis
PWC	Pore water conductivity
SD	Standard deviation
TDS	Total dissolved solids

1. INTRODUCTION

Thawing permafrost is a major concern in Arctic landscapes (Schuur et al., 2008; Jorgenson et al., 2006; Kokelj and Jorgenson, 2013). Permafrost degradation can increase carbon availability, which can lead to increased emission of CO_2 and CH_4 (Zona et al., 2009; Zhuang et al., 2006; Wickland et al., 2006; Schuur et al., 2009). It can also cause changes in soil biogeochemical cycling (Frey and McClelland, 2009; Hinzman et al., 2013) and release previously frozen solutes and nutrients to freshwater ecosystems (Keller et al., 2007; Malone et al., 2013; Bowden et al., 2008; Lantz et al., 2009). Although the future degree of permafrost degradation is uncertain (Delisle, 2007; Lawrence et al., 2008; Etzelmuller et al., 2011; Callaghan et al., 2011a), there is a general consensus over the predicted warming trends in the Arctic and particularly western Canadian Arctic. In these regions, air temperatures are expected to increase by 0.5-2^{o}C over the next century (Callaghan et al., 2011b) which would be sufficient to thaw the uppermost 2-3 m of permafrost in some areas (Derksen et al., 2012; Serreze et al., 2000; Lantz et al., 2013; Forbes et al., 2010; Tape et al., 2006; Callaghan et al., 2011a). Similarly, northwestern Canada experienced an increase in summer air temperature of up to 7^{o}C during the Early Holocene (Ritchie, 1984; Delorme et al., 1997; Clark et al., 2004). During this warm period, the depth of the permafrost table was on average 2-3 times greater than at present, reaching up to eight times the modern thickness in some regions (Burn, 1997; Fritz et al., 2012; Burn et al., 1986; Lauriol et al., 2002; Kotler and Burn 2000; Sanborn et al. 2006; Kokelj et al. 2002; Kokelj and Burn 2003; Murton, 2001).

To date, most studies of carbon, soluble ions and/or nutrient content and cycling have focused on the active layer (Keller et al., 2007; Lacelle et al., 2008; Lipson et al., 2010, 2012; Zona et al., 2011; Hubbard et al., 2013; Newman et al., 2015), while the few investigations of the biogeochemistry of permafrost are mostly limited to its uppermost 1.5 m (Kokelj et al., 2002; Malone et al., 2013; Kokelj and Burn, 2005; Lacelle et al., 2014). Based on these studies, physical, chemical and biological weathering occur mainly in the active layer, and consequently, the permafrost table represents a weathering boundary. This is reflected by distinct biogeochemical profiles between the active layer and near-surface permafrost with the permafrost typically containing higher concentrations of total soluble ions but lower concentrations of organic carbon (Kokelj and Burn, 2005; Keller et al., 2007; Kokelj and Lewkowicz, 1999; Lacelle et al., 2008; Tarnocai et al., 2009; Keller et al., 2010; Malone et al., 2013; Lacelle et al., 2014). Natural disturbances (e.g. active layer detachment slides, retrogressive thaw slumps) that lead to active layer deepening, therefore, may release solutes and carbon previously stored in the permafrost. For example, in northwestern Canada, hundreds of small to medium-sized stream catchments are now impacted by large, long-lived

retrogressive thaw slumps that expose a few to tens of meters of permafrost to thawing (Lacelle et al., 2015). These disturbances have significantly increased stream sediment and solute loads, affecting stream water quality across a range of watershed scales (Kokelj et al., 2013; Malone et al., 2013). However, little is known about the biogeochemical profiles in the active layer and the uppermost 2-5 m of permafrost at the regional scale. Information on the concentration and distribution of soluble ions and carbon in the active layer and uppermost 5 m of permafrost is needed to evaluate the potential consequences of permafrost degradation over the next century, including carbon availability and effects on freshwater ecosystems.

In this study, active layer and permafrost samples from eight sites across the northwestern Canadian Arctic were collected to depths of 5 m. The selected sites include the Tundra and Taiga Ecoregions (ECG, 2010), and both undisturbed (n=6) and disturbed (n=4) sites. The latter include two retrogressive thaw slumps located in the Richardson Mountains and two recently fire-disturbed sites (i.e. last 50 years). The active layer and permafrost cores were analyzed for ground ice content, carbon content and soluble ions concentration. The results will provide quantities and trends that allow an assessment of the potential biogeochemical changes in terrestrial and aquatic ecosystems due to thawing permafrost under a warmer climate.

1.1 RESEARCH QUESTIONS AND OBJECTIVES

This thesis aims to answer the following research questions:

(1) How are gravimetric water content (GWC), carbon content, pore water conductivity (PWC), leached conductivity (LC), and soluble ions distributed in the active layer and uppermost 5 m of permafrost in the northwestern Canadian Arctic?

(2) Are ground ice and biogeochemical profiles in the active layer, relict active layer and permafrost below the paleo thaw unconformity (hereafter termed Layer 1, Layer 2 and Layer 3, respectively) statistically different?

(3) Do the biogeochemical profiles in the active layer and uppermost 5 m of permafrost in the northwestern Canadian Arctic relate to the history of permafrost?

Based on these research questions, the objectives of this thesis are to: (1) determine the GWC, carbon content, conductivity and soluble ions concentration and distribution in the active layer and uppermost 5 m of permafrost in the northwestern Canadian Arctic by collecting active layer and permafrost samples across a latitudinal and longitudinal gradient; (2) compare the ground ice content and biogeochemical variations between layers at individual sites and to test the significance; (3) compare all variables across sites to determine potential relationships

between response and explanatory variables; and (4) investigate the findings in relation to the regional history of permafrost.

To achieve the objectives, analyses were conducted to measure: (1) gravimetric water content (GWC) in the active layer and permafrost; (2) pore water conductivity in active layer and permafrost, where possible; (3) total soluble ions in the active layer and permafrost using a leached extraction method; (4) organic matter and inorganic carbon contents semi-quantitatively using loss on ignition (LOI); and (5) organic carbon content by elemental analysis (EA). Subsequent data analyses included: (1) data transformation and simple, descriptive univariate analysis; (2) ANOVA with post-hoc Tukey HSD tests; and (3) a principal components analysis. Overall, this study contributes to baseline information on permafrost geochemistry in the northwestern Canadian Arctic that is needed to quantify ecosystem and watershed changes due to the anticipated permafrost degradation over the next 100 years.

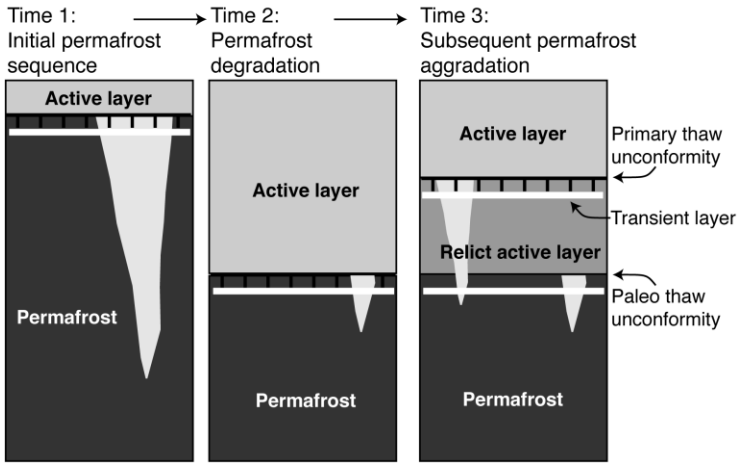

Figure 1 Schematics of terminology used in this thesis (Source: French, 1998).

2. BACKGROUND

2.1 Active Layer and Permafrost

The active layer is the uppermost soil layer that thaws in summer and freezes in winter. The active layer is important as hydrological, biogeochemical and pedological processes tend to be restricted to this layer. The boundary between the active layer and permafrost is termed the permafrost table. An ice-rich transition zone, or “transient layer”, can sometimes be observed in the upper part of permafrost. This transient layer serves as a buffer zone and protects soil at greater depths from permafrost degradation (Shur et al., 2005). This is because a higher energy input, or latent heat absorption, is required to melt the ice in this layer compared to thawing ice-poor permafrost. As a result, one can expect permafrost beneath the transient layer to persist, even through warmer summers, until the net energy budget overcomes this threshold (Shur et al., 2005).

The spatial distribution of permafrost can be classified into zones of continuous permafrost (>90 %), discontinuous permafrost (≥50 to <90 %), sporadic permafrost (≥10 to <50 %) and isolated patches of permafrost (0 to <10 %) (Brown et al., 1997). This distribution is mainly controlled by climatic factors, where the southern boundary of continuous permafrost corresponds with the mean annual air temperature isotherm of -6°C to -8°C (Fig. 2) (Burn, 2012). In addition, ecological factors have been shown to influence, and in some cases control, permafrost distribution to varying degrees. For example, a mature ecosystem assemblage (i.e. with a thick, well-developed surficial organic layer) is required to develop new permafrost within the discontinuous zone, while in the continuous zone, permafrost persists independently of vegetation cover (Shur and Jorgenson, 2007). As a result, Shur and Jorgenson (2007) proposed a permafrost classification that considers the interplay between climate and biophysical factors. The categories, from most to least independent of vegetation, are: i) climate-driven permafrost; ii) climate-driven, ecosystem-modified permafrost; iii) climate-driven, ecosystem-protected permafrost; iv) ecosystem-driven permafrost; and v) ecosystem-protected permafrost. In settings where climate is the dominating factor, interactions with permafrost are relatively simple. They become more complex where surface vegetation plays a greater role due to its lower thermal conductivity and ability to maintain permafrost stability. Vegetation is an important factor affecting snow interception, topographical properties (with associated consequences for surface roughness and air redistribution/turbulence), thermal and hydraulic properties in the ground, and albedo (Shur and Jorgenson, 2007).

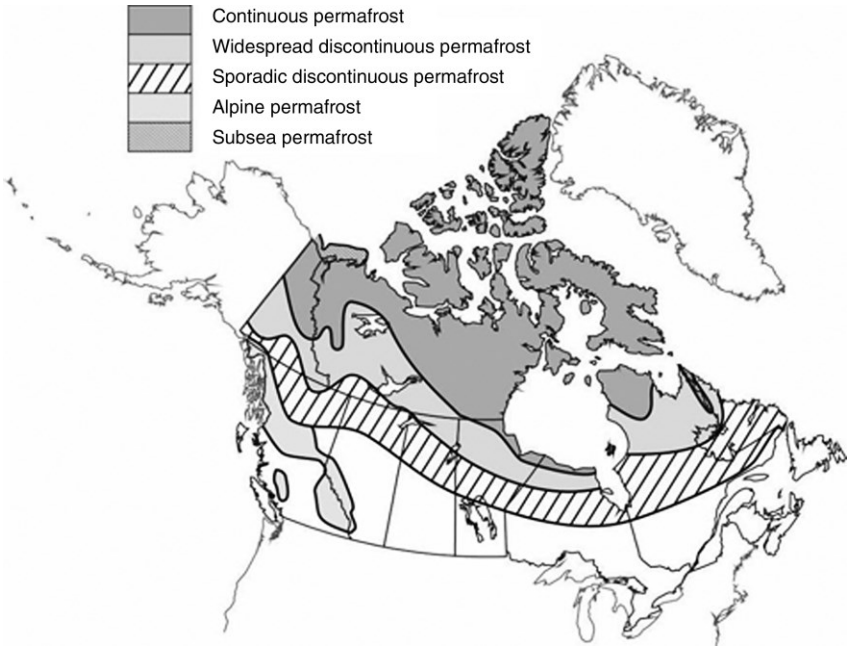

Figure 2 The regions of permafrost distribution in Canada (Source: Burn, 2011).

2.2 Contemporary Climate and Active Layer Thickness

Over the last few decades, Arctic air temperature has increased by ca. 1^{o}C per decade in spring and winter, a rate twice as high as the global mean annual air temperature and the region is also experiencing an increase in precipitation (Hartmann et al., 2013; Larsen et al., 2014). Responses to this changing climate are numerous and varied including storm frequency/severity, and summer warmth index which relates to positive plant productivity (Xu et al., 2013). At the ecosystem-level, warmer freshwater systems can lead to shifts in community assemblages (Christoffersen et al., 2008; Heino et al., 2009; Jansson et al., 2010). Other responses have been observed, such as an increase in permafrost temperatures (Romanovsky et al., 2010), a northward proliferation of tall shrubs and trees (Lantz et al., 2013; Forbes et al., 2010; Myers-Smith et al., 2011), and the development of retrogressive thaw slumps and thermokarst lakes (Kokelj et al., 2013) with subsequent changes in nutrient availability among terrestrial and aquatic systems (Lantz et al., 2009; Thienpont et al., 2013; Lewis et al., 2012; Kokelj et al., 2009).

Active layer deepening is another response to climate change. Since 1990, active layer thickness has been monitored at a number of sites in both the Northern and Southern Hemispheres through the Circumpolar Active Layer Monitoring (CALM) Program. In the Canadian Arctic, measurements from 18 sites show a fluctuation in active layer thicknesses between 25-120 cm (Fig. 3). Inter-annual variability in active layer thickness is a result of several factors, but primarily variations in snow cover and summer air temperature (French, 2007). However, persistent increased temperatures and/or more severe disturbances, (e.g. alterations in vegetation cover, forest fires, physical and thermal characteristics of overlying soil and moisture content), can lead to deepening of the active layer and thermokarst (Anisimov et al., 2007; Brown et al., 2000). Since the 1990s, only 6 of 18 sites in Arctic Canada have shown an increase in active layer thickness: Alexandria Fjord, Pump Station, Great Bear River, Ochre River, Tanquary Fjord and Bake Lake. All other sites show a decreasing trend in active layer thickness, including all sites along the Mackenzie River Corridor (Fig. 4). However, linear regression models and subsequent regression analysis suggest that the changes in active layer thickness are only significant at three sites (Fort Simpson, Rengleng River, Taglu). All others' significance is unable to be determined certainly due to small datasets.

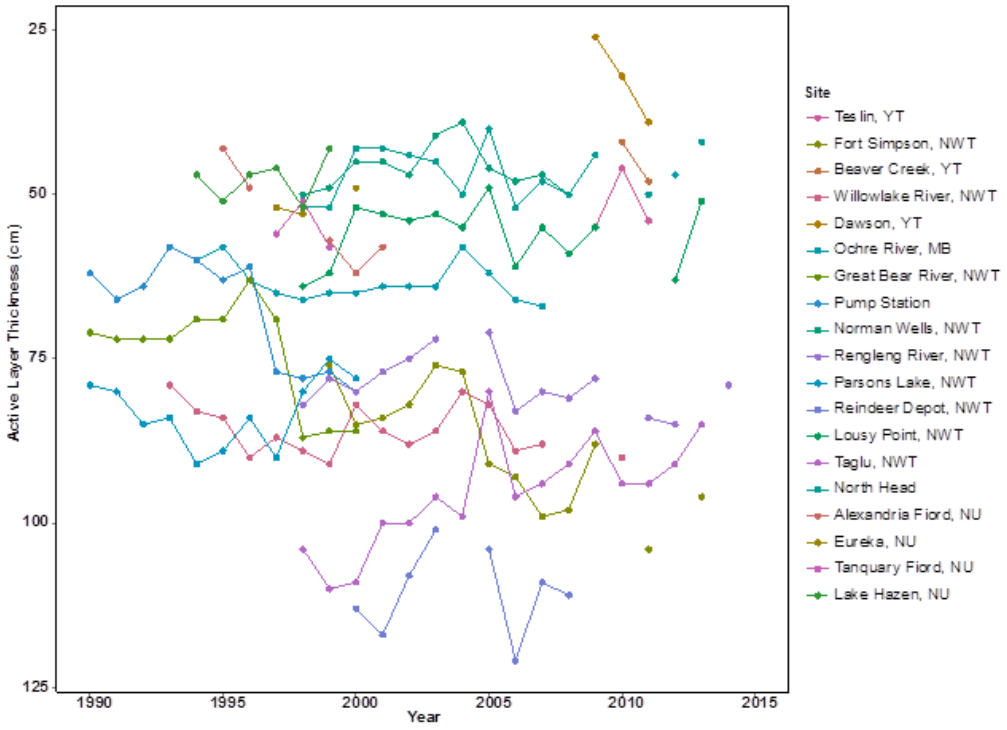

Figure 3 Active layer thickness (in cm) measured at 19 sites in the Canadian Arctic. Data was obtained from the CALM monitoring network.

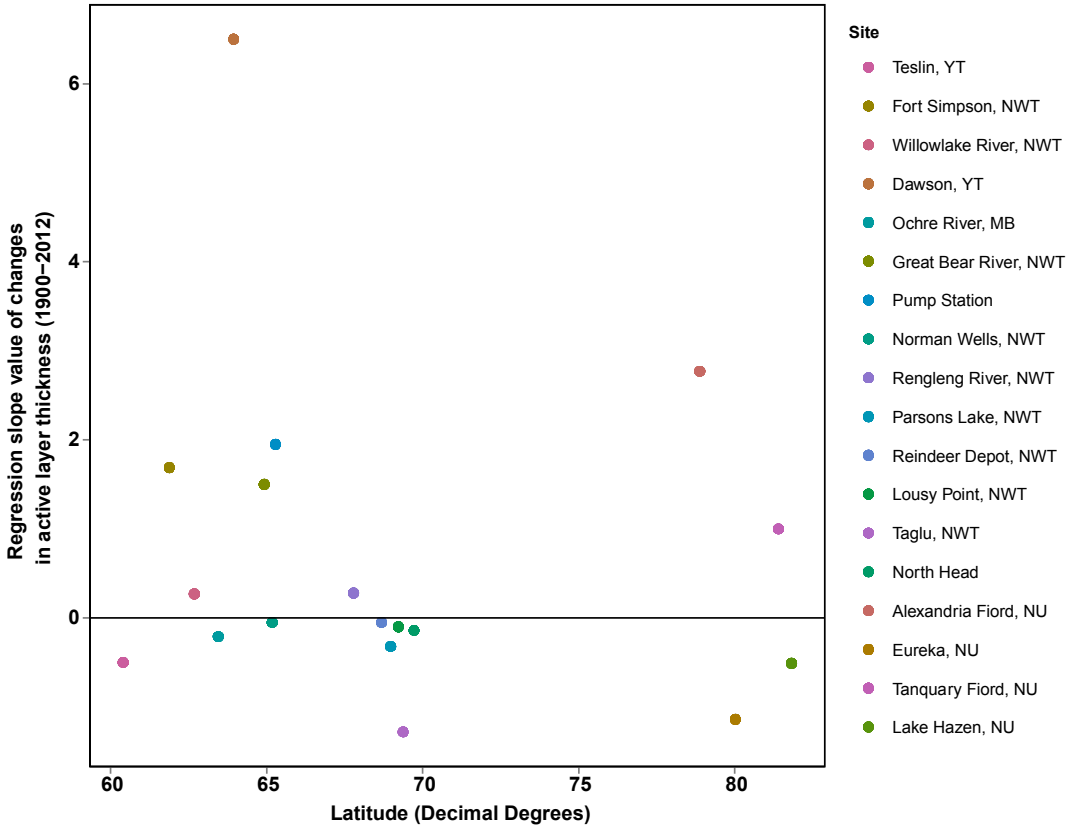

Figure 4 Regression slope values of changes in ALT between 1990-2012 along a latitudinal gradient. Data used in the calculation of slope values was obtained from the CALM program.

2.3 Early Holocene Climate and Paleo-Active Layer

During the Early Holocene, summer air temperatures in northwestern Canada were 2-7^{o}C warmer than present-day (Ritchie, 1984; Delorme et al., 1977; Clark et al., 2004). This Holocene Thermal Maximum (HTM) was driven by Milankovitch cycles, corresponding to an interval with high obliquity and increased insolation, the presence of an anti-cyclone over the nearby receding Laurentide Ice Sheet that brought southern air masses to the region, and perhaps to the greater continentality due to the Beaufort Sea coastline being ca. 100 km further north (Ritchie, 1984; Burn, 1997; Miller et al., 2010; Fritz et al., 2012; Gajewski, 2015).

Proxy data suggest that the thermal maximum began in northwestern Canada around 10,600 BP. Palynological analyses reveal that pollen from several species (e.g. spruce – *Picea*, cat-tail – *Typha,* bog myrtle – *Myrica*, and poplar – *Populus*) were found north of their modern range during this time (Burn, 1997 and references therein). In some cases, the displacement was in the order of several hundred kilometers, such as for *Typha*, where it was located approximately 500 km to the north of its present-day distribution (Vardy et al., 1997). Mechanisms of dispersal particular to this species restrict displacement, further confirming the paleoclimatic conditions of the Early Holocene (Ritchie et al., 1983). Tamarack and spruce macrofossils were found buried within a peat deposit, almost 100 km outside present-day ranges. Dating of these specimens provided ages of 7,510 ± 140 BP (Vardy et al., 1997). In the Mackenzie Delta and Peel Plateau region, evidence of beaver-chewed wood was dated to 7,800 ± 300 BP (Delorme et al., 1977) and 5,810 ± 40BP (Lauriol, unpublished results) in areas no longer occupied by beavers. Furthermore, the evolution from herb-tundra to woodland was documented by the change in pollen input of less than 500 to over 2000 around the thermal maximum (Ritchie et al., 1983; Meyer et al., 2010). Other (micro)biological examples of a warmer climate during the early Holocene include the presence of endostromatolites formed under peak thermal conditions and methanogenesis reactions (Clark et al., 2004), as well as a lack of cryophiles between 14,410-6,820 BP (Delorme et al., 1977). Analyses of $\delta^{18}O$ isotope profiles from endostromatolites support indications of a transition from a cooler period at the onset to warmer temperatures of the Holocene Thermal Maximum (Clark et al., 2004; Lauriol et al., 2009).

The warmer summer air temperatures during the Early Holocene led to a much thicker active layer in the western Canadian Arctic than today (Burn, 1997; Fritz et al., 2012; Burn et al., 1986; Lauriol et al., 2002; Kotler and Burn 2000; Sanborn et al. 2006; Kokelj et al. 2002; Kokelj and Burn 2003). The paleo-active layer is defined as “a horizon corresponding to the depth to which previous thawing of permafrost had proceeded” (French, 2007). The permafrost table is an example of a primary thaw unconformity, while a paleo-active layer is considered a

secondary thaw unconformity. It is worth noting that a secondary thaw unconformity need not always be a paleo-active layer (e.g. talik). The paleo-active layer can be identified along natural or anthropogenic exposures by ice-wedge truncation, variations in permafrost cryostructures and sediment colour, with sediments above the unconformity often being lighter (Burn, 1997; French and Shur, 2010). A paleo-active layer associated with the Early Holocene warm interval has been documented at numerous sites in northwestern Arctic Canada. Near Mayo (central Yukon Territory), a paleo-active layer was observed at 1.3 m depth, approximately twice the depth of the modern active layer. On Herschel Island (northern Yukon Territory), a thaw unconformity is found 1.5 to 3.0 m below the depth of the modern active layer (Burn et al., 1986; Fritz et al., 2012; Burn, 1997). In the latter case, an increase in the upper range would have likely caused the development of a talik. In the Tuktoyaktuk Coastlands (NWT), the paleo-active layer has been measured at ca. 2 m depth, corresponding to 2-8 times the depth of the modern active layer (Murton, 2001). It should be noted that observations of paleo-active layers in Arctic Canada are restricted to northwestern Canada as no studies have yet documented the presence of a paleo-active layer in the mid, high and eastern Canadian Arctic.

2.4 Future Climate Change and Response of the Active Layer

Results from 25 models under different climate scenarios predict an increase in Arctic temperatures of 3 to 6^{o}C by 2100 (Overland et al., 2011; Collins et al. 2013). Consequently, the uppermost 2-3 m of permafrost is expected to thaw in some areas over the next century (Callaghan et al., 2011a). Models generally fail to consider the effect of wild fire on future permafrost conditions, and particularly on active layer thickness (Lawrence et al., 2008; Koven et al., 2011, 2013; Saito et al., 2007; Eliseev et al., 2013). Although this natural or human-induced phenomenon most often occurs in forested areas, other vegetated regions – including tundra – can also be affected due to moisture content change (French, 2007). Following a fire disturbance, water availability significantly increases at the base of the active layer simultaneously.

Although the impact of future air temperature warming, forest fires, and permafrost degradation has yet to be fully understood, the complexity of climatic interactions and feedbacks in the Arctic is certain. In turn, these processes are anticipated to affect active layer thickness, with some Arctic regions predicting increases, while others will experience little to no changes and possibly thinning of the active layer (Callaghan et al., 2011a). With a thicker active layer, greater water storage capacity in this zone could allow for more baseflow annually, and particularly over the winter months, potentially contributing to a thermal perturbation of permafrost and a modification of Arctic hydrology (Adam et al., 2009; St Jacques and Sauchyn,

2009). The increased water availability and deeper active layer would also likely lead to additional chemical weathering of the near-surface permafrost (Lacelle et al., 2008). This would have a positive feedback on solute concentrations within the seasonally-frozen layer as well as those being leached from the soil into the surrounding watersheds and ecosystems.

2.5 Ground Ice and Water Content in Permafrost

The presence of permafrost in the landscape is a major factor in controlling hydrological processes. With the exception of taliks, water movement tends to be limited to the active layer as the permafrost table acts as a physical boundary, preventing water infiltration to great depths (Osterkamp and Burn, 2003; Cheng, 1983). However, unfrozen water in permafrost can occur in small amounts due to the presence of solutes that lower the freezing point below $0^{o}C$ (Osterkamp and Burn, 2003). Further, finer-grained soils have a high specific area that allows water to remain adsorbed on the soil surface (Cheng, 1983). For example, unfrozen water content (Wu, as gravimetric water content %) in clayey-silt soils near Inuvik have been shown to have the following non-linear relationship with temperature below $0^{o}C$ (T, in ^{o}C): $Wu=12.97T^{-0.51}$ (Kokelj and Burn, 2003). The unfrozen water found at the base of the active layer and uppermost permafrost may move along thermal and hydraulic gradients from the base, with the downward migration flux of water in the summer being higher than the upward movement in winter (Cheng, 1983; Mackay, 1983). The greater downward water flux in summer can be attributed to the temperature dependency of hydraulic conductivity in permafrost. The seasonal differences in hydraulic conductivity can be up to three orders of magnitude higher in summer (Burn and Michel, 1988). These processes have been confirmed by different methods, including neutron probing (Cheng 1983), indirectly by heavemeter (Mackay, 1983; Smith, 1985; Burn, 1988) and tritium measurements (Chizhov et al., 1983; Burn and Michel, 1988).

Ground ice content in permafrost is related not only to moisture availability and migration, but also to soil porosity. Finer-textured soils with moderate permeability and porosity (e.g. “frost-susceptible” silts) allow capillary forces to draw unfrozen water towards a freezing front (French, 2007). This process is responsible for the formation of segregation ice within a soil profile, with the ice layers ranging from mm to m thick. In permafrost terrain, there is potential for the freezing of water to supersaturate unconsolidated soils, resulting in excess ice. The thaw of this excess ice can account for loss of soil bearing strength. Excess ice is formed when water content exceeds available pore space causing layers of ice to form between soil layers during freezing. The type of ground ice found within a particular area can be a product of the climate and ecosystem interactions previously mentioned. Pore and lenticular ice are found mainly in climate-driven permafrost, and turn into layered reticulate and ataxitic ice when the

role of vegetation becomes important. All these types are present in ecosystem-driven and ecosystem-protected permafrost, further depending on the soil drainage capacity (Shur and Jorgenson, 2007).

Ground ice is one of the most dynamic components of permafrost. Its concentration and distribution vary in large part due to the thermal history of permafrost and vegetation change. Jorgensen et al. (2010) provided a generalization of ground ice content and its distribution in 6 common types of permafrost (Fig. 5). These include: A) epigenetic permafrost with overall little ice content but possible presence of ice-rich layers at depths if the downward freezing front reaches available groundwater; B) permafrost formed under parasyngenetic conditions in closed taliks in lacustrine or glacio-lacustrine sediments leading to high ground ice content; C) epigenetic permafrost with little ice content overlain by an organic and ice-rich layer near the surface; D) syngenetic permafrost with high ice content formed during sediment accumulation (e.g. in fluvial, aeolian and some glacial deposits). In this case, upward growth of ice wedges is linked to the increase in ground ice content; E) ice-rich syngenetic permafrost with an increase in ice content just below the surface of permafrost from accumulation of organic matter; and F) syngenetic permafrost with high overall ground ice content and an ice-poor layer near the surface due to the thawing and refreezing of soils during a warmer climate or surface disturbances in addition to an ice-rich layer near the surface of permafrost caused by the accumulation of organic matter.

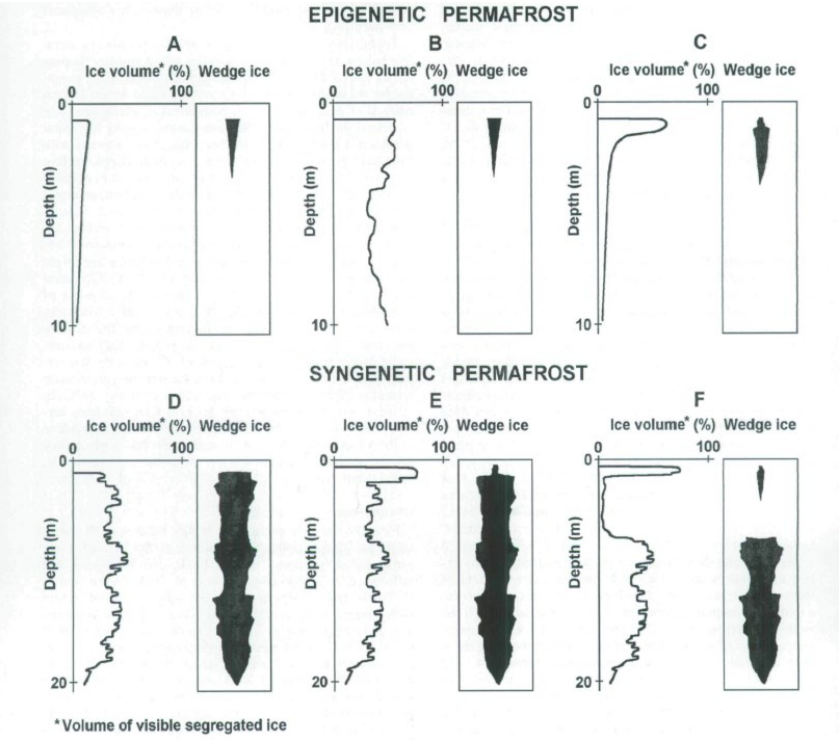

Figure 5 Generalization of ground ice abundance in 6 different types of permafrost based on formation processes, as outlined by Jorgenson et al. (2010). See the text for descriptions of the different types of permafrost.

2.6 Weathering and Geochemistry of the Active Layer and Permafrost

As in any other environment, weathering processes in permafrost regions play a role in modifying the landscape, primarily in the active layer (French, 2007). In permafrost environments, physical weathering is related to the volumetric expansion of water during phase changes and thermal stress, which causes ground alteration at micro to macro-scales (Komishchev and Rogov, 1993; Prick and Pissart, 1993; Lewkowicz, 2001). Climate ultimately plays a large role in this type of weathering process, primarily during seasons with cross-zero temperature variations (i.e. spring, summer and autumn) (Konishchev and Rogov, 1993). Its intensity is divided based on the number of days with freeze-thaw: weak (<50 days), average (50-70 days) and strong (>70 days) (Konishchev and Rogov, 1993). Although more effective in the active layer, physical weathering also occurs within permafrost. The effects of physical weathering in periglacial environments include frost-heave, patterned ground, thermal contraction/dilation, and cryoturbation (French, 2007).

Conversely, chemical weathering in permafrost areas is associated with solution/karstification, salt weathering and leaching (French, 2007). Blake et al. (1991) suggested that chemical weathering, although prevalent, is limited by water availability in the

soil, which is typically restricted to the short thaw season. The type and degree of chemical weathering can be determined by analyzing the presence of secondary minerals (Allen et al., 2001). It can also be assessed indirectly through measurement of solutes in rivers and streams (Etienne, 2002 and references within). As observed in Ball et al.'s study (2011), lateral flow can create geochemical homogenization as the soil is progressively de-salinized, while water ponding may lead to salinization. Topography and local water sources determine the resulting effect. In a study of physical and chemical weathering in the active layer from the high Arctic, Lacelle et al. (2008) observed a change in micro-morphologies of sand grains (decrease in grain angularity with depth) and geochemical profile (increase in ionic content with depth). The transition from dominant physical weathering near the surface to increasing chemical weathering with depth was attributed to decreasing frequency and intensity of mechanical weathering and to the presence of permafrost which allows for a greater availability of water for chemical reactions at the base of the active layer (Fig. 6).

Early work on permafrost geochemistry was undertaken near Fairbanks and Barrow, Alaska, USA (e.g. Péwé and Sellman, 1973; Brown, 1968; O'Sullivan, 1966). Results from these unglaciated regions indicated a step-like change at the boundary between interglacial and glacial aged-sediments. These features were found to be a result of enhanced freshwater leaching during the warmer-wetter interglacial periods. This finding was used to infer that geochemical discontinuities in permafrost can provide information on past permafrost conditions (e.g. Mackay and Dallimore, 1992). Subsequent studies of permafrost geochemistry focused on the active layer – permafrost boundary, though these remain quite limited in number. For example, studies on the geochemical composition of the active layer and near-surface permafrost from the Mackenzie Delta (Kokelj and Burn, 2005; Lacelle et al., 2014), Herschel Island (Kokelj et al., 2002) and northern Alaska (Ping et al., 1998; Bockheim et al., 1998; Keller et al., 2007) have all shown that soluble ion content is lowest in the active layer but increases ca. 2 to 7 fold in the top of permafrost. These studies have been conducted in fine-grained materials, which can contain significant amounts of unfrozen water at temperatures below 0°C due to their higher specific surface area (Anderson et al. 1973; Williams and Smith 1989). As such, the increase in soluble ions in the top of permafrost has been attributed to leaching in the active layer and the downward transport of soluble ions during summer by water migrating along the negative soil thermal gradient. Therefore, the distribution of soluble ions in the top of permafrost may be used to infer decadal to centennial stability of the active layer and associated growth of the transient layer (e.g., Kokelj and Burn 2003; Lacelle et al. 2014).

Most of the aforementioned geochemical studies were limited to an investigation of the geochemical composition of the active layer and near-surface permafrost (<1.5 m). All of these

studies were performed at the local scale, unlike the present thesis which investigates biogeochemistry variations at the regional scale. Considering that the active layer thickness varies from year to year, and that it was much thicker during past warm climate intervals, such as the early Holocene (Burn, 1997; Lauriol et al., 2002), or following forest fires (Mackay, 1995; Burn, 1998), these studies likely only analyzed the geochemical profiles above the maximum depth of thaw during the Holocene (in the relict active layer), but not in permafrost below that. The permafrost comprising the relict active layer likely experienced intermittent thawing and leaching. As such, its geochemical profiles are expected to be different from both the active layer above (i.e. greater than) and the permafrost below it (i.e. less than). This assumption pertains primarily to sites with stable conditions and could differ amongst those subject to, for example, erosional or accumulation processes (e.g. hillslopes, taliks).

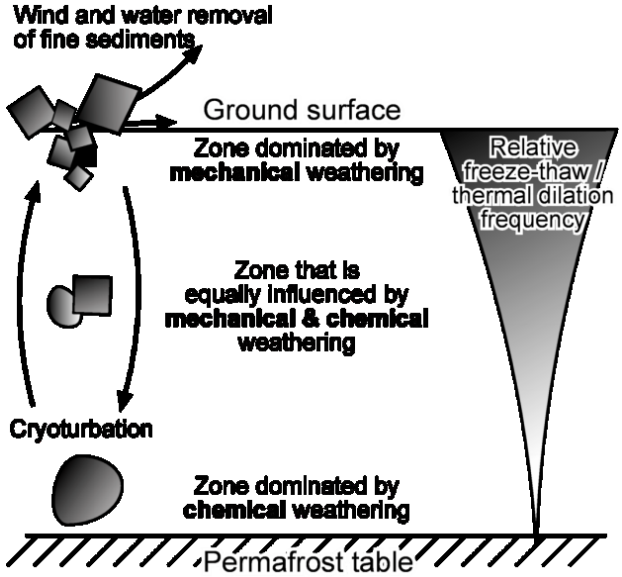

Figure 6 Relationship between mechanical and chemical weathering in periglacial environments (Source: Lacelle et al., 2008).

3. STUDY AREA

3.1 Physiography

The study area is situated in the northwestern part of the Northwest Territories, Canada, extending from the Richardson Mountains and Peel Plateau to the uplands east of the Mackenzie Delta region (Fig. 7). The Richardson Mountains consist of a series of north-south ridges separated by broad valleys (Catto, 1996). Elevation is typically more than 500 m a.s.l., the lowest point being Summit Lake in McDougall Pass (320 m a.s.l.) and the highest point being Mount Sittichinli (1574 m a.s.l.). The Peel Plateau slopes gently eastward with elevation ranging from 650 m a.s.l. in the foothills of the Richardson Mountains to 100 m a.s.l. west of the Peel River (Catto, 1996; Duk-Rodkin and Lemmen, 2000). The upland terrain east of the Mackenzie Delta belongs to the Taiga Plains ecozone and is covered by hummocks in varying stages of development. Elevation in this region varies between 100-300 m a.s.l. (ECG, 2010).

3.2 Geology

The majority of the study area is located within the Interior Platform geological province, (Geological Survey of Canada, 1997). Bedrock geology in the Richardson Mountains-Peel Plateau region consists primarily of Cretaceous marine shales, conglomerates and sandstones of the Boundary Creek, Arctic Red, Rat River, Mount Goodenough and Martin Creek Formations (Norris, 1981a). To the South-East of the Mackenzie Delta, bedrock geology is comprised of Devonian marine shales, siltstones, and sandstones from the Imperial Formation (Norris, 1981b). Towards the coast of the Beaufort Sea, there are some pockets of Upper Cretaceous marine shales, and siltstones from the Horton River Formation, Devonian marine limestone and dolomite of the Gossage Formation, in addition to Permian clastics and conglomerates (Norris, 1981b,c). With the exception of the Mackenzie Delta, a till blanket or till veneer covers the study sites.

3.3 Late Pleistocene Glaciation

During the Late Pleistocene, the Laurentide Ice Sheet (LIS) advanced onto the eastern slopes of the Richardson Mountains up to an approximate elevation of 750 m a.s.l. and extended beyond the Tuktoyaktuk Coastland (Fig. 7) (Duk-Rodkin and Lemmen, 2000). The LIS is inferred to have been warm-based as evidenced from the occurrence of eskers, drumlins and reconstructed low glacier profile (Beget, 1987; Rampton, 1988). It was initially thought that the maximum extent of the LIS was reached ca. 30 kcal yr BP (Duk-Rodkin and Lemmen, 2000),

however, new U/Th ages indicate that the ice sheet reached its maximum extent at ca. 18 kcal yr BP (Lacelle et al., 2013). Retreat of the LIS from the Peel Plateau was characterized by two standstills or readvances named the Tutsieta Lake Phase dated just prior to 15 kcal yr BP and an unnamed phase situated a few kilometers to the east (Duk-Rodkin and Hughes, 1992). The Richardson Mountains – Peel Plateau region has been ice-free since ca. 13 kcal yr BP, as suggested by the presence of *Bison priscus* near the community of Tsiigetchic (Zazula et al., 2009) and the upland terrain east of the Mackenzie Delta was deglaciated shortly after 12 kcal yr BP (Geological Survey of Canada, 1973).

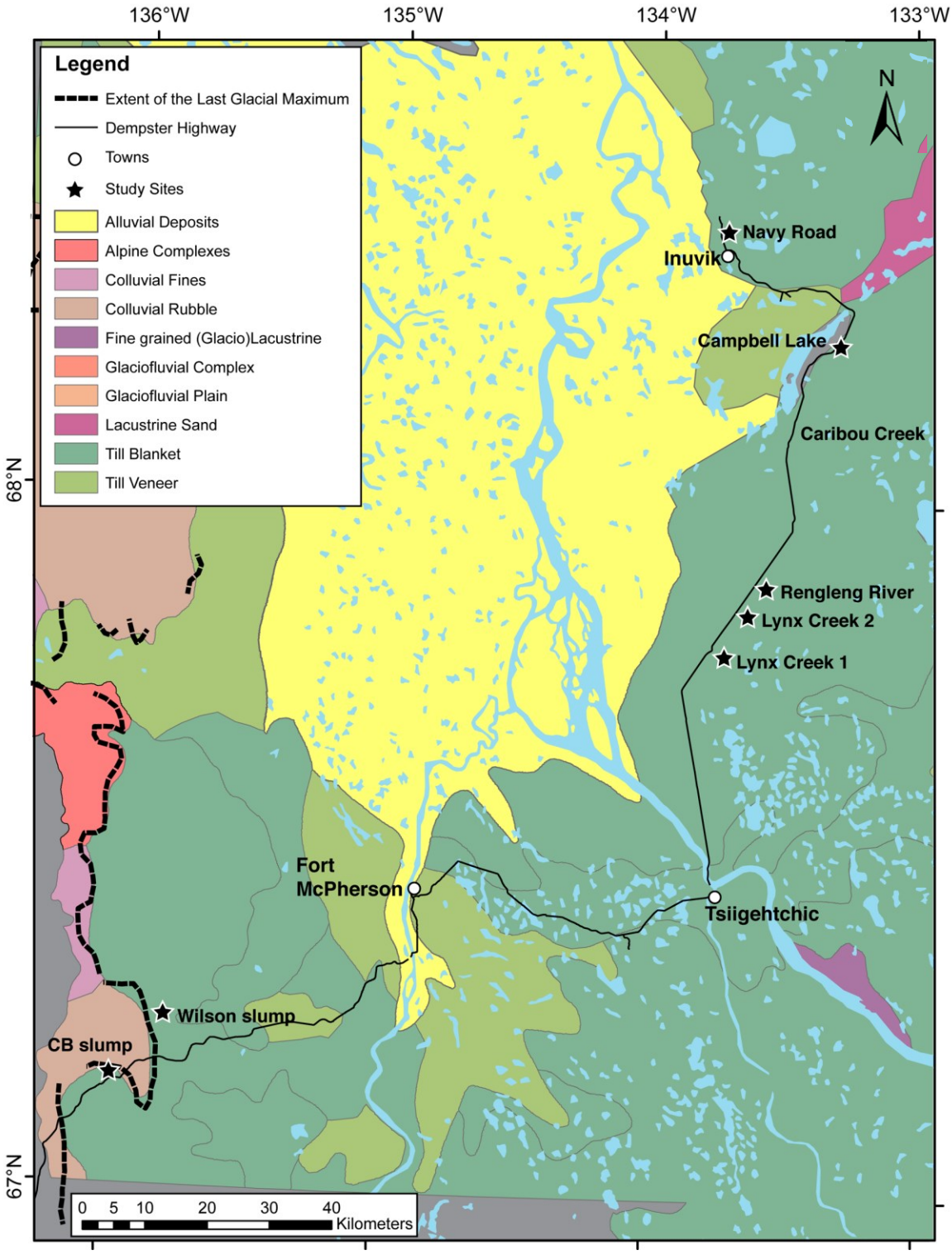

Figure 7 Location of the eight sampling sites in the Northwest Territories, Canada with surficial geology of the region and the extent of the Laurentide Ice Sheet maximum delimited by a thick black dashed line. Two cores were collected at Navy Road (NRD and NRT2) as well as at Rengleng River (R2T2 and R2T3).

3.3 Climate, Vegetation and Permafrost Conditions

The regional climate is characterized by short cool summers and long cold winters. Climate data from weather stations in Fort McPherson and Inuvik indicate that the mean annual air temperature (MAAT) is approximately -7.3°C (Environment Canada, 2012). Mean temperatures in January reach close to -26°C; whereas mean temperatures in July approach 15°C (Environment Canada, 2012). Air temperature in the Tuktoyaktuk Coastal Plain is slightly colder, with mean winter, summer and annual air temperatures of -26.5°C, 4.5°C and -9.8°C, respectively (Environment Canada, 2012). Since the 1970s, the MAAT in this region has been increasing at a rate of 0.77°C per decade (Fig. 8A; Burn and Kokelj, 2009). Trends are similar at all three locations. Total annual precipitation at Fort McPherson and Inuvik ranges from 250 to 300 mm, with ca. half falling as rain. The Tuktoyaktuk coastal plain, receives less precipitation overall, with a total annual precipitation of 125-200 mm (Fig. 8B; Environment Canada, 1995). Total annual precipitation shows little temporal changes. Precipitation totals for June–July show that six of the ten wettest summers in an intermittent record extending back to 1915 have occurred since 1994, with 2010 and 2012 being the wettest two summers on record (Kokelj et al., 2015).

The Richardson Mountains and Peel Plateau regions are part of the Tundra Cordillera ecozone with vegetation consisting mainly of Arctic tundra assemblages, sedges, and some dwarf shrubs (ECG, 2010). The upland region east of the Mackenzie Delta falls in to the Taiga Plains ecozone with open, generally stunted black spruce woodlands and willows, alders, mosses and lichen composing the understory (ECG, 2010). The present-day tree line is situated between Inuvik and Tuktoyaktuk.

These climate and vegetation conditions result in continuous permafrost within the study area. Permafrost thickness in the region varies between ca. 300 m in the northern Peel Plateau area, to approximately 100 m in Inuvik, NT, and increases northward towards the Beaufort Sea reaching a thickness of nearly 500 m (French, 2007; Burn and Kokelj, 2009). The active layer thickness in the study area ranges from about 30-50 cm on vegetated surfaces in fine-grained tills or in organic deposits, to more than 100 cm in disturbed areas and gravelly floodplains (Brown et al., 2000b). Regional active layer monitoring (e.g. Rengleng River, Parson Lake and Reindeer Depot) shows significant year-to-year variability, and longer-term trends vary with ecological change, soil moisture and climate (Fig. 3) (Smith et al., 2009). In areas with stable vegetation conditions, the inter-annual variation in thickness of active layer is largely dependent on the thawing degree-days and conditions during the previous winter (Smith et al., 2009). Soil horizons are primarily mineral in nature, with a thin organic layer consisting of mosses, shrubs

and woody materials overlying oxidized and gleysolic horizons, respectively. However, cryoturbation plays an important role in soil formation processes as evidenced by patterned ground (e.g. earth hummocks).

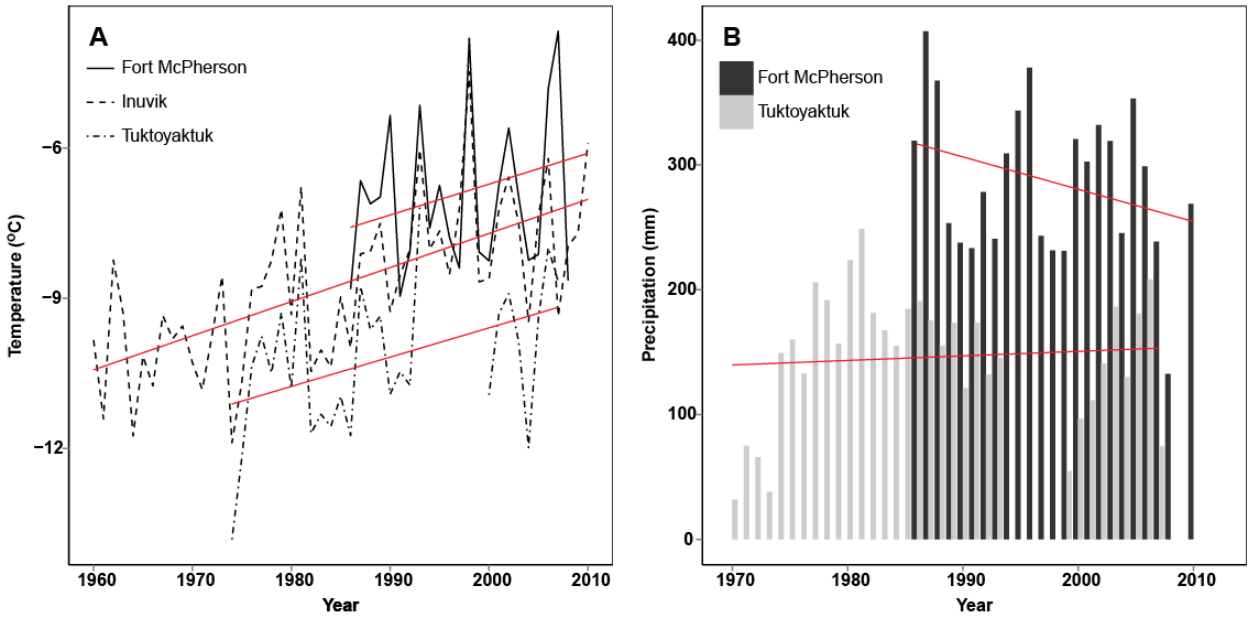

Figure 8 (A) Mean annual air temperature (MAAT), in ^{o}C, and linear regression analysis (red lines) between 1960-2012 in Fort McPherson, Inuvik and Fort Tuktoyaktuk, NT. Data was obtained for Fort McPherson A, Inuvik A, and Tuktoyaktuk weather stations from Environment Canada. (B) Total annual precipitation, in mm, with associated linear regression analysis (red lines) at Fort McPherson and Tuktoyaktuk, between 1970-2010. Data was obtained from Environment Canada. Linear regression MAAT trends show an increase of approximately the same magnitude across all sites. Total annual precipitation regression trends show little temporal changes at Tuktoyaktuk and what appears to be a decreasing trend at Fort McPherson. However, this could be a result of the short data collection range.

4. METHODOLOGIES

4.1 Active Layer and Permafrost Sampling

Active layer and permafrost samples were collected from 8 sites (10 cores) in the Peel Plateau and upland terrain east of the Mackenzie Delta (Fig. 7). The sampling sites were selected based on accessibility, surficial geology, ecoregion type and disturbance incidence over the last 50 years. Table 1 provides a summary of site characteristics, including geographical coordinates, elevation and active layer thickness.

Active layer and permafrost samples in the upland terrain east of the Mackenzie Delta were collected at 6 sites (8 cores) in late summer 2014. All sampled sites are on till blanket surfaces and fall within the Taiga Plain ecoregion. Two of the sites in this region had previously been burned by forest fire (NRD and Lynx 2) in 1968 and 1999, respectively (Natural Resources Canada, 2014). The active layer soils were sampled at 3-5 cm intervals from the surface using a spade and placed in polyethylene bags. The permafrost was sampled using a CRREL corer with an inner diameter of 3.5-in with a Viper powerhead (Fig. 9A). The cores were sub-sectioned into 3-5 cm segments in the field and placed in sealed plastic jars.

On the Peel Plateau, active layer and permafrost samples were collected in summer 2013 from the headwall of two thaw slumps (CB and Wilson slumps; Figs. 10 and 11). The CB slump and Wilson slumps are located on undivided till blanket and till veneer and are found within the Taiga Plains ecozone. These sites have not been subjected to recent fire disturbances (i.e. since the 1960s; Natural Resources Canada, 2014). The active layer samples were collected every 3-5 cm interval using a spade and the samples placed in polyethylene bags. The permafrost samples were collected from the headwall of thaw slumps using a 3-in. diameter handheld HILTI corer by coring horizontally 15-20 cm into the permafrost (Fig. 9B-C). The permafrost samples were acquired over a 2-3 m continuous section and placed in sealed plastic jars.

Figure 9 (A) Sampling with a CRREL corer and Viper powerhead at Lynx 1 during summer 2014. (B) Thaw slump headwall sampling in summer 2013 with a handheld HILTI corer at the CB and (C) Wilson sites.

Figure 10 Aerial photograph of the surrounding landscape at the Wilson slump site (left) and headwall with the paleo thaw unconformity delimited by the dotted white line (right). Person standing for scale.

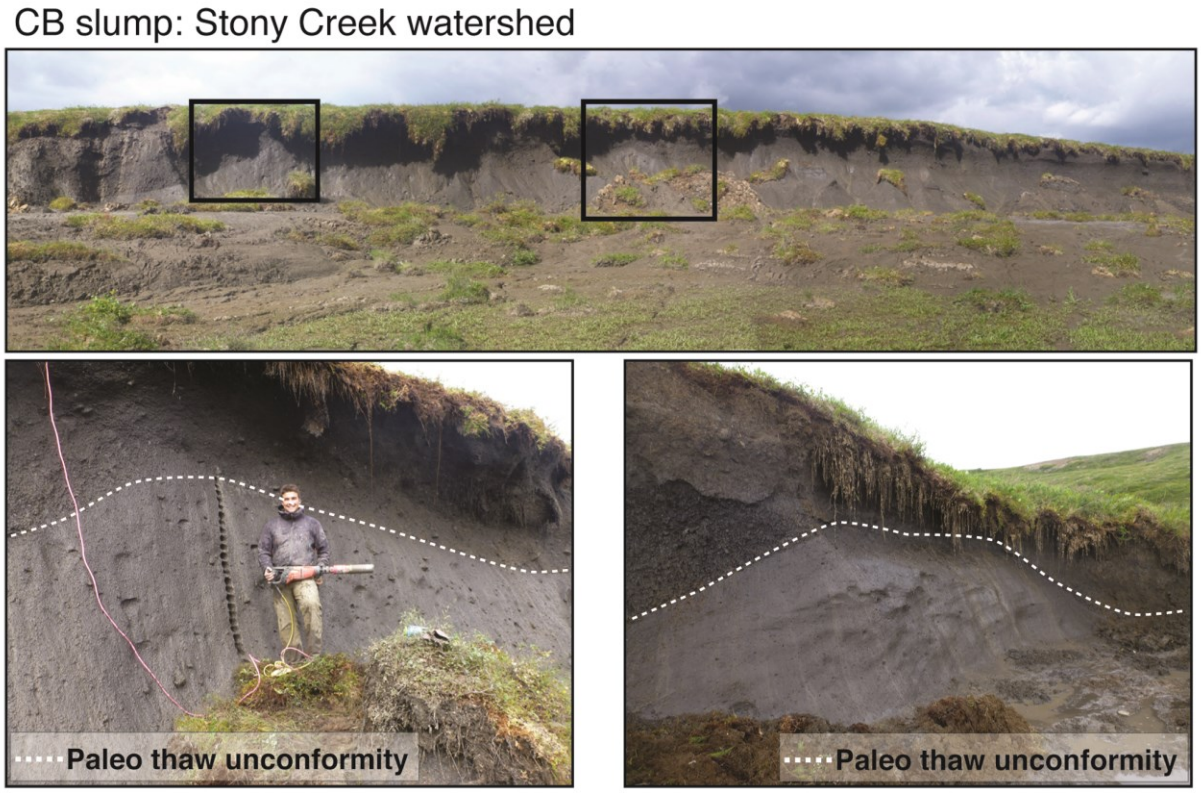

Figure 11 Photograph of the CB slump landscape (above) with HILTI corer sampling method (bottom left) and boundary of the paleo thaw unconformity indicated by the dotted white line (bottom right).

Table 1 The characteristics of the 10 active layer and permafrost cores collected in the western Canadian Arctic, including latitude and longitude (in decimal degrees), elevation (in m), active layer thickness (in cm), ecozone, surficial geology and year of post-1950 forest fire when applicable.

Site	Name	Latitude	Longitude	Elevation (m a.s.l.)	Slope (degree)	Aspect (degree)	Frost Table Depth (cm)	Ecozone	Surface Geology	Post-1950 forest fire
Peel Plateau										
CB slump	CB	67 ^{o} 10.558'	-135 ^{o} 43.507'	595	10.5	194	48	Tundra Cordillera	Till blanket	-
Wilson slump	Wilson	67 ^{o} 27.734'	-135 ^{o} 16.145'	610	2.4	135	32	Tundra Cordillera	Till blanket	-
Eastern Mackenzie Delta										
Navy Road 2	NRD	68 ^{o} 23.036'	-133 ^{o} 45.285'	32	1.4	225	107	Taiga Plains	Till blanket	1968
Navy Road 1	NRT2	68 ^{o} 22.988'	-133 ^{o} 45.241'	32	1.4	225	28	Taiga Plains	Till blanket	-
Lynx Creek 1	Lynx 1	67 ^{o} 47.532'	-133 ^{o} 47.193'	107	0.8	-1	31	Taiga Plains	Till blanket	-
Lynx Creek 2	Lynx 2	67 ^{o} 51.153'	-133 ^{o} 40.254'	71	0.3	270	74	Taiga Plains	Till blanket	1999
Rengleng River –T2	R2T2	67 ^{o} 51.946'	-133 ^{o} 38.893'	76	0	-1	56	Taiga Plains	Till blanket	-
Rengleng River – T3	R2T3	67 ^{o} 51.946'	-133 ^{o} 38.893'	76	0	-1	31	Taiga Plains	Till blanket	-
Caribou Creek	Caribou	68 ^{o} 05.964'	-133 ^{o} 29.325'	5	0	-1	15	Taiga Plains	Till blanket	-
Campbell Lake	Campbell	68 ^{o} 14.002'	-133 ^{o} 18.051'	57	2.0	315	33	Taiga Plains	Till blanket	-

4.2 Laboratory Analyses

4.2.1 Gravimetric Water Content

All active layer and permafrost samples were brought to the Aurora Research Institute in Inuvik, NT. The samples were analyzed for gravimetric water content (GWC). Samples were weighed and then dried in beakers at 105°C for a minimum of 24 h, after which the dry weight (g) was noted. The following equation was used to calculate the gravimetric water content in each sample (van Everdingen, 1998):

[1] $$\text{GWC}\ (\%) = \left(\frac{\text{Weight of moist soil (g)} - \text{Weight of dry soil (g)}}{\text{Weight of dry soil (g)}}\right) * 100\ \%$$

4.2.2 Conductivity and Concentration of Soluble Ions

The concentration of soluble salts and ions in the active layer and permafrost are largely dependent on the methodological approach used to extract the ions. A variety of methods have been employed to extract soil water and pore water in the active layer and permafrost, including *in situ* soil water sampling, extraction pore water, soil:water extractions and acid extractions (Lacelle et al., 2015). For this study, the conductivity and soluble ions concentration was determined by two different methods: 1) extraction of pore water and 2) soil:water extractions (Conklin, 2014; Lacelle et al., 2015). Extraction of pore water in the sample was done by decanting, squeezing, or centrifuging the sample. For the samples that were super-saturated, the soil water was readily collected by these methods, however pore water cannot always be extracted from samples that are under-saturated. When extractable, the pore water was filtered through 0.45 μm pore diameter cellulose nitrate filters and transferred to 20 mL polyethylene bottles. The pore water conductivity (PW) was then measured using a handheld SympHony 3P90MS multimeter (accuracy < 0.5%), which provides bulk soluble ion concentrations at field water concentration. The conductivity was standardized to 100% gravimetric water content in the samples using the following equation (Kokelj and Burn, 2005):

[2] $$Corrected\ conductivity\ \left(\frac{mS}{cm}\right) = conductivity\ \left(\frac{\mu S}{cm}\right) \times \frac{GWC}{1000}$$

Given that most of the active layer and some of the permafrost samples were under-saturated in water, the soil-water extraction technique was also used with deionized water. To determine the most efficient and complete extraction method (total soluble ions), various soil-water ratios were first tested (1:1, 1:5, 1:10, 1:25). The soil-water mixture was shaken for 1 h with a Burrell wrist-shaker model 75 at speed setting 5, and then left to stand for 24 h.

Following this step, samples were centrifuged for 10 minutes at 2,500 rpm, and the leachate water decanted, filtered and analyzed for its ionic content. Figure 12 shows the results of a salt-rich permafrost sample collected near Navy Road (Inuvik, NT, Canada) using different soil-water ratios. Based on the results, soluble ions at this site were completely leached with a soil-water ratio > 1:5. To ensure complete soluble ions extraction, a soil:water ratio of 1:10 was used for all active layer and every other permafrost samples. Conductivity of the leachate water (LC) was measured with a SympHony H30PCO multimeter.and standardized to soil:water ratio used for the extraction.

The leached water was then analyzed for major cations and anions at the Advanced Research Complex, University of Ottawa (Ottawa, ON). For cation analysis (Ca^{2+}, Mg^{2+}, Fe^{2+}, K^{+}, Na^{+}, Mn^{2+}), the samples were acidified with 100 µL of HNO_3 prior to inductively coupled plasma atomic emission spectroscopy analysis. The anion concentration (Cl^{-}, SO_4^{2-}) was determined unacidified by ion chromatography using a Dionex ICS-2100. A set of internal standards was run simultaneously. Analytical reproducibility for leachate conductivity is >95 % on average and >85 % at minimum. Analytical error for cations and anions by ICP-AES is <5 %. Individual sample detection limits were based on the final dilution of the sample (Ca^{2+}: 0.006 mgL^{-1}; Fe^{2+} and Mn^{2+}: 0.003 mgL^{-1}; K: 0.038 mgL^{-1}; Mg^{2+}: 0.0003 mgL^{-1}; Na: 0.010 mgL^{-1}; SO_4^{2-}: Cl^{-}:). A charge balance analysis:

[3] $$charge\ balance\ (\%) = \frac{\sum cations - \sum anions}{\sum cations + \sum anions} \times 100$$

showed that, for the majority of sites, the ionic charge balance in the active layer was positive (~60-70%), suggesting that HCO_3^{-} should be added as an anion to balance the charges. Except for a few samples, the ionic charge balance in the permafrost below the paleo-active layer was always negative, with an average value of -13 %. This suggests that this layer likely has a slight excess of SO_4^{2-}. All soluble ion concentrations are expressed as milliequivalence by mass of 100 g of dry soils (meq 100 g^{-1} soil).

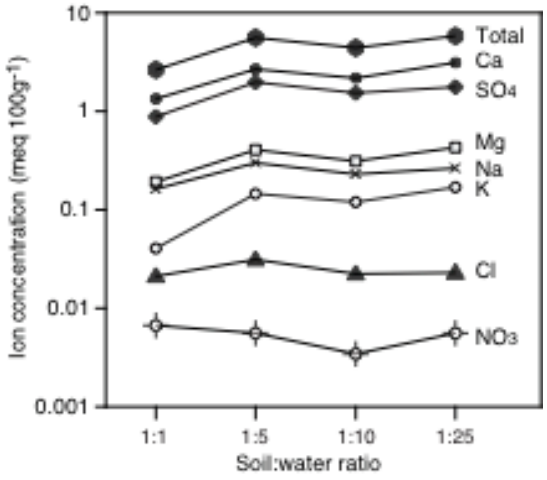

Figure 12 Graph of soluble ion concentrations measured at different soil-water ratios. The permafrost sample (150 cm depth) is from a hummock near Navy Road, Inuvik, NT, Canada.

4.2.3 Organic Matter, Organic Carbon and Inorganic Carbon Concentration

The concentration of organic matter, organic carbon and inorganic carbon in the active layer and permafrost were determined using two different methods. Organic matter and inorganic carbon contents were determined following the loss-on-ignition method outlined by Heiri et al. (2001). A small amount (2-3 g) of oven-dried samples (LOI_{105}) was placed in a crucible at 550°C in a muffle furnace for 6 h, weighed (LOI_{550}), and returned for 6 h at 950°C. The final weight is then noted (LOI_{950}) in order to complete the equations and calculate the respective carbon contents.

The organic matter content was determined using the following equation:

[4] $$\text{Organic matter}\ (\%) = \left(\frac{\text{LOI}_{105}\ (\text{g}) - \text{LOI}_{550}\ (\text{g})}{\text{LOI}_{105}\ (\text{g})}\right) * 100\ \%$$

The inorganic carbon content was determined using the following equation:

[5] $$\text{Inorganic carbon}\ (\%) = \left(\frac{\text{LOI}_{550}\ (\text{g}) - \text{LOI}_{950}\ (\text{g})}{\text{LOI}_{550}\ (\text{g})}\right) * 100\ \%$$

The total organic carbon content in a sub-set of active layer and permafrost samples (i.e. NRD, CB slump, Wilson, Lynx 2, R2T2 and R2T3) was determined to establish a relation between organic matter and total organic carbon. Total organic carbon was measured on an Elemental Analyzer (EA) at the University of Ottawa's G.G. Hatch Stable Isotope Laboratory after acidification (10 % HCl) to remove the possible presence of inorganic carbon. The acidified

samples were left to react for 72 h, centrifuged at 2500 rpm for five minutes with an IEC Centra GP8 and rinsed twice with deionized water. The powdered samples were oven dried at 105^{o}C for 24 h and mixed with a few milligram of tungstic oxide (WO_3) in tin capsules. The organic carbon content was then determined using the EA with combustion at high temperature (1800^{o}C). The evolved gases were separated in a chromatographic column such that carbon, nitrogen and sulphur could be quantified. A set of certified standards were analyzed simultaneously to provide a calibration curve. The routine analytical precision of the Vario Micro Cube is +/-0.1%.

4.3 Data and Statistical Analysis

4.3.1 Setting Layer Boundary Depths

The depth of the frost table was determined during sample collection given the physical observation between the thawed surficial layer and permafrost below. The boundary between the relict active layer and the permafrost below the paleo-thaw unconformity differed between sites. At Peel Plateau sites, this boundary depth was determined in the field as a result of an observed change in soil colour and cryostructures. The layer 3 boundary at all other sites was set based on a large spike in conductivity at depth (typically >6 mS cm^{-1}). If values in that range were not measured, it was assumed that the paleo-thaw unconformity had not been reached during sample collection.

4.3.2 Data Interpolation for Missing Values, Outliers and Data Transformations

For all ions that had concentrations below detection limit, a value half that of the detection limit was assigned. These corrections were done prior to any data analysis. Issues typically arise when dealing with environmental data, particularly so in this case given that samples are spatially autocorrelated and fail to meet assumptions of normality and independence. The following transformations and analyses were conducted using the statistical programme R (R Core Team, 2013). After performing an exploratory data analysis, it was determined that any further statistical analysis required some form of data transformation. The log transformation was most appropriate for GWC, LC, all ions, organic and inorganic carbon, whereas the square root transformation was best for PWC. In some cases, there were a few outliers following the transformation. These were typically associated with the active layer where the topmost sample, composed of mosses and lichen with high porosity and low specific gravity, retained a large volume of water and thus had higher GWC, PWC and/or LC. Given the small number of samples in the active layer, the outliers were not removed. One sample at the Lynx 2

site (14-LC-30) had a considerably lower LC value (by an order of magnitude) than the surrounding values, and likely had not completely dissolved all ions during the leaching process.

4.3.3 Assumptions of Normality and Independence

To test whether the transformed variables met the assumptions of normality and independence, the Shapiro-Wilk normality test was performed in R statistical software using the following equation (Acevedo, 2013):

[6] $$W = \frac{(\sum_{i=1}^{n} a_i x_{(i)})^2}{\sum_{j=1}^{n} (x_i - \overline{X})^2}$$

Results with associated *p*-values are presented in Table 2. All transformed variables were significant, met the assumption of normality and, as a result, were used in subsequent data and statistical analyses.

Table 2 The result of the Shapiro-Wilk test (W), with associated *p*-value, of each transformed variable.

Transformed Variable	W	*p*-value
logGWC	0.9593	1.500×10^{-9}
logLC	0.9771	3.649×10^{-4}
sqrtPWC	0.9459	2.699×10^{-8}
logCa	0.9496	4.134×10^{-5}
logSO4	0.9352	3.296×10^{-6}
logMg	0.9684	1.963×10^{-3}
logFe	0.8521	9.224×10^{-11}
logNa	0.9271	9.038×10^{-7}
logK	0.9420	1.044×10^{-5}
logMn	0.9102	7.854×10^{-8}
logCl	0.9559	1.394×10^{-4}
log(Organic Carbon)	0.8987	3.735×10^{-12}
log(Inorganic Carbon)	0.9408	1.048×10^{-8}

4.3.4 ANOVA and Post-Hoc Tukey HSD Test

The ANOVA measures whether two or more means are similar. This test was performed at each individual site for comparison between the same variable in all different layers (the active layer – layer 1, the residual thaw layer – layer 2, and permafrost below the thaw unconformity – layer 3). Here, the alternate hypothesis stipulated that H_1: $\overline{x}_1 \neq \overline{x}_2 \neq \overline{x}_3$.

[7] $$F = \frac{\Sigma n_j(\bar{X}_i - \bar{X})^2/(k-1)}{\Sigma\Sigma(X-\bar{X}_j)^2/(N-k)}$$

where n_j is the sample size in the jth group, $\bar{x}_j$ is the jth group sample mean, $\bar{x}$ is the overall mean, k is the number of independent groups and N is the total number of observations in the analysis (Boston University, 2013).

Following this treatment, the post-hoc Tukey HSD test was applied to determine between which layers the mean difference is occurring. The Q-critical is set using the inverse Studentized Range distribution, the number of treatments, degrees of freedom for the error term and the alpha-level (Vasavada, 2014). The Q-statistic is calculated using the following equations:

[8] $$Qi,j = \frac{|\bar{X}_i - \bar{X}_j|}{s_{i,j}}$$

[9] $$s_{i,j} = \frac{\hat{\sigma}_\epsilon}{\sqrt{H_{i,j}}}$$

where $\bar{x}$ is the mean in each respective treatment, $\hat{\sigma}_\epsilon$is the square root of the Mean Square Error, and $H_{i,j}$ is the harmonic mean of the number of observations in each treatment.

4.3.6 Principal Components Analysis

A principal components analysis (PCA), scaled and centered around mean=0 with a correlation matrix, was conducted on explanatory (i.e. depth) and response variables. This was computed in R with the “vegan” package (Oksanen et al., 2015). In addition to those included initially, elevation (extracted from a Natural Resources Canada digital elevation model, DEM, in ArcMap), and latitudinal and longitudinal coordinates were added as explanatory variables. A PCA aims to constrain multiple variables to few dimensions, or components, which can explain the majority of variance within the original dataset (Sheskin, 2011).

5. RESULTS

5.1 Relation Between Conductivity and Total Dissolved Solids

Electrical conductivity of water is dependent on the concentration of ionic species in solution and therefore is expected to be correlated with the total dissolved solids (TDS) (Wood, 1976). To assess if this is the case for soil water extractions, the transformed leachate water electrical conductivity measurements were compared to the transformed sum of major ions (total soluble ions) determined in the laboratory (i.e. Ca^{2+}, Mg^{2+}, Fe^{2+}, K^{+}, Mn^{+}, Na^{+}, SO_4^{2-}, Cl^{-}). Figure 13 shows that the transformed leachate water conductivity and total dissolved solids of the water samples are highly correlated (adjusted R^2: 0.95; $\rho < 0.001$).

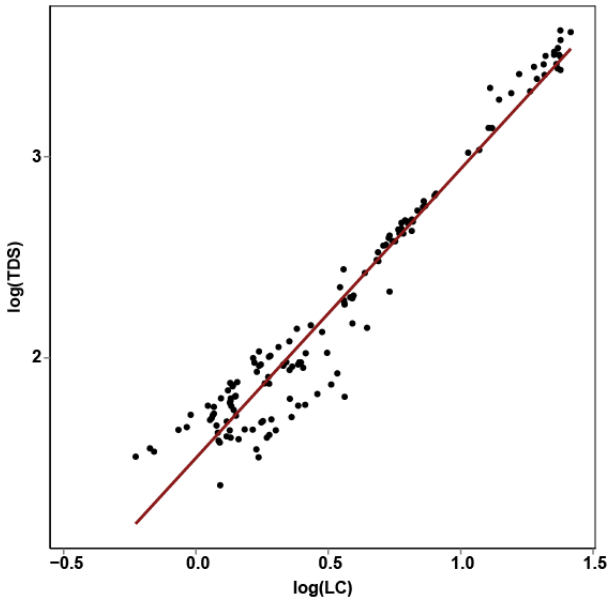

Figure 13 Linear regression for the log of total dissolved solids (TDS) as a function of the log of leached conductivity (LC) provided an equation of log(TDS) = 1.4373*log(LC) + 1.5020 (adjusted R^2: 0.95; $\rho < 0.001$).

5.2 Relation Between Organic Matter and Organic Carbon

Loss on ignition, albeit a simple and economical method, is a semi-quantitative method for determining organic carbon content as it provides an estimation of organic matter content (in %) which includes elements other than C in the mass (O, H and N) (Schumacher, 2002). Empirical research has shown that organic carbon constitutes approximately 40-60 % of organic matter, depending on the type of soil (Navarro, 1992 and references within). In this study, the organic matter content obtained by the loss on ignition method was compared to the quantitative elemental analysis method that provides organic carbon content (Fig. 14). Here, the linear

regression equation between the two transformed variables at a subset of sites (R2T2, R2T3, Lynx 2, NRD, CB and Wilson slumps) was determined to be:

[9] $$\log(\text{Organic Carbon}) = 0.823 * \log(\text{Organic matter}) - 0.276$$

with adjusted R^2: 0.74 and ρ <0.001. This equation was used to calculate the organic carbon content for all the samples at eight sites.

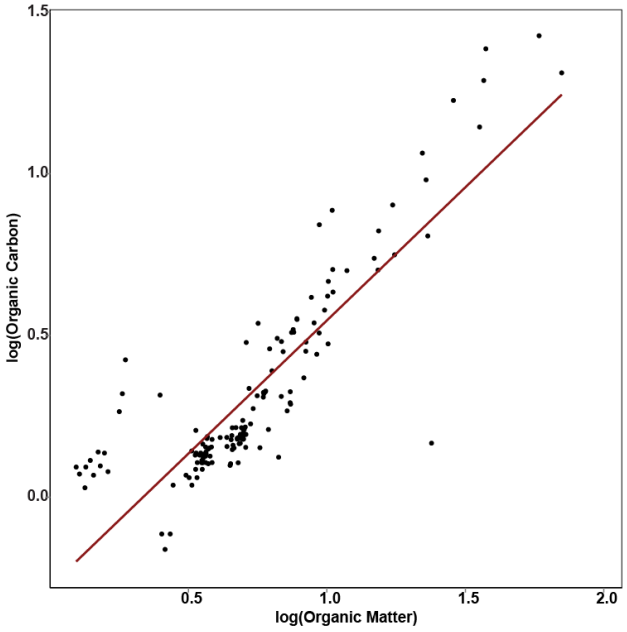

Figure 14 The relationship between the logarithm of elemental analysis organic carbon (%) as a function of the logarithm of loss on ignition organic matter content (%) for samples at the R2T2, R2T3, Lynx 2, NRD, CB and Wilson slump sites (n=145) , with the linear regression model indicated as the red line (Eq. 9). Adjusted R^2: 0.74; ρ -value < 0.001.

5.3 Gravimetric Water Content and Geochemical Profiles

The results from the 8 sites are presented by location, from west to east, which follows the timing of retreat of the Laurentide Ice Sheet in the study area.

5.3.1 CB Slump

CB slump is situated on the Peel Plateau at 595 m a.s.l. elevation. The frost table depth at this site was 48 cm in August 2013. The core was collected from the group surface to 305 cm depth. Based on changes in cryostructures observed in the headwall of the slump (from reticulate to suspended), the depth of the paleo-thaw unconformity was inferred at 115 cm (Fig. 15). The source of the thaw unconformity is likely to be both climatic and geomorphic in nature.

The GWC ranged from 20 to 178 %. With the exception of the O horizon and the base of active layer where GWC increases to 160 %, GWC is lowest in the active layer and relict active layer (20-60 %). The GWC is highest below the paleo-thaw unconformity where it ranges from 118 to 178 %. Pore water conductivity could only be measured in the permafrost below the paleo-thaw unconformity. The pore water conductivity values follow a similar trend to the GWC. Pore water conductivity is highest immediately below the paleo-thaw unconformity (2.1 mS cm^{-1}) and then varies from 1.1 to 1.9 mS cm^{-1}. The conductivity values determined from leachate (1:10 soil-water ratio) is 3 to 6 times higher than the pore water values. Leachate conductivity values are lowest in the active layer (1.2-3.4 mS cm^{-1}) and increase to 3.4 mS cm^{-1} at the top of permafrost. Leachate conductivity values progressively increase from the top of permafrost to the top of the paleo-thaw unconformity (115 cm depth). Below this depth, leachate conductivity values range from 5.2 to 11.8 mS cm^{-1}. The dominant soluble ions in the active layer and permafrost are SO_4^{2-}, Ca^{2+} and Mg^{2+}. Their concentration is lowest in the active layer (<1.15 meq 100 g^{-1} soils) and highest in the permafrost below the paleo-thaw unconformity (>1.20 meq 100 g^{-1} soils). Cl^-, which is very soluble, has the lowest concentration in the active layer and permafrost. The uppermost samples are high in organic carbon content (9-29 %) but rapidly decline with depth in the active layer. Concentrations within permafrost remain below 2.3 %. Inorganic carbon is highest in the first sample of the active layer (4.0 %), while its percentage in the rest of the core fluctuates little and remains below 2.9 %.

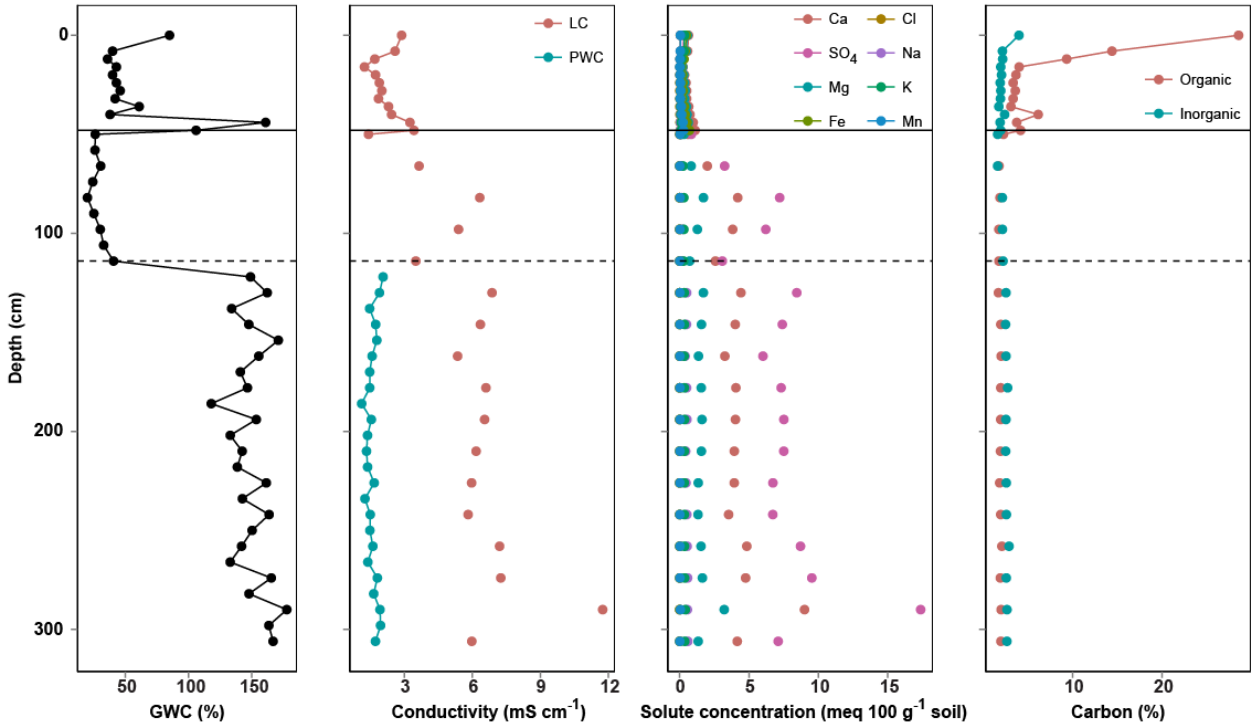

Figure 15 Gravimetric water content (GWC), pore water and leachate (1:10 soil water ratio) conductivity (PWC and LC, respectively), leachate ion concentration and carbon contents (organic and inorganic) in the active layer and shallow permafrost at the CB slump site from the ground surface to 305 cm depth. The solid black line represents the depth of the frost table (48 cm) and the dashed line represents the depth of the paleo active layer (115 cm). Note that pore water was only recovered from layer 3.

5.3.2 Wilson Slump

Wilson slump is situated on the Peel Plateau at 610 m elevation. The frost table depth at this site was 32 cm in August 2013. Based on changes in cryostructures observed in the headwall of the slump (from reticulate to suspended), the depth of the paleo-thaw unconformity was inferred at 175 cm (Fig. 16). The core was collected to a depth of 265 cm.

At this site, the GWC ranged from 30 to 295 % with peaks occurring at 80 and 192 cm depths (295 % and 200 %, respectively). The GWC is lowest within the active layer (<60 %). Unlike at the CB slump site, there is little difference in GWC above and below the paleo-thaw unconformity. Pore water conductivity could only be measured in the permafrost. Pore water conductivity fluctuates throughout the uppermost 3 m of permafrost, from 0.6 to 2.5 mS cm^{-1}, the latter occurring as peaks at 80 and 192 cm depth, which corresponds to GWC maximum values. Leachate conductivity values are 2 to 9 times higher than those from the pore water. Leachate conductivity is lowest in the active layer (<3.6 mS cm^{-1}) and highest in the permafrost below the paleo-thaw unconformity (>5.1 mS cm^{-1}). Between the top of permafrost and the top of the paleo-thaw unconformity, leachate conductivity values have intermediate values, fluctuating

between 3.6 and 6.5 mS cm^{-1}, which contrasts with the CB slump site. The dominant soluble ions in the active layer and permafrost are SO_4^{2-}, Ca^{2+} and Mg^{2+}. Their concentration is lowest in the active layer (<2.4 meq 100 g^{-1} soils) and highest below the paleo-thaw unconformity (> 3.2 meq 100 g^{-1} soils for SO_4^{2-} and Ca^{2+}, >1.1 meq 100 g^{-1} soils for Mg^{2+}). Cl^- has the lowest concentration overall and shows little variation with depth. Organic carbon peaks just below the top of the active layer (7.1 %), while the rest of the active layer remains around 2.5-3.0 %. Within permafrost, this remains <2.0 %. Inorganic carbon follows a similar trend in the active layer, where a peak is present just below the surface (2.6 %). The remainder of the active layer varies between 1.8-2.2 %, and increases below the permafrost table boundary to range between 2.2 and 2.8 %.

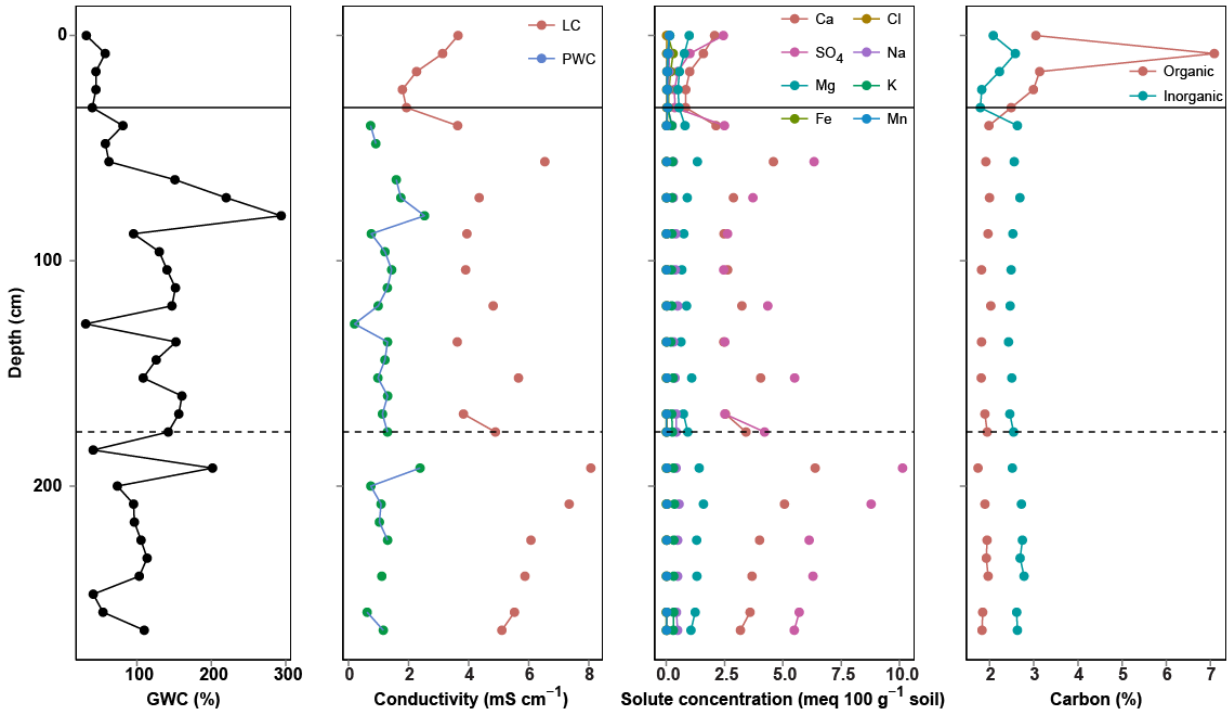

Figure 16 Gravimetric water content (GWC), pore water and leachate (1:10 soil-water ratio) conductivity (PWC and LC, respectively), leachate ion concentration and carbon contents (organic and inorganic) in the active layer and shallow permafrost at the Wilson slump site. The solid black line represents the depth of the frost table (32 cm) and the dashed line represents the depth of the paleo-active layer (175 cm). Pore water was recovered from layers 2 and 3 at this site.

5.3.3 Navy Road – Disturbed site (NRD)

The Navy Road site is situated ca. 5 km north of Inuvik where a fire-break was put in place in 1968 to prevent a wildfire from reaching the town of Inuvik (Mackay, 1995). The site is situated in the burned region. In August 2014, the frost table depth at this site was 107 cm at

time of sampling. The increase in leachate conductivity at depth resulted in the paleo-thaw unconformity being inferred at 136 cm (Fig. 17). The core was collected from the ground surface to 170 cm depth.

The GWC ranged from 34 to 262 % and was lowest in the active layer (< 92 %). GWC increased in the relict active layer to a value of 177 %. Below the paleo-thaw unconformity (here likely caused by the increase in active layer thickness following the 1968 fire; Mackay, 1995), GWC is highest reaching a maximum value of 260 %. Pore water conductivity could only be measured below 131 cm depth. Pore water conductivity ranged from 0.49 to 4.66 mS cm^{-1} and was highest below the paleo-active layer. Leachate conductivity was measured in the active layer and permafrost and values are ca. 5 times higher than the pore water conductivity values. The leachate conductivity was lowest in the active layer (< 3 mS cm^{-1}) and showed little variation with depth. Leachate conductivity progressively increased below the active layer to reach a maximum value of 24 mS cm^{-1} just below the paleo-active layer. The dominant soluble ions in the active layer and permafrost are SO_4^{2-} and Ca^{2+}. Peaks reach values of 75 and 24 meq 100 g^{-1} soil just below the paleo-thaw unconformity. Cl^- has the lowest concentrations and showed little variation with depth. Peaks in organic carbon content occur in the active layer at 25 cm, 41 cm, 82 cm depth (>6 %) and below the paleo-thaw unconformity at 151 cm (9 %). Carbon content within the relict active layer shows intermediate values (2.5-4.8 %). Inorganic carbon fluctuates little throughout the entire core and remains under 3 %.

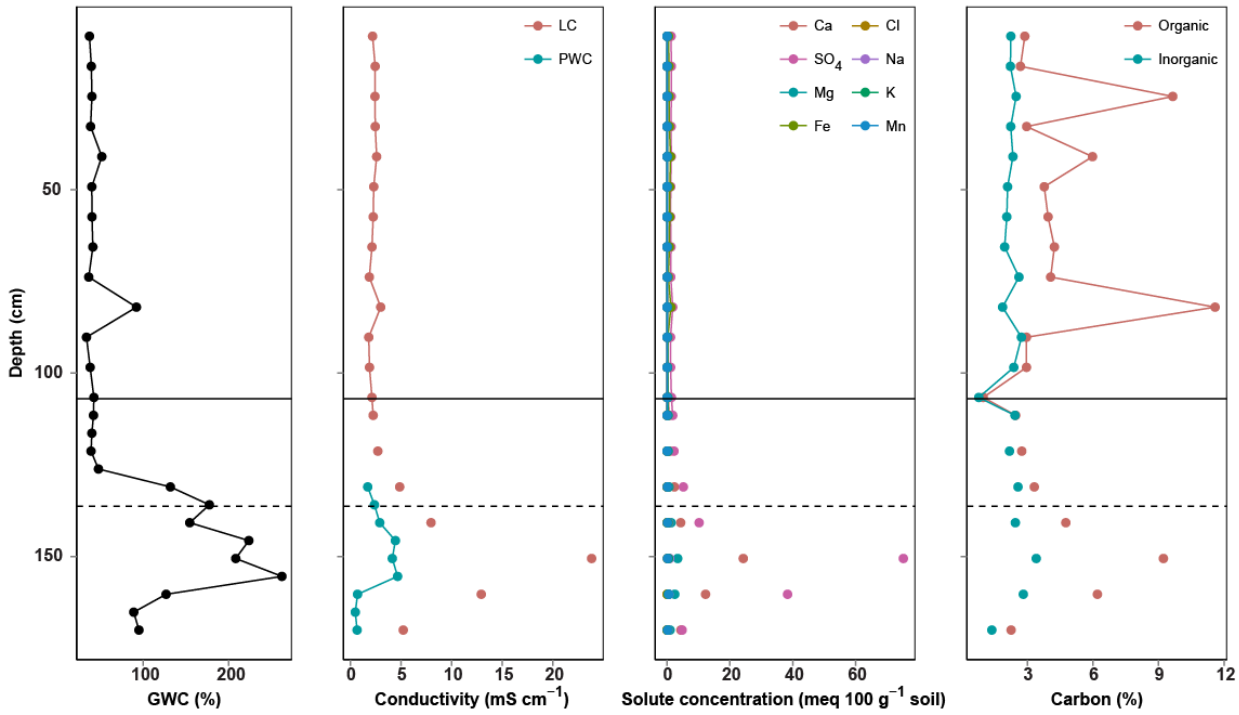

Figure 17 Gravimetric water content (GWC), pore water and leachate (1:10 soil-water ratio) conductivity (PWC and LC, respectively), leachate ion concentration and carbon contents (organic and inorganic) in the active layer and shallow permafrost at the NRD site. The solid black line represents the depth of the frost table (107 cm) and the dashed line represents the depth of the paleo-active layer (136 cm). Pore water was recovered from layers 2 and 3 at this site.

5.3.4 Navy Road – Undisturbed Site (NRT2)

The NRT2 site is situated on the unburned side of the fire-break ca. 50 m south of the NRD site. The frost table depth at this site was 28 cm in August 2014; the core was collected from the ground surface to 149 cm depth (Fig. 18). A thaw unconformity was not identified at this site.

The GWC ranged from 20 to 312 % and was lowest at the base of the active layer and top of permafrost (< 90 %). GWC peaked in the relict active layer to 312 % at 106 cm. Pore water conductivity in the permafrost ranged from 0.03 to 0.30 mS cm^{-1} and was highest in the first couple samples of the active layer (1.10 mS cm^{-1}). Leachate conductivity was measured in the active layer and permafrost and values are >5 times higher than the pore water conductivity values. The leachate conductivity ranged from 2.0 and 5.9 mS cm^{-1} throughout. Peaks occurred at the top of the active layer and at 127 cm depth. Organic carbon content ranges from 3-19 %, with the highest values at the surface. A small peak occurs at 127 cm depth (10 %), corresponding to a peak in leachate conductivity. Inorganic carbon is stable at all depths and remains under 2 %.

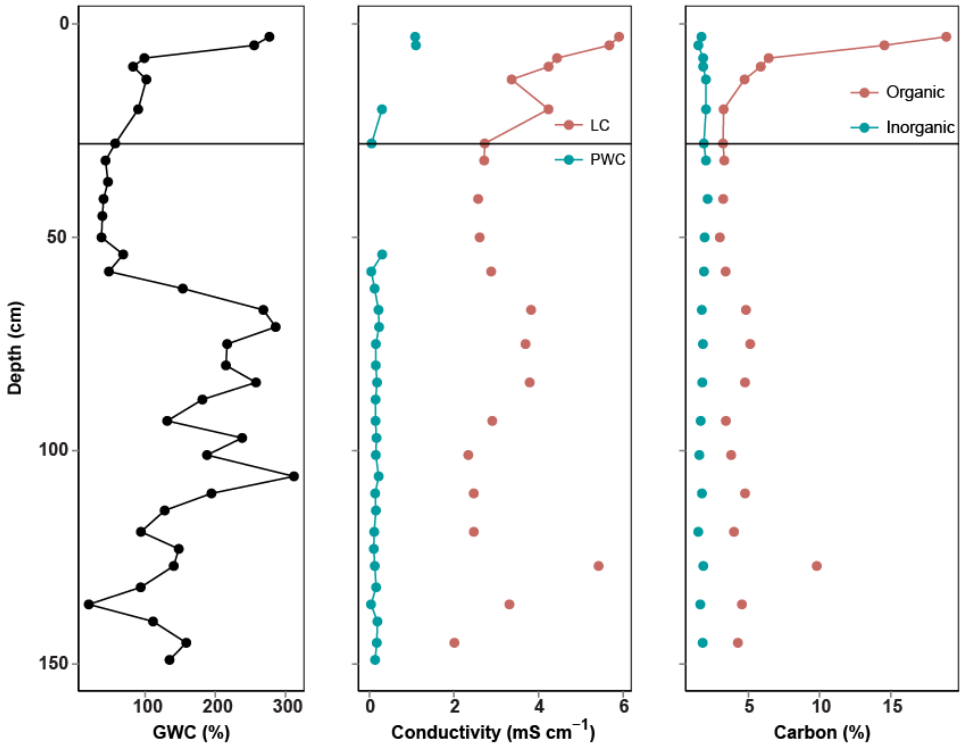

Figure 18 Gravimetric water content (GWC), pore water and leachate (1:10 soil water ratio) conductivity (PWC and LC, respectively), and carbon contents (organic and inorganic) in the active layer and shallow permafrost at the NRT2 site. The solid black line represents the depth of the frost table (28 cm). Pore water was recovered from both layers at this site.

5.3.5 Lynx 1

The Lynx 1 site is situated in flat upland terrain along the eastern Mackenzie Delta, at an elevation of 107 m. The frost table depth at this site was 31 cm at time of sampling in August 2014 (Fig. 19). The core was collected from the ground surface to 345 cm depth. A thaw unconformity was not identified at this site

The GWC ranged from 20 to 2740 %, with maximum values (1000-2740 %) occurring from the surface to 123 cm. The peak occurs at 119 cm, while below 254 cm, lower GWC values are found (<100 %). Pore water conductivity in the active layer was < 0.7 mS cm^{-1}. In permafrost, pore water conductivity ranged from 0.001 to 3.8 mS cm^{-1} and was highest between 55 and 175 cm (1.5-3.8 mS cm^{-1}). Leachate conductivity was measured in the active layer and permafrost and values are generally 5-20 times higher than the pore water conductivity values. The leachate conductivity ranged from 3.7 to 6.4 mS cm^{-1} in the active layer, and between 1.1 and 10.9 mS cm^{-1} in permafrost. The latter occurs at 160 cm and corresponds to the overall peak in leachate conductivity. Organic carbon content ranges from 15-38 % in the active layer and permafrost until 164 cm, with highest values nearer to the surface. Below this depth,

organic carbon content is minimal (<5 %). Inorganic carbon is <5 % in the active layer, and fluctuates between 1-10 % in permafrost. Below 169 cm, inorganic carbon remains below 3 %.

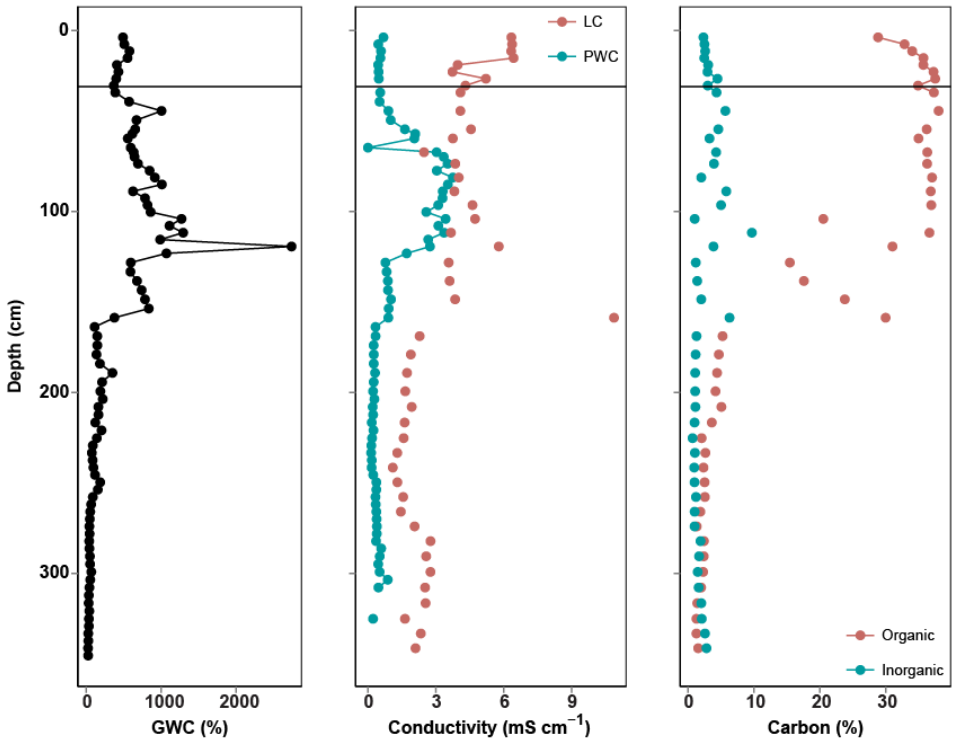

Figure 19 Gravimetric water content (GWC), pore water and leachate (1:10 soil-water ratio) conductivity (PWC and LC, respectively), and carbon contents (organic and inorganic) in the active layer and shallow permafrost at the Lynx 1 site. The solid black line represents the depth of the frost table (31 cm). Pore water was recovered from both layers.

5.3.6 Lynx 2

The Lynx Creek 2 site on the eastern perimeter of the Mackenzie Delta was subjected to a forest fire in 1999 (NRCan, 2014). The frost table depth is deeper compared to most other sites, with a value of 74 cm (Fig. 20). The paleo-thaw unconformity was inferred at 136 cm given the corresponding peak in LC below this depth. The core was collected from the ground surface to 202 cm depth at this site.

GWC is highest at the top of the active layer (96 %), then ranges from 18-30 % within that layer. The GWC in permafrost fluctuates slightly but remains <50 %, with no large peaks observed. PWC fluctuates little throughout permafrost and is below <0.9 mS cm^{-1}. Conversely, LC remains relatively constant throughout the active layer and most of the relict active layer (≤2.5 mS cm^{-1}). A small peak occurs at the top of layer 1 (2.5 mS cm^{-1}) and a larger one at the base of layer 2 (20.6 mS cm^{-1}). Below the paleo-thaw unconformity, these values range between 1.7 and 21.8 mS cm^{-1}. SO_4^{2-} and Ca^{2+} are the dominant ions. From the active layer to

136 cm depth, values remain <1.5 meq 100 g^{-1} soil. At greater depths, concentrations for these ions range between 1.3 and 57 meq 100 g^{-1} soil. Organic carbon ranges from 0.7-7 % in the active layer, with the highest values being at the surface and a small peak occurring at 53 cm. These peaks correspond to higher values in GWC. The organic carbon fluctuates between 0.5 and 1.3 % within the permafrost. In the active layer, inorganic carbon ranges from 0.4-2.7 %, with highest values occurring at the base. Permafrost inorganic carbon ranges from 0.8 and 3.0 %, and more fluctuations are found in the relict active layer.

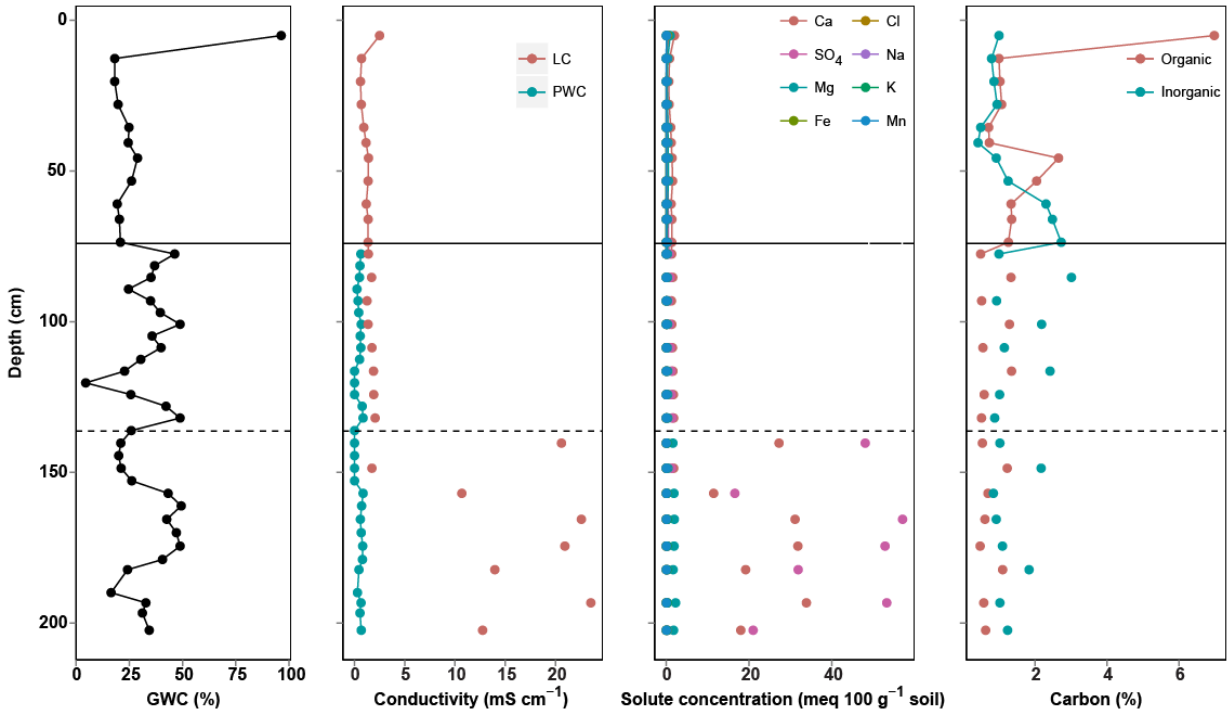

Figure 20 Gravimetric water content (GWC), pore water and leachate (1:10 soil-water ratio) conductivity (PWC and LC, respectively), leachate ion concentration and carbon contents (organic and inorganic) in the active layer and shallow permafrost at the Lynx 2 site. The solid black line represents the depth of the frost table (74 cm) and the dashed line represents the inferred depth of the paleo-active layer (136 cm). Pore water was extracted from layers 2 and 3.

5.3.7 R2T2

The R2T2 site is one of two cores collected near Rengleng River along the eastern perimeter of the Mackenzie Delta. The frost table depth at time of sampling in August 2014 was 56 cm (Fig. 21). Given patterns of downward migration and accumulation of water often 20-30 cm below the permafrost table as well as corresponding peaks in leachate conductivity, the paleo-thaw unconformity was inferred at 157 cm. The core was collected from the ground surface to 188 cm depth at this site.

GWC is highest at the top of the active layer (142 %), then remains close to 30 % within that layer. In permafrost, it ranges between 23 and 145 %. The largest peak occurs at 74 cm. PWC fluctuates little throughout permafrost and ranges from 0.2-1.0 mS cm^{-1}. LC remains relatively constant throughout the active layer and the relict active layer, ranging from 0.9 to 4.0 mS cm^{-1}. Small peaks occur at the top of the active layer and base of the relict active layer. Below the paleo-thaw unconformity, LC values are over 20 times the pore water conductivity values. The former ranges between to 10.1 to 26.1 mS cm^{-1}. SO_4^{2-} and Ca^{2+} are the dominant ions. Their concentrations fluctuate between 0.1-4.0 meq 100 g^{-1} soil throughout the active layer and relict active layer. In layer 3, these spike and range between 23.5 and 71.1 meq 100 g^{-1} soil. Apart from the top of the active layer where organic carbon is 23.7 %, the rest of this layer and all of permafrost fluctuates little and is below 2.8 %. Inorganic carbon ranges from 1.1 to 3.2 %, and generally increases with depth from the mid-relict active layer.

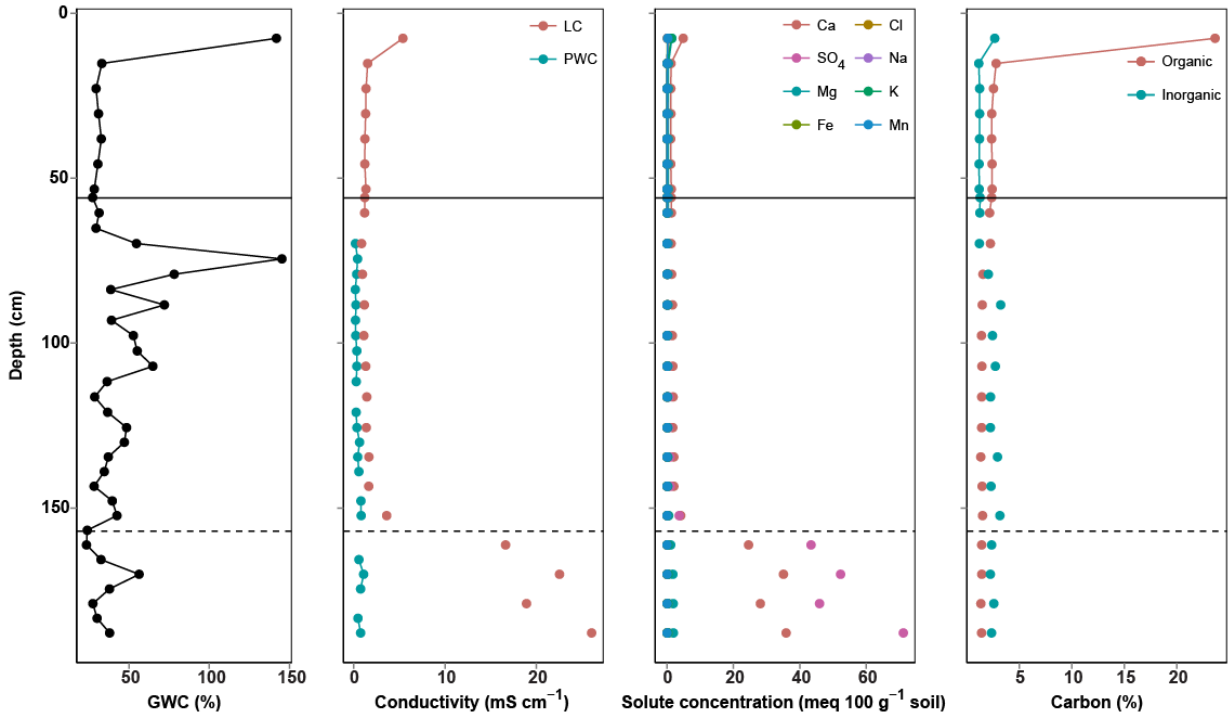

Figure 21 Gravimetric water content (GWC), pore water and leachate (1:10 soil-water ratio) conductivity (PWC and LC, respectively), leachate ion concentration and carbon contents (organic and inorganic) in the active layer and shallow permafrost at the R2T2 site. The solid black line represents the depth of the frost table (56 cm) and the dashed line represents the depth of the paleo-active layer (157 cm). Pore water was recovered from layers 2 and 3.

5.3.8 R2T3

The R2T3 core was collected ca. 2 m from the R2T2 core near Rengleng River. The frost table depth in August 2014 was 31 cm (Fig. 22). The peak in leachate conductivity led to the paleo-thaw unconformity to be inferred at 116 cm. The core was collected from the ground surface to 223 cm depth at this site.

GWC ranges from 135 % at the top of the active layer to 30 % at its base. GWC in permafrost ranges from 30-520 %. The largest peak occurs just below the permafrost table. Lowest values are found below the paleo-thaw unconformity. PWC ranges from 0.2 to 1.4 mS cm^{-1}, with few fluctuations. In the active layer and relict active layer, LC fluctuates between 1.1 and 4.4 mS cm^{-1}. Small peaks occur at the top of the active layer and top of the relict active layer. At the paleo-thaw unconformity depth, LC ranges between 7.8 to 23.8 mS cm^{-1}, over 5 times the value of pore water conductivity. SO_4^{2-} and Ca^{2+} are the dominant ions in the active layer and relict active layer, with their concentrations fluctuating between 0.1-4.2 meq 100 g^{-1} soil. Below the paleo-thaw unconformity, these range between 15.8 and 62.4 meq 100 g^{-1} soil. Peaks in organic carbon occur at the top of the active layer and the top of permafrost (15 %). The rest of the active layer ranges from 2.7 to 4.1 %, while the rest of the relict active layer ranges from 1.4 to 11.9 %. Below the paleo-thaw unconformity, organic carbon is minimal (<1.5 %). Inorganic carbon ranges between 1.0 and 2.8 %. Small peaks occur below the permafrost table and at 168 cm. Higher values are generally at depth.

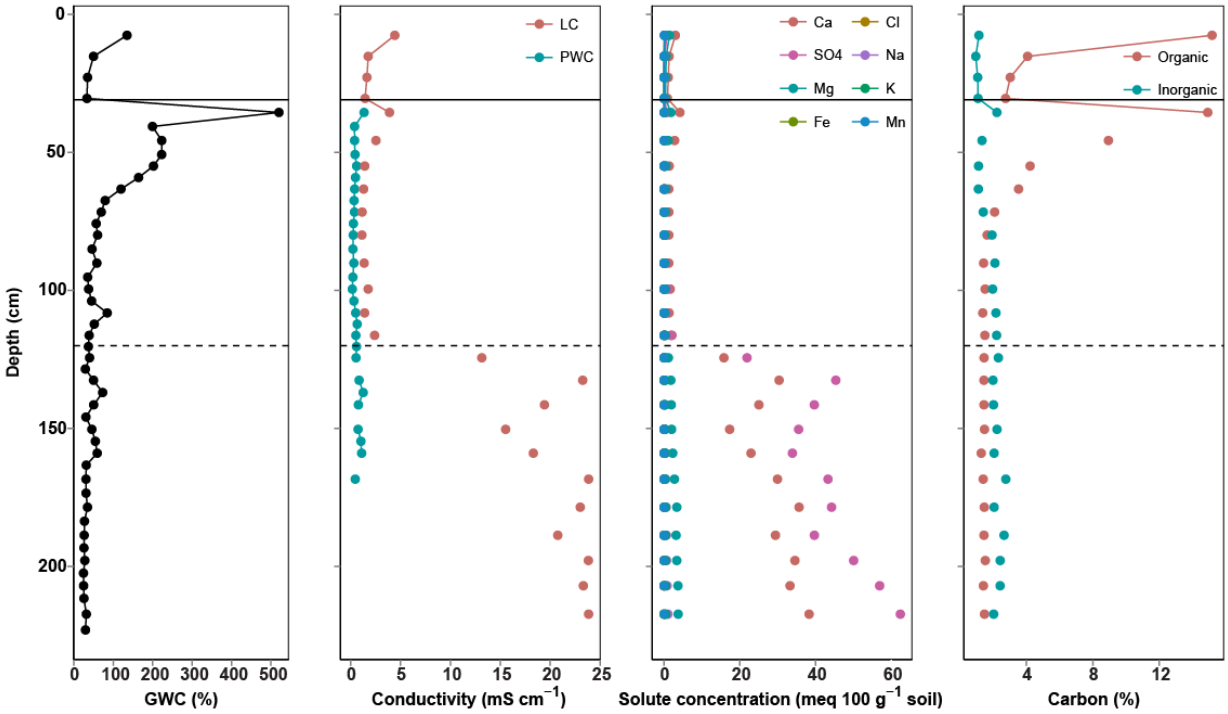

Figure 22 Gravimetric water content (GWC), pore water and leachate (1:10 soil-water ratio) conductivity (PWC and LC, respectively), leachate ion concentration and carbon contents (organic and inorganic) in the active layer and shallow permafrost at the R2T3 site. The solid black line represents the depth of the frost table (31 cm) and the dashed line represents the depth of the paleo-active layer (116 cm). Pore water was recovered from layer 2 and the top part of layer 3.

5.3.9 Caribou Creek

The Caribou Creek site is situated in the upland terrain near Inuvik, NT. The frost table depth at this site was 15 cm in August 2014. Samples from this core were collected from the ground surface to 193 cm depth. A thaw unconformity was not identified at this site.

The gravimetric water content was highest in the active layer (ranging from 350 to 460 %). In the permafrost, the GWC showed little variation with depth, being <100 %, except at 35 cm depth where GWC increased to 380 % corresponding most likely to an ice-rich layer. The leachate conductivity is high in the active layer, ranging from 6.4 to 9.3 mS cm^{-1}. The leachate conductivity values decreased in the uppermost 30 cm of permafrost, where they ranged from 7.9 to 0.7 mS cm^{-1} in the first few samples. Below 40 cm, the leachate conductivity is <1 mS cm^{-1}, with a maximum value of 0.97 mS cm^{-1} occurring at a depth of 184 cm. The organic carbon trend corresponded to that of the leachate conductivity. Values are highest in the active layer, ranging from 30.5 to 36.4 %. At the top of permafrost, organic carbon decreased

from 18.9 to 6.6 %. Below 43 cm, values remain under 1 %. Inorganic carbon decreases in the active layer from 22 to 13 %. In permafrost, it ranges from 0.4 to 3.6 %.

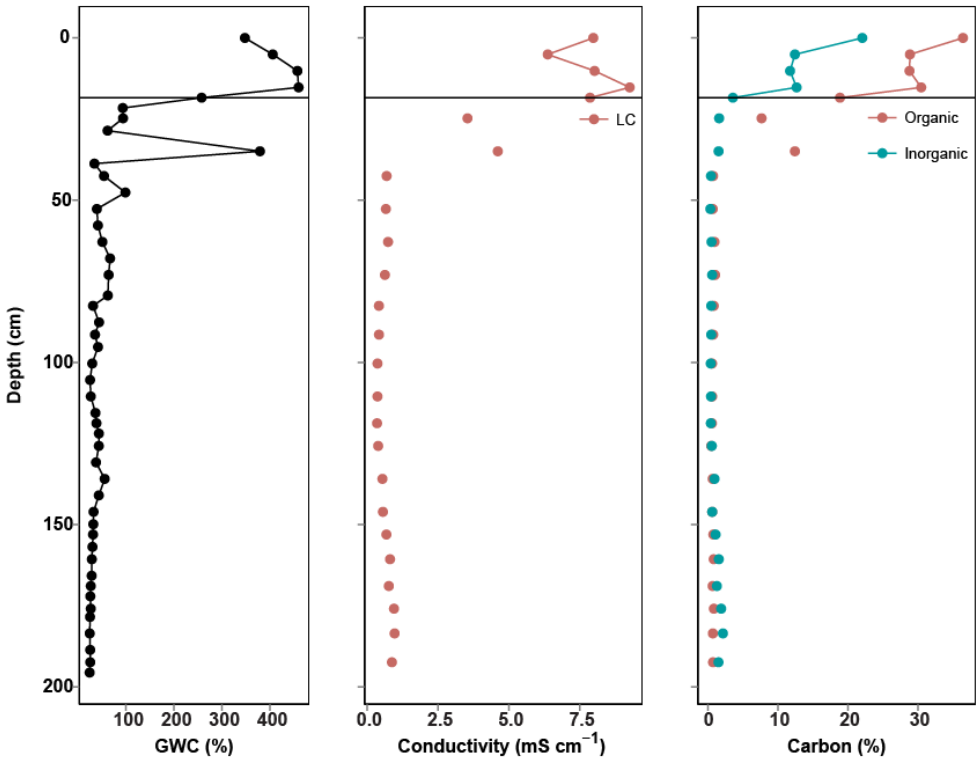

Figure 23 Gravimetric water content (GWC), pore water and leachate (1:10 soil-water ratio) conductivity (LC), and carbon contents (organic and inorganic) in the active layer and shallow permafrost at the Caribou site. The solid black line represents the depth of the frost table (15 cm). No pore water data is available.

5.3.10 Campbell Lake

Campbell Lake is situated in the upland terrain near Inuvik, NT. The frost table depth at this site was 33 cm in August 2014. The core was collected from the ground surface to 193 cm depth. A thaw unconformity was not identified at this site.

The uppermost sample contains the highest gravimetric water content (233 %) due to the high water retention capacity of organic material within the O horizon. Otherwise, gravimetric water content remains < 100 % throughout the core, with ice-rich layers just below the modern active layer (89 %) and around the 100 cm depth (75 %). Pore water was not extractable from the active layer and pore water conductivity was only measured in the permafrost. From 58 to 152 cm, pore water conductivity ranges from ca. 0.6 to 0.3 mS cm^{-1}. Below that depth, pore water conductivity increases to 0.7 mS cm^{-1} and then fluctuates between 0.3 and 0.5 mS cm^{-1}. The leachate conductivity values are highest at the surface of the active layer, with values of ca. 2.5-5 mS cm^{-1}, and decrease to values <0.6 mS cm^{-1}. In the permafrost, leachate conductivity

increases to 3.1 mS cm^{-1} just below the active layer and below 48 cm, leachate conductivity increases linearly from under 1 to 1.7 mS cm^{-1}. Organic carbon follows the same trend as leachate conductivity, with the highest values occurring in the topmost samples of the active layer (8-33 %) and decreasing to <1.5 %. A small peak occurs below the permafrost table (7 % at 48 cm), with values being under 1.5 % below this depth. Inorganic carbon fluctuates little with values being below 2.5 %.

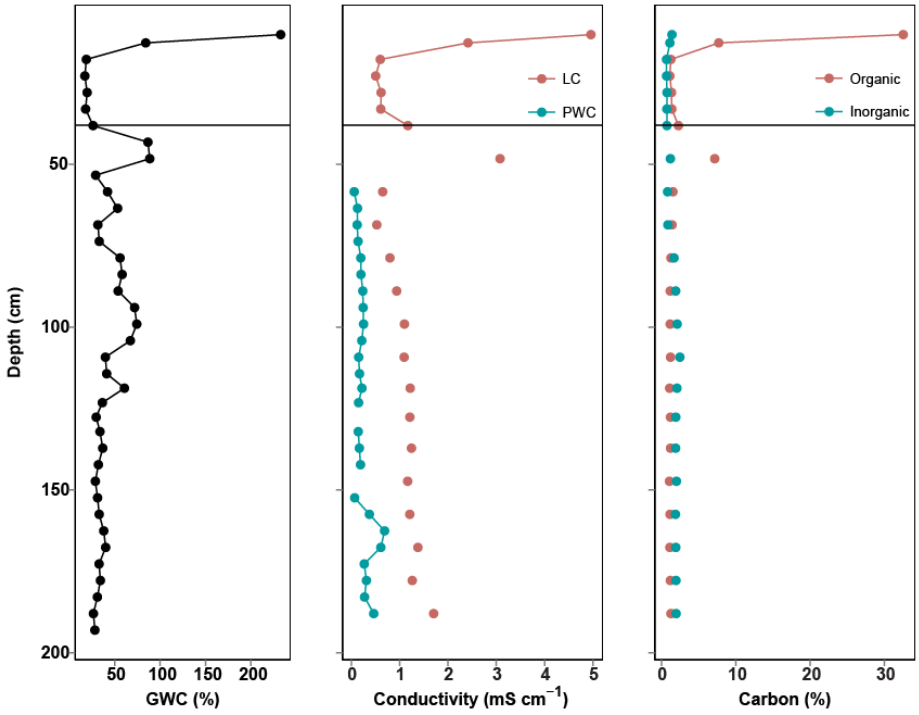

Figure 24 Gravimetric water content (GWC), pore water and leachate (1:10 soil-water ratio) conductivity (PWC and LC, respectively), and carbon contents (organic and inorganic) in the active layer and shallow permafrost at the Campbell site. The solid black line represents the depth of the frost table (33 cm). Pore water was only recovered from layer 2.

5.3.11 Summary

In summer 2013 and 2014, 10 active layer and permafrost cores were collected from 8 sites; all samples were collected from till veneer or blanket. The Peel Plateau cores (CB and Wilson slumps) were collected from sites with vegetated areas limited to tussocks, grasses and few short shrubs. All other sites were in areas where vegetation consisted of sparse black spruce, elderberry, Labrador Tea, and mosses, with the exception of Lynx 1 situated in a sedge meadow. The deepest cores were collected at CB slump (305 cm), Wilson (265 cm), Lynx 1 (345 cm), and the shallowest cores were collected at NRT2 (149 cm) and NRD (170 cm). Figure 25 shows the GWC, PWC, LC, total dissolved solids (TDS), organic and inorganic carbon contents from the 8 sites (10 cores), presented on a longitudinal gradient (i.e. west to east from

left to right) for ease of comparison. In this figure, the solid line represents the depth of the frost table and the dashed line represents the inferred depth of the paleo-thaw unconformity.

The GWC at the 8 sites was very variable, ranging from 18 to 2740 % across all sites. However, general trends with depth were observed (i.e., the active layer, relict active layer and below the paleo thaw unconformity). At the CB and Wilson slumps situated on the Peel Plateau, GWC was lowest in the active layer (< 60 %), with the exception of the base of the active layer at CB slump where GWC increased. GWC was highest in the paleo active layer at CB slump and within the relict active layer and paleo active layer at Wilson, where values > 120 % were measured. Similarly, GWC at the Navy Road site (NRD and NRT2) was lowest in the active layer (< 90 %) and highest in the relict active layer permafrost and below (> 90 %). At the Lynx Creek sites (Lynx 1 and Lynx 2), distinct patterns in GWC were observed. Lynx 1 is situated in a sedge meadow and GWC is highest in the uppermost 2 m (>500 %), corresponding to an organic-rich zone. Below that depth, GWC is < 100 %. At Lynx 2, the area was burned in 1999 and GWC shows little variations with depth (across the 3 layers). At the other 4 sites situated in the upland terrain east of the Mackenzie Delta (Rengleng River, Campbell Lake and Caribou Creek), similar GWC trends are observed. The active layer contained the lowest GWC (<100 %), with peaks corresponding to organic-rich layers. Figure 26 shows the positive correlation between organic carbon and gravimetric water content at all sites. All four sites showed an ice-rich zone in the upper relict active layer (i.e. below the permafrost table) and GWC showed little variations between the relict active layer and below it.

Pore water was recoverable from the active layer and permafrost at NRT2 and Lynx 1, and from the permafrost only at all other sites except for Caribou Creek where pore water data was unavailable. At all sites where pore water was recoverable, conductivity ranged from 0.001 to 4.7 mS cm^{-1}. Variations in pore water conductivity seemed to correspond to those in GWC, and Figure 27 shows the positive correlation between these variables. Otherwise, no specific trend is observed across the active layer and permafrost. This could be an effect of the pore water recovery method.

All active layer and permafrost samples were leached in milli-Q water and leached water conductivity ranged from 0.001 to 26.1 mS cm^{-1}. In contrast to pore water conductivity, leachate conductivity showed variations between the active layer, relict active layer and beneath the paleo active layer. At all sites, except for Lynx 1, Campbell Lake and Caribou Creek, leachate conductivity was lowest in the active layer (< 4.4 mS cm^{-1}) and 2 to 5 times higher below the paleo thaw unconformity (> 8.1 mS cm^{-1}). In the relict active layer, leachate conductivity values were similar to those in the active layer or slightly higher, and only Wilson slump and R2T3 sites showed an increase in leachate conductivity immediately below the permafrost table. Unlike

other sites, leachate conductivity values at Lynx 1 were highest in the active layer and top of the relict active layer, whereas Caribou Creek and Campbell Lake were only highest in the active layer. The two latter sites showed an increase in leachate conductivity immediately below the permafrost table. Since a positive linear relation exists between leachate conductivity and total dissolved solutes, the TDS trends are very similar to those of leachate conductivity at the sites where it was measured (i.e. CB slump, Wilson, NRD, Lynx 2, R2T2 and R2T3). TDS values are < 72.0 mg L^{-1} in the active layer and reach values up to 4,173.4 mg L^{-1} below the paleo thaw unconformity.

Organic carbon content in the active layer and permafrost varies from 1 to 38 %. At all sites, organic carbon is highest at the ground surface (>7 %), corresponding to the O-horizon. Below this soil horizon, organic carbon remained <5 % in the active layer, except for discrete organic-rich layers. In the relict active layer and below the paleo thaw unconformity, organic carbon content shows little variation with depth (1-5 %). Lynx 1, a sedge meadow, is the only exception where organic carbon is >20 % to 2 m depth. Below that depth, organic carbon reaches values similar to all other sites (<5 %).

Inorganic carbon content in the active layer and permafrost varies from 0.4 to 22.0 %. At most sites, inorganic carbon is highest in the active layer. In the permafrost, inorganic carbon content shows little variation with depth, being < 4 %. The higher inorganic carbon in the active layer supports the positive ionic charge balance in this layer due to the absence of dissolved carbonate ions in calculation.

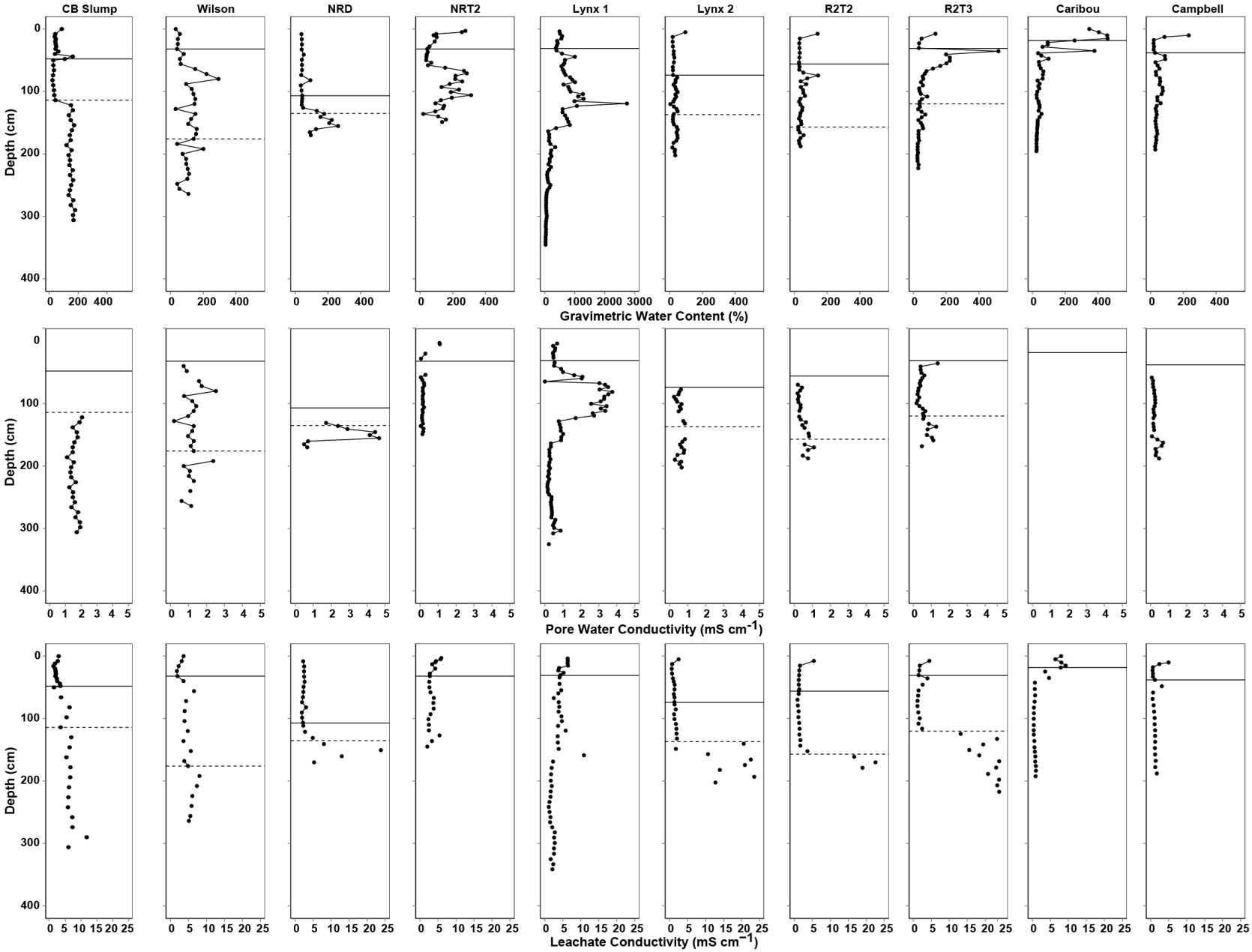
CB Slump
Wilson
NRD
NRT2
Lynx 1
Lynx 2
R2T2
R2T3
Caribou
Campbell
Depth (cm)
0
100
200
300
400
0 200 400
0 1000 2000 3000
Gravimetric Water Content (%)
0 1 2 3 4 5
Pore Water Conductivity (mS cm^{-1})
0 5 10 15 20 25
Leachate Conductivity (mS cm^{-1})

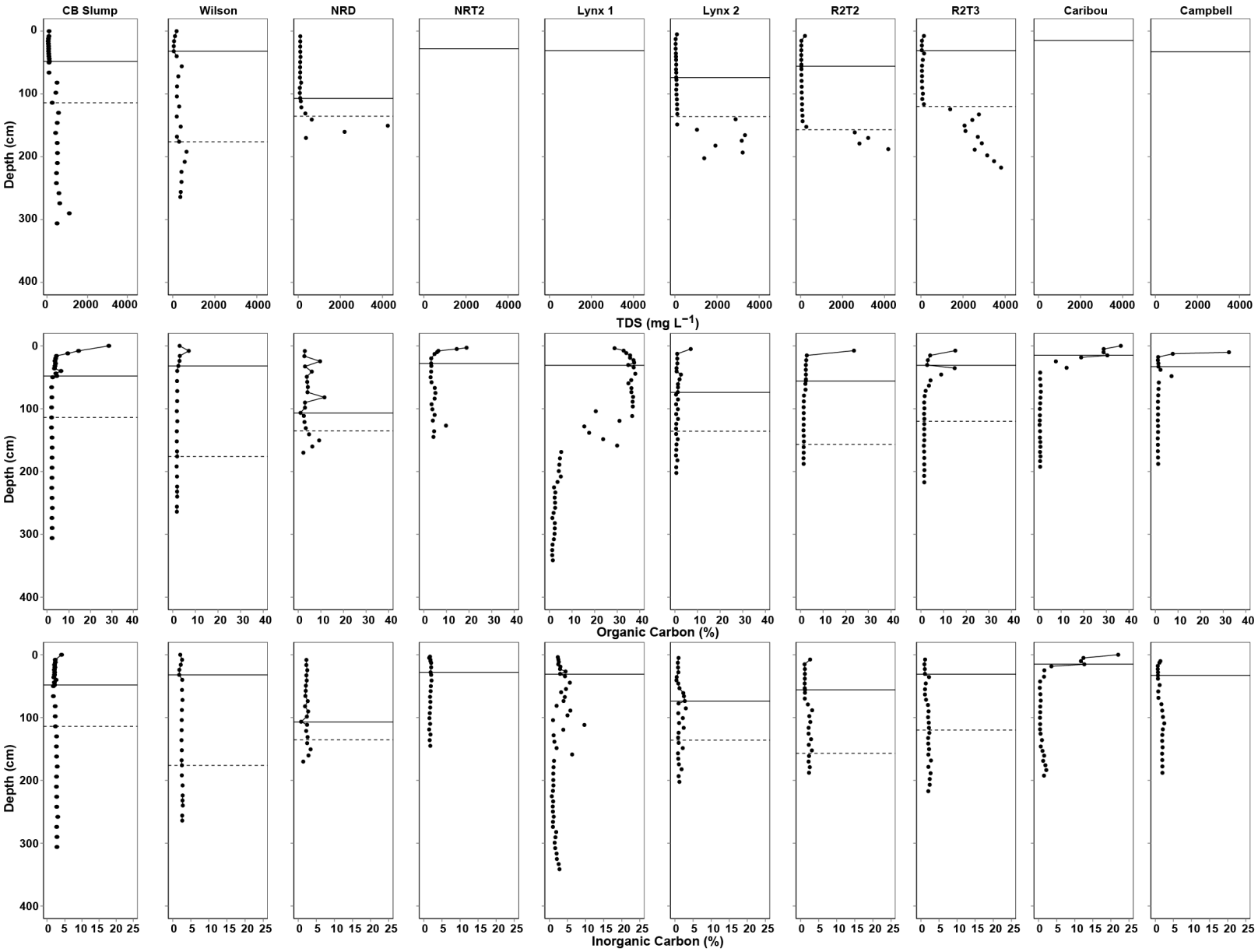

Figure 25 A summary of gravimetric water content (GWC, in %), pore water and leachate conductivity (PWC and LC respectively, in mS cm^{-1}), total dissolved solids (TDS, in mg L^{-1}), organic carbon and inorganic carbon at all sites (in %), arranged along a longitudinal gradient from left to right. The solid black line indicates the depth of the frost table, while the dashed line represents the paleo-thaw unconformity depth. Note that the Lynx 1 GWC x-axis scale is greater than other sites.

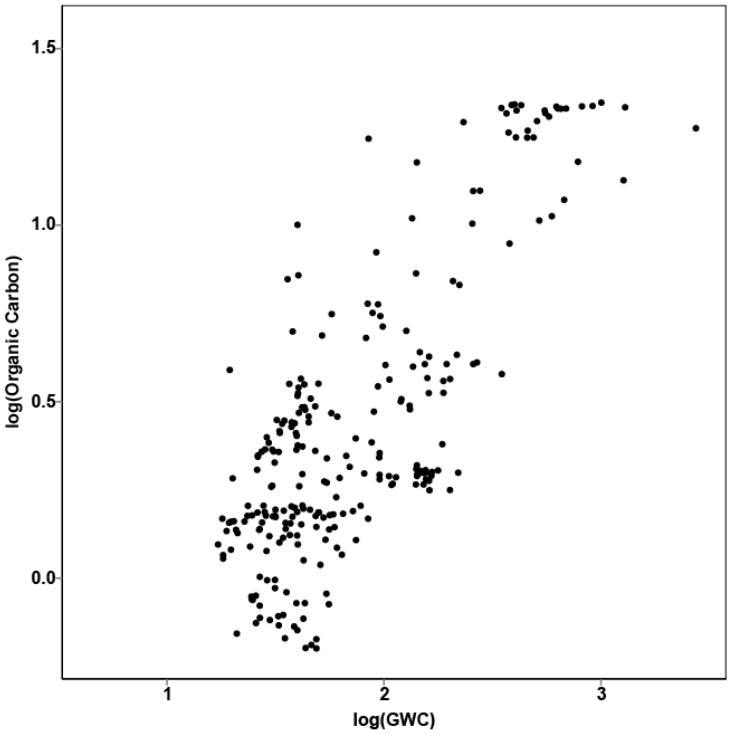

Figure 27 Relationship between log-transformed organic carbon and log-transformed gravimetric water content at all sites.

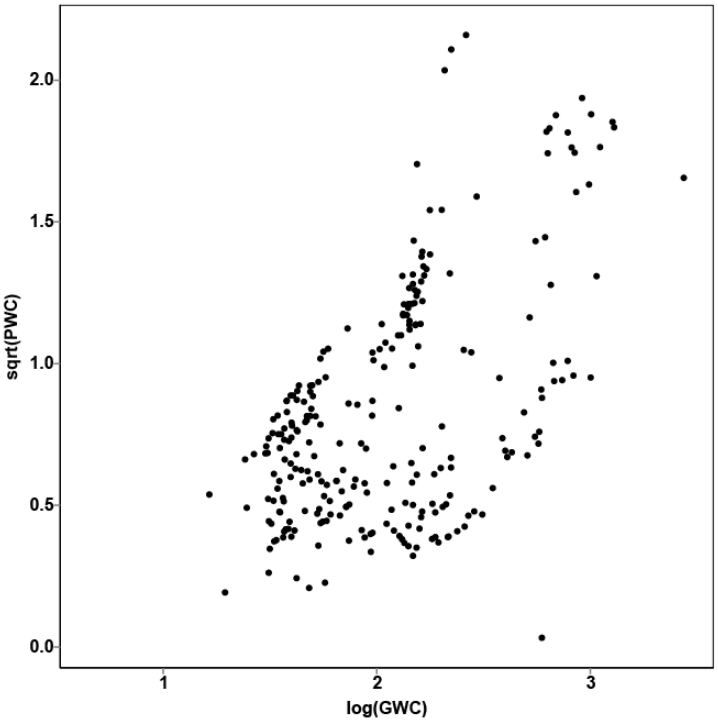

Figure 28 Relationship between square-root transformed pore water conductivity and log-transformed gravimetric water content at all sites.

5.4 Data Analysis

Figure 28A-C shows the transformed mean and standard deviation of GWC, pore water conductivity and leachate conductivity in the active layer (layer 1), relict active layer (layer 2) and below the paleo-thaw unconformity (layer 3) at each site; values are presented in Appendix A. An ANOVA followed by the post-hoc Tukey HSD Test was performed to verify if the mean transformed GWC, pore water conductivity, leachate conductivity as well as each individual ion are significantly different among the three layers (Appendix B and C, respectively).

The mean log(GWC) in layer 1 is significantly higher relative to the layer 2 at CB slump (1.74 ± 0.21 vs 1.45 ± 0.09) and Caribou Creek (2.62 ± 0.06 vs 1.63 ± 0.26) sites, whereas mean log(GWC) is significantly higher in the layer 2 than in the layer 1 at the Wilson slump site (2.08 ± 0.23 vs 1.64 ± 0.09). At all other sites (Campbell, Lynx 1, Lynx 2, NRD, NRT2, R2T2 and R2T3), there are no significant differences in mean log(GWC) between the layers 1 and 2. The higher mean log(GWC) in layer 1 or lower mean log(GWC) in layer 2 is associated with a period of thaw and freeze-back that removed water from the relict active layer (i.e. CB slump), flat sites with impeded drainage (i.e. Caribou Creek), or sites with organic-rich active layers where the water is absorbed in the O horizon (i.e. Lynx 1). The mean log(GWC) in layer 3 is significantly higher than in the layer 2 at CB slump (2.18 ± 0.04 vs 1.45 ± 0.09) and NRD (2.19 ± 0.19 vs 1.81 ± 0.29), whereas this value is significantly greater in layer 2 than layer 3 at R2T3 (1.93 ± 0.34 vs 1.54 ± 0.14). The four other sites show no significant differences between the GWC in layers 2 and 3. GWC is significantly higher in layer 3 compared to layer 1 at CB slump (2.18 ± 0.04 vs 1.74 ± 0.21), NRD (2.19 ± 0.18 vs 1.63 ± 0.11) and Wilson (1.93 ± 0.21 vs 1.64 ± 0.09), whereas the remaining sites' differences are not significant.

Given the limited samples with recoverable pore water, PWC was only measured at 6 sites, and only 2 had water extractable from layer 1. The mean sqrt(PWC), a surrogate for available dissolved solids within the recoverable water fraction, was significantly higher in the layer 1 compared to layer 2 at NRT2 (0.72 ± 0.40 vs 0.39 ± 0.08). Below the paleo-thaw unconformity (i.e. layer 3), mean sqrt(PWC) was significantly lower than in layer 2 at Rengleng River (R2T2 and R2T3) (1.66 ± 0.17 vs 1.51 ± 0.13 and 1.93 ± 0.34 vs 1.54 ± 0.14, respectively); the differences at the other 3 sites were not significant.

Leachate conductivity (LC), a surrogate for total soluble ions, was measured at all sites for all available layers. The mean log(LC) in layer 1 was significantly higher than in the layer 2 at 3 sites (Caribou, Lynx 1 and NRT2) (0.89 ± 0.07 vs -0.10 ± 0.37; 0.72 ± 0.10 vs 0.43 ± 0.22; 0.60 ± 0.13 vs 0.48 ± 0.12, respectively); by contrast the mean log(LC) was significantly higher in the layer 2 than in layer 1 at 2 sites (CB and Wilson slumps) (0.56 ± 0.25 vs 0.34 ± 0.13; 0.65 ± 0.09 vs 0.39 ± 0.13, respectively). All 6 sites with leachate conductivity measurements in the

three layers showed that mean log(LC) was significantly higher in layer 3, when comparing both layers 1 and 2 against layer 3 (i.e. CB and Wilson slumps, Lynx 2, NRD, R2T2, R2T3).

Figure 29A-C shows the mean transformed values for Ca^{2+}, SO_4^{2-} and Mg^{2+} for the three layers. The mean transformed Ca^{2+} is greater in layer 2 than layer 1 at three sites (CB slump: 0.34 ± 0.34 vs -0.27 ± 0.20; Wilson: 0.47 ± 0.11 vs 0.07 ± 0.18; NRD: 0.04 ± 0.29 vs -0.97 ± 0.32). When comparing layers 1 and 3 as well as layers 2 and 3, all sites have significantly higher Ca^{2+} in layer 3. In terms of SO_4^{2-}, a significant difference is observed between layers 1 and 2, where layer 2 is higher at all sites but R2T3. All sites show a greater SO_4^{2-} mean in layer 3 when compared to layers 1 and 2 separately. Mg^{2+} is significantly higher in layer 2, compared to layer 1, at CB Slump and NRD (-0.08 ± 0.28 vs -0.39 ± 0.16 and -0.37 ± 0.14 vs -1.01 ± 0.17), whereas layer 1 is higher than layer 2 at R2T2 (-0.33 ± 0.20 vs -0.56 ± 0.12). When comparing layers 1 and 2 to layer 3, all sites show a significant difference, where layer 3 is higher.

Figure 30A-B shows the mean transformed organic and inorganic carbon contents. Organic carbon is significantly higher in layer 1 comparative to layer 2 at Caribou, CB slump, Lynx 1, Lynx 2, R2T2 and Wilson sites (1.27 ± 0.04 vs -0.09 ± 0.37; 0.66 ± 0.25 vs 0.28 ± 0.04; 1.31 ± 0.03 vs 0.76 ± 0.47; 0.18 ± 0.23 vs -0.04 ± 0.16; 0.47 ± 0.29 vs 0.21 ± 0.06; 0.49 ± 0.15 vs 0.28 ± 0.01, respectively). All other sites and layers are not significant with the exception of a higher mean in layer 1 relative to layer 3 at CB slump, Lynx 2, R2T2, R2T3 and Wilson sites (0.66 ± 0.25 vs 0.29 ± 0.02; 0.18 ± 0.23 vs -0.07 ± 0.12; 0.47 ± 0.29 vs 0.17 ± 0.01; 0.61 ± 0.28 vs 0.18 ± 0.01; 0.49 ± 0.15 vs 0.27 ± 0.01, respectively).

Inorganic carbon content is significantly higher in layer 1 relative to layer 2 at Caribou (1.15 ± 0.13 vs -0.07 ± 0.29), whereas it is higher in layer 2 compared to layer 1 at Campbell, R2T2, and R2T3 (0.21 ± 0.17 vs -0.07 ± 0.14; 0.35 ± 0.15 vs 0.12 ± 0.12; 0.23 ± 0.12 vs 0.03 ± 0.03, respectively), At the other 4 sites inorganic carbon content is not significantly different between layer 1 and 2. Layer 3 is only higher in inorganic carbon than layer 2 at CB slump and R2T3 (0.42 ± 0.02 vs 0.29 ± 0.07 and 0.35 ± 0.05 vs 0.23 ± 0.12, respectively). Inorganic carbon is significantly higher in layer 3 comparatively to layer 1 at CB slump, R2T2, R2T3 and Wilson (0.42 ± 0.02 vs 0.33 ± 0.09; 0.38 ± 0.02 vs 0.12 ± 0.12; 0.35 ± 0.05 vs 0.03 ± 0.03; 0.43 ± 0.01 vs 0.32 ± 0.07, respectively). At all other sites, no significant differences are observed between layers.

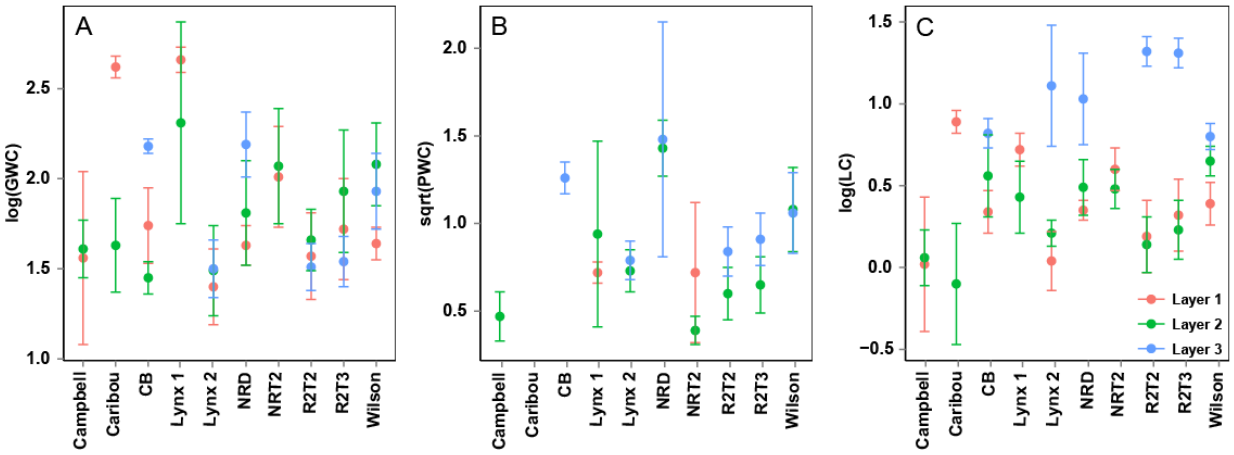

Figure 29 The mean log(GWC), sqrt(PWC), log(LC) ± SD, in A, B and C, per layer at each individual site.

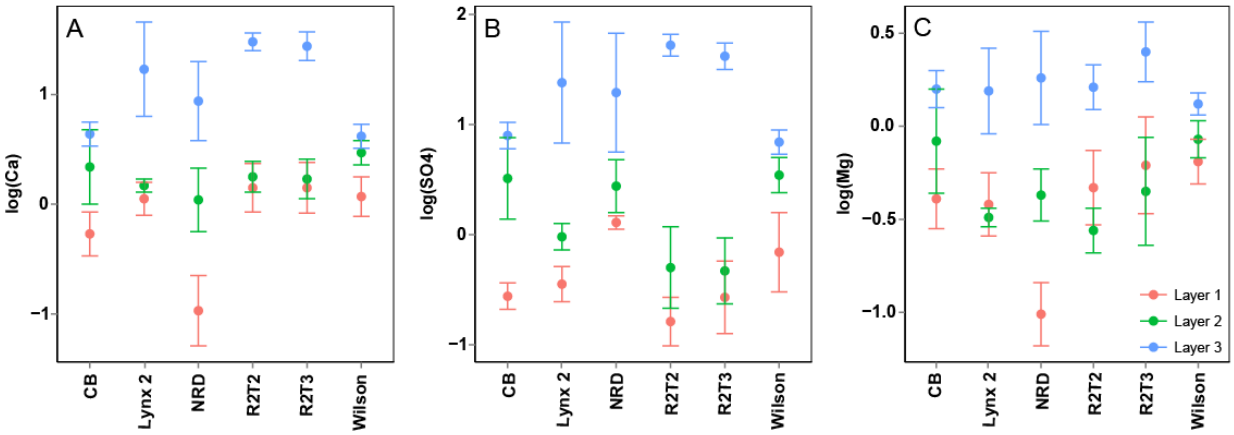

Figure 30 The mean log(Ca), log(SO_4), and log(Mg) ± SD, in A, B, and C, per layer at each individual site.

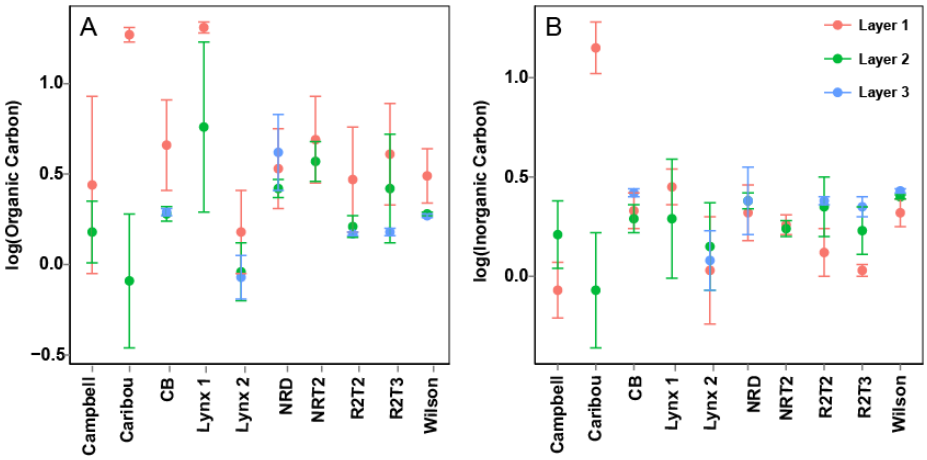

Figure 31 The mean log(Organic carbon), and log(Inorganic carbon) ± SD, in A, and B, per layer at each individual site.

6. DISCUSSION

6.1 Effect of Extraction Method on Concentration of Soluble Ions

Geochemical analyses in permafrost environments have been conducted using varying extraction techniques, including extraction of pore water (e.g. Kokelj et al. 2002; Kokelj and Burn 2005; Conklin, 2014), or following a leaching with milli-Q water and a pre-determined soil:water ratio (e.g. Blum et al. 2002; Keller et al. 2007; Conklin, 2014). The former method has been applied in soil salinity studies to determine solute availability for plants. The latter method allows determining total soluble ions in soils. Lacelle et al. (2015) determined that the majority of soluble ions at a particular Navy Road site in Inuvik, NT were dissolved with a soil:water ratio of at least 1:5. It was suggested that a different soil:water ratio might be required to leach all dissolved solutes at other sites, depending on the soil's mineral composition since the salt concentration is a factor in determining this ratio. Within this study, a 1:10 soil:water ratio was selected to ensure that the leaching process would be complete for all sites.

The measurements of pore water and leachate conductivity in relation to GWC are compared in Figure 31. Pore water conductivity is positively correlated with gravimetric water content, with some sites showing a stronger (e.g. NRT2) or weaker (e.g. NRD) relationship with GWC. The Lynx 1 site was an outlier given its greater organic carbon content that was consistently high in the upper 2 m of permafrost. In comparison, LC values (1:10 soil:water ratio, or GWC = 1000 %) show a wide range of values (0.001 to 26.1 mS cm^{-1}). As a result, the pore water extraction technique may not provide the total amount of dissolved solids, but rather the dissolved solids readily available within the volume of extracted pore water (i.e. relation between solubility of salt (K_{sp}) and volume of water). The use of the pore water extraction method may underestimate the total soluble ions, by as little as 2 to more than 20 times the leachate conductivity values. This distinction between methods should therefore be considered when evaluating a study's purpose and objectives as it could alter the results as well as their interpretation, especially in terms of soluble ion concentrations and distributions in a soil column. For example, Kokelj et al. (2002) and Kokelj and Burn (2005) assessed the distribution of ground ice and soluble ions in the active layer and shallow permafrost in northwestern Canada and found that the ice-rich transient layer contained higher soluble ions concentration. However, this particular conclusion was likely reached as a bias of using the specific pore water extraction method.

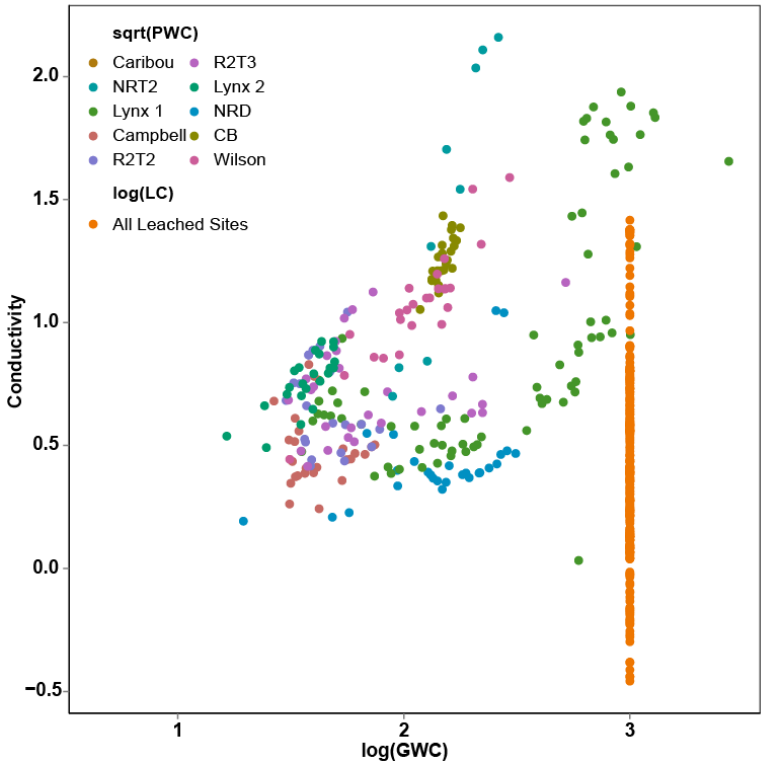

Figure 32 The correlation between pore water conductivity and leachate conductivity (square-root and log-transformed, respectively) as a function of log-transformed gravimetric water content for each individual site (PWC) and all leachate sites together (LC; Sites included are CB and Wilson slumps, Lynx 2, NRD, R2T2 and R2T3).

6.2 Distribution of Gravimetric Water Content, Soluble Ions and Organic Carbon Contents in the Active Layer and Permafrost

6.2.1 Gravimetric Water Content

GWC measurements in permafrost have frequently found ice accumulations within near-surface permafrost that have been linked to the development of an ice-rich zone termed the transient layer (Shur et al. 2005). The development of the transient layer has been attributed to the formation of segregated ice within upper permafrost horizons over decades to centuries (Cheng 1983; Mackay 1983; Shur et al. 2005). In this study, several sites show an ice-rich layer either near the top of contemporary permafrost (Campbell Lake, Caribou Creek, Lynx 1, R2T2, R2T3) or below the paleo active layer (CB and Wilson slump, NRD, R2T2). All other sites have low GWC throughout the active layer and permafrost with only a small increase in GWC. Based on the ANOVA and post-hoc Tukey HSD test results, GWC was significantly greater in the active layer relative to the relict active layer at 3 sites (Caribou, CB and Wilson slumps) and not statistically significant at all others. This measurement considers the average of the layer, and in the case of layer 1 includes the O-horizon which often contains much higher water content. If

the O-horizon samples are removed, the GWC would be lower or similar to layer 2. Following an investigation of GWC at a nearby site, Kokelj and Burn (2003) determined that ice-poor permafrost is due to rapid permafrost aggradation. This would suggest that permafrost at Campbell, Caribou, CB slump (layer 2), Lynx 2, NRD, R2T2, R2T3 formed rather quickly as they all contained relatively low GWC contents. Although this is likely a result of limited water availability, site and slope conditions could also be important contributing controlling factors.

Several distinctions in GWC between sites should be noted. The large GWC spikes at the top of layer 2 at Caribou and R2T3 are likely due to the presence of a single thin ice layer, as opposed to segregated lenticular ice spread over a certain vertical distance. Lynx 1 shows by far the most GWC across all sites within the upper 175 cm (i.e. > 500 %). This site was rich in organic matter between the surface and this depth. Visually, mosses and humic soil were abundant during laboratory analyses translating to organic carbon results being positively correlated to GWC across these depths. Despite being located at higher elevation (107 m) than other sites east of the Mackenzie Delta, site-specific characteristics must have favoured organic matter accumulation at this site. Lynx 2 and NRD sites likely had higher GWC within the permafrost table (top of layer 2) prior to the fire disturbances that occurred in 1999 and 1968, respectively. The fires would have removed the surficial vegetation, exposing the underlying soil to post-fire thaw and potentially melting any ice layers to the depth at which the fire reached. The greater GWC observed at Lynx 2 than NRD could be due to a reflection of varying site conditions that would have impeded drainage or due to a less severe disturbance at Lynx 2. This would have allowed water to accumulate at the base of the active layer and thus be incorporated to the permafrost table as it aggraded. Slope may also have been a factor in the development of the GWC profile, or lack thereof, in layer 2 at CB slump. At this highly elevated site (595 m), the 10^{o} slope in addition to rapid permafrost aggradation likely prevented the formation of segregated ice lenses and contributed to its overall low ice content. GWC is also a function of soil physical properties, such as grain size and porosity. It tends to be high in areas of fine-grained, unconsolidated Quaternary soils (French, 2007). Although the majority of till deposits of the Canadian Cordillera are formed within silt and clay matrices, till veneer in high relief areas of the Richardson Mountains-Peel Plateau can be more coarse-grained (Fulton, 1989). This may explain the low GWC of layer 2 at CB.

6.2.2 Soluble Ions Content

The total soluble ions and leachate conductivity were significantly lower in the active layer compared to the relict active layer at 4 out of the 8 sites (CB and Wilson slumps, Lynx 2 and NRD), whereas the total soluble ions and leachate conductivity were significantly higher in

the active layer compared to the relict active layer at 3 out of the 8 sites (Caribou Creek, Lynx 1 and NRT2). The latter sites contained higher organic carbon content in the active layer. Kokelj and Burn (2003; 2005) and Lacelle et al. (2014) suggested that soluble ions tend to accumulate just below the permafrost table following movement of water along thermal gradients leading to a progressive accumulation of ice and solutes. Leachate conductivity and total soluble ions' distributions from the 8 sites in this study do not necessarily follow this trend. For example, at NRD, Lynx 2, R2T2, R2T3, Caribou and Campbell, the leachate conductivity shows near-vertical profiles within the first two layers (no solute-rich layer within the top of permafrost), aside from a few samples with increased values associated with peaks in organic carbon. At CB and Wilson slumps, leachate conductivity does show an increase at the top of layer 2, however, the increase is not restricted to the permafrost table as leachate conductivity varies throughout the relict active layer. It should be noted that the aforementioned studies strictly analyzed the samples' extractable pore water, including a 1:1 soil:water ratio for under-saturated samples. This distinction in observed trends between those studies' results and this thesis reflects back to the differing methods used to measure conductivity – pore water vs. leachate conductivity at a 1:10 soil:water ratio. The pore water extraction method should be used when the outcome is to analyze the water fraction and elucidate patterns of water movement in the soil, knowing that this method likely underestimates the total dissolved solids. As a result, leachate conductivity should be the preferred method when analyzing the soil fraction to investigate its composition.

All sites showed a step-like increase in total soluble ions and leachate conductivity at the paleo thaw unconformity (in the order of 2 to 10 times higher) and concentrations remained high over the sampled depth. This finding is similar to those obtained by Kokelj et al. (2002) on Herschel Island, where soluble cation concentrations below the paleo thaw unconformity were several orders of magnitude greater than those in the active layer and relict active layer. Since the increase in total soluble ions and leachate conductivity occurs right at the paleo permafrost table, and not ca. 20-30 cm below it (as observed in the contemporary permafrost table), the solute enrichment cannot be attributed to movement of water and soluble ions along a thermally-induced gradient. Instead, the much higher total dissolved ion concentrations and leachate conductivity can be attributed to reduced chemical weathering (freshwater leaching) that these soils experienced relative to those above. For example, soils in the active layer annually experience seasonal leaching by rainfall or groundwater flow whereas the soils below the paleo thaw unconformity have likely remained frozen throughout the Holocene.

The active layer, relict active layer and permafrost below the paleo thaw unconformity are characterized by a (Ca+Mg)-SO_4 geochemical facies. The source of soluble ions can be assessed by examining ionic relationships. Figures 32-37 examine the potential of $CaSO_4$,

(Ca+Mg)-SO_4 and halite mineral dissolution as contributing processes in each layer for the six cores where geochemical analyses were undertaken. For example, the dissolution of gypsum can be expressed by the following equation:

[10] $$(CaSO_4)_2H_2O \rightarrow Ca^{2+} + SO_4{}^{2-} + 2H_2O$$

Assuming that Ca^{2+} and $SO_4{}^{2-}$ in the waters originate from the dissolution of gypsum, their concentration (expressed in equivalent units) should plot close to the 1:1 line. At all sites and for the three layers, a strong relation exists between (Ca+Mg)-SO_4 and ions are distributed close to the dissolution line suggesting CaMg-sulfate dissolution. According to Malone et al. (2013), the origin of sulphate in the tills of this region is likely from the sulfate-bearing geological units at Bear Rock and Saline River Formations further east in the central Mackenzie Valley and from the local shale sediments. Although Na-Cl shows no relation in layers 2 and 3 at all sites, the Na-Cl ratio in the active layer (layer 1) is close to the dissolution line. Keene et al. (1986) found that the sea-salt ratio is 0.86, suggesting an input of marine salts from precipitation in the active layer. This suggests that the increased [Na^+] in the active layer likely originates from precipitation originating from the Beaufort Sea.

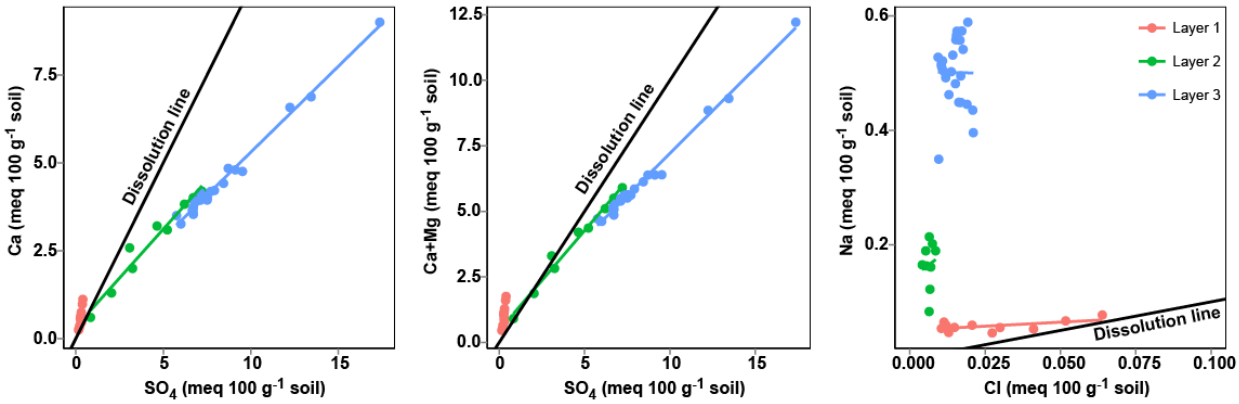

Figure 33 Relation between major ion species measured at CB slump from soil water extractions to assess the potential for gypsum/anhydrite, (Ca+Mg)SO_4 and halite dissolution.

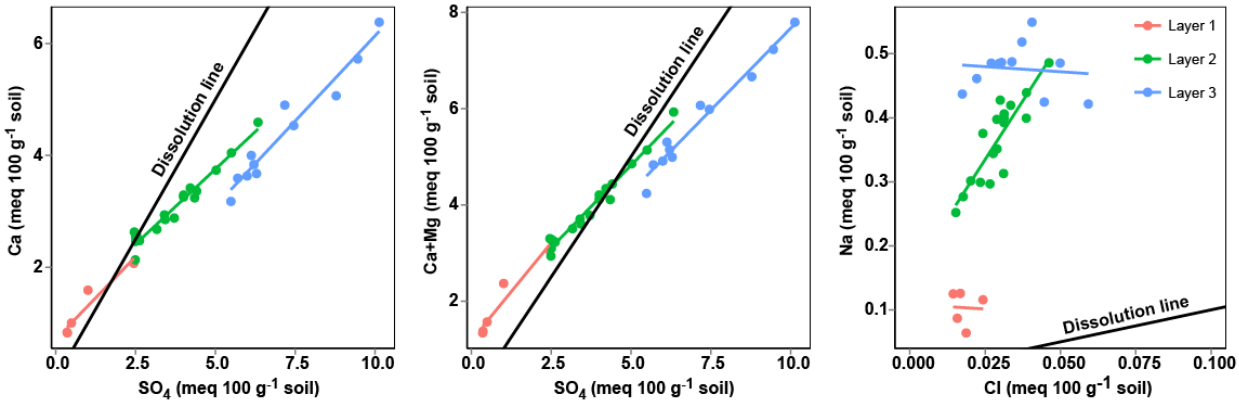

Figure 34 Relation between major ion species measured at Wilson from soil water extractions to assess the potential for gypsum/anhydrite, (Ca+Mg)SO_4 and halite dissolution.

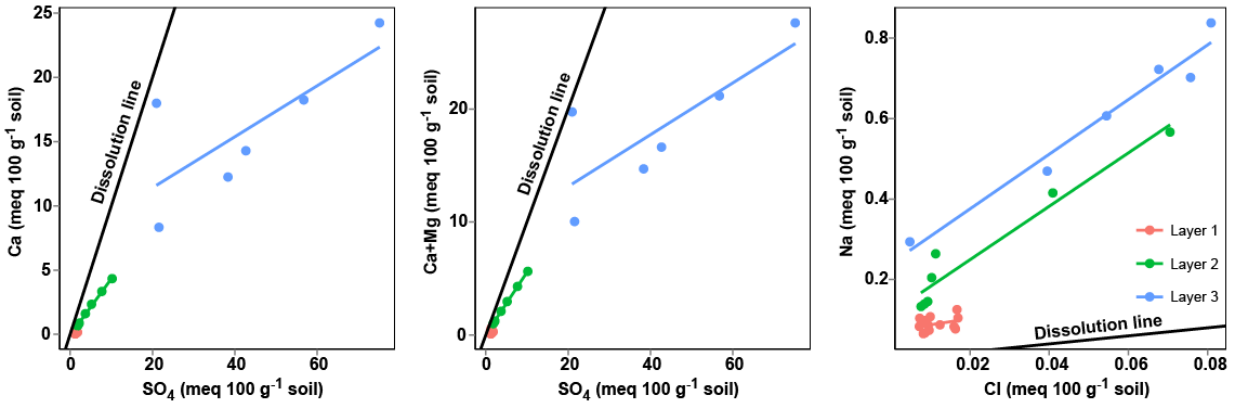

Figure 35 Relation between major ion species measured at NRD from soil water extractions to assess the potential for gypsum/anhydrite, (Ca+Mg)SO_4 and halite dissolution.

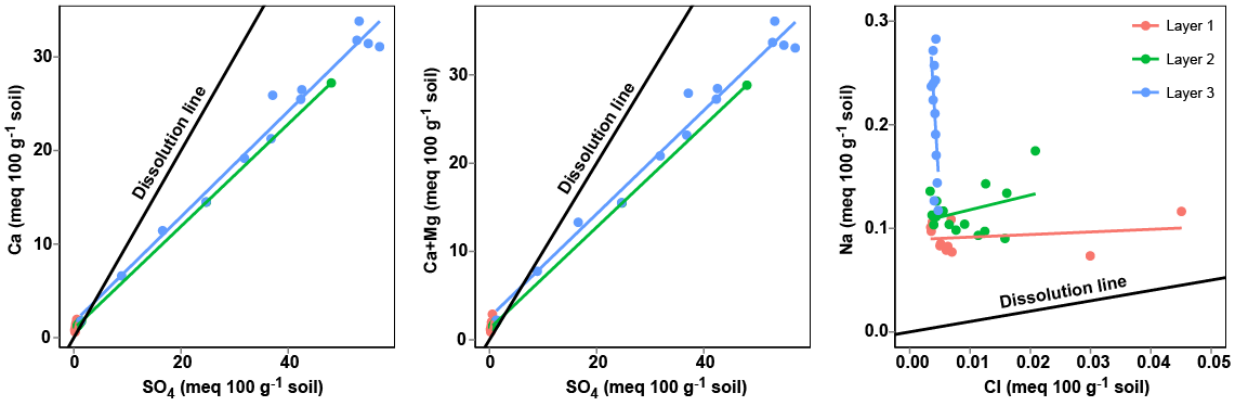

Figure 36 Relation between major ion species measured at Lynx 2 from soil water extractions to assess the potential for gypsum/anhydrite, (Ca+Mg)SO_4 and halite dissolution.

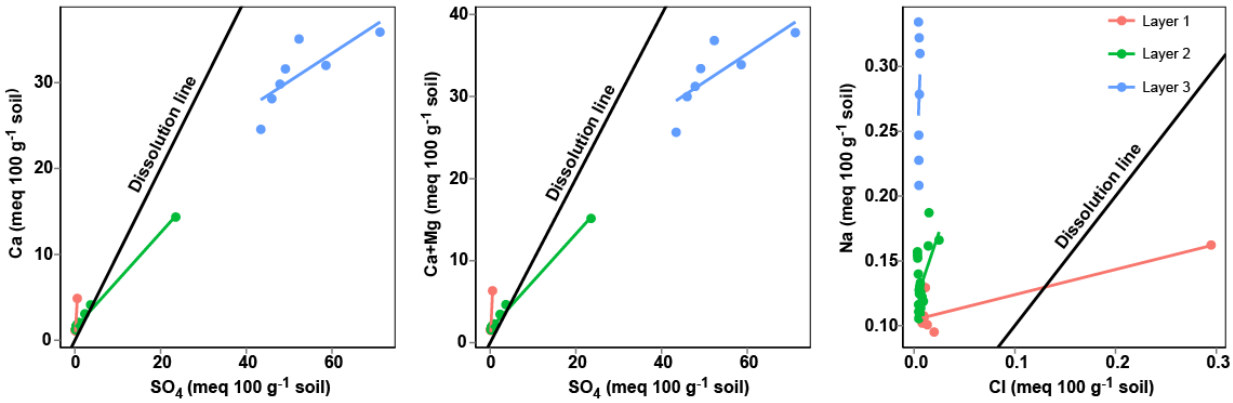

Figure 37 Relation between major ion species measured at R2T2 from soil water extractions to assess the potential for gypsum/anhydrite, (Ca+Mg)SO_4 and halite dissolution.

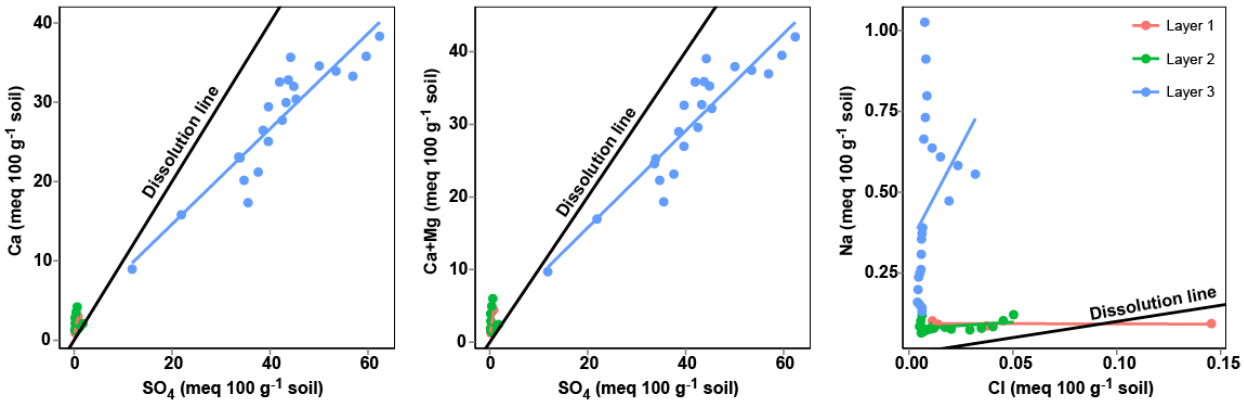

Figure 38 Relation between major ion species measured at R2T3 from soil water extractions to assess the potential for gypsum/anhydrite, (Ca+Mg)SO_4 and halite dissolution.

6.2.3 Organic Carbon Content

Organic carbon content was highest in the active layer in 6 out of the 10 cores (Caribou, CB and Wilson slumps, Lynx 1, Lynx 2, R2T2) and this is attributed to the O-horizon at the ground surface. At most sites, the organic carbon content is <5 % in the relict active layer and below the paleo thaw unconformity. At the two fire-disturbed sites (NRD and Lynx 2), peaks of organic carbon were observed at various depths in the active layer and relict active layer. Organic carbon content is lowest at CB and Wilson slumps likely due to the harsher growing conditions at higher elevation. Organic carbon content is highest at the Lynx 1 site, a sedge meadow, and concentration remains >30 % in the uppermost 1.75 m.

The soils examined in this study mostly contained organic carbon in the active layer with the soils in the relict active layer and below the paleo thaw unconformity containing little carbon. This is because the vegetation in this region is typically shallow-rooted and contributes little to no carbon to the deeper, frozen soil layers. The potential mechanisms to move organic carbon deeper in the soils include cryoturbation and leaching during past periods of deeper thaw or burial of surface organic matter followed by permafrost aggradation, as observed in hummock troughs (e.g. Kokelj et al., 2009).

6.3 Ground ice and Biogeochemical Discontinuities in the Active Layer and Permafrost: Relation with History of Permafrost

Past studies of ground ice content and biogeochemistry of permafrost have considered the permafrost as a single layer, and where applicable, have identified the depth of maximum thaw during the Early Holocene as a thermal discontinuity. Recent studies have explored intra-site variability of a parameter (i.e. GWC, soluble ions, organic carbon) on small spatial scales (e.g. Lacelle et al. 2014) and found that large variations in GWC can occur over very short distances due to the capability of water to migrate in the active layer and permafrost. Variability is much less in terms of soluble ions and organic carbon, making generalizations in permafrost areas quite challenging. However, treating permafrost as a single layer may not be ideal given the site-specific differences and varying thaw unconformity depths that can arise due to variations in physical characteristics (e.g. vegetation cover, slope, aspect).

Statistical analysis of mean values of transformed GWC, leachate conductivity and total soluble ions and organic carbon in the active layer, relict active layer and below the paleo thaw unconformity (section 5.3) suggest that layers in permafrost soils of the western Canadian Arctic can be differentiated based on a single parameter or a combination of parameters. For example, leachate conductivity is a parameter that best differentiates among layers. Layers were particularly distinct in terms of LC below the paleo thaw unconformity, where values were 2 to

10 times higher than in the active layer and relict active layer. A combination of the other parameters (GWC, organic carbon) can also be used to distinguish between layers, though this varies by site and is often less significant. These results suggest that there are at least three distinct layers in permafrost regions of the western Canadian Arctic.

To elucidate possible explanations for the generation of distinct biogeochemical layers in the active layer and permafrost, a PCA was performed (Table 3; Fig. 38). The analysis indicates that the greatest loading in the first principal component is attributed to organic carbon, followed closely by inorganic carbon and GWC. LC is positively correlated to these variables. All are inversely related to depth, suggesting that as depth increases, GWC and carbon contents decrease with LC following the same trend but to a lesser degree. This is expected given that organic carbon is typically restricted to shallower depths. In addition, the PCA's second component is loaded on the explanatory variable, depth, which is positively related to LC and inversely to organic carbon. LC thus takes on opposing characteristics: it increases at shallow depths in correspondence with organic carbon content, but also increases independently at greater depth. The latter, I propose, is a reflection of the varying lengths of time and degrees of chemical weathering (i.e. freshwater leaching) to which the soil layers were exposed since the early Holocene Thermal Maximum. More precisely, deeper permafrost layers (layer 3) would have been exposed to soil leaching less frequently than intermediate layers (layer 2), and less so than surficial layers (layer 1). Although additional explanatory variables – geographic coordinates or elevation, for example – might have shed light on other spatial patterns resulting from the maximum extent of the LIS and its retreat, the clustering of study sites in the Peel Plateau and east of the Mackenzie Delta would have introduced bias into the results.

Table 3 The loadings from the first principal components of all samples and variables at the study sites.

	PC 1	PC 2	PC 3	PC 4	PC 5
Depth	0.543	-4.711	2.823	-1.751	1.502
logGWC	-3.082	0.532	3.905	1.346	-2.990
log(Organic Carbon)	-3.236	1.882	0.903	-0.738	4.517
log(Inorganic Carbon)	-3.091	-0.987	-2.449	-3.928	-1.956
logLC	-2.441	-2.964	-2.398	3.863	0.597

Climatic and geomorphic processes, whether acting co-dependently or independently, lead to the outlining of different hypotheses to explain the biogeochemical signatures between the three distinct layers that are observed in this thesis in relation to depth. The first climatic hypothesis relates to the entire study area being covered by the warm-based LIS at 18 kcal yr BP (Lacelle et al., 2013). This type of glacier would have deposited basal till over the course of its persistence. The Richardson Mountains and Peel Plateau (western portion of the study area) were deglaciated by 13 kcal yr BP as evidenced by the dating of *Bison priscus* near Tsiigetchic (Fig. 39) (Zazula et al., 2009). During this time, air temperatures were much lower than present and epigenetic permafrost would have had ca. 1,500 years to aggrade in the till veneer and blanket before the onset of the early Holocene warm interval at ca. 11.5 kcal yr BP. Conversely, the Inuvik upland sites were deglaciated only after 12 kcal yr BP, which would have given less than 500 years for epigenetic permafrost to aggrade in the tills (note that the precise timing of permafrost aggradation in the Inuvik uplands is unknown). During the early Holocene warm interval, summer air temperatures were 2-7^{o}C higher than present-day, allowing for a deep active layer to develop. In northwestern Canada, the paleo-active layer has been measured to depths of 2-3 m, corresponding to 2-8 times deeper than the modern active layer (Burn, 1997; Fritz et al., 2012; Burn et al., 1986; Lauriol et al., 2002; Kotler and Burn 2000; Sanborn et al. 2006; Kokelj et al. 2002; Kokelj and Burn 2003; Murton, 2001).

The geomorphic hypothesis relates to the possibility, or rather the likelihood, of fire or topographic disturbances over the last 10,000 years that would have led to the development of a thaw unconformity at depth. Similar to modern-day climatic processes (Hinzman et al., 2005), the air temperature increase in the order of 2-7^{o}C that occurred during the early Holocene surely would have increased the frequency of those types of natural events. Furthermore, thaw slumping, for example, would have likely re-occurred in the same areas due to landscape susceptibility (i.e. polycyclic thaw slumping) (Kokelj et al., 2009a); this process could have affected the depth and profile of the thaw unconformity. Given that these types of natural disturbances are a positive feedback of increased air temperatures, it is difficult to say whether

the development of the thaw unconformity observed in the western Canadian Arctic is a direct product of warming air temperature or the result of the interplay between the early Holocene climate and natural disturbances. However, the precise formation process(es) of the distinct layers and their geochemical variations are irrelevant. Soils in the residual thaw layer, whether a product of climatic and/or geomorphic conditions, would have experienced freshwater leaching by infiltrating precipitation. Below the paleo permafrost table, soils would not have experienced chemical weathering at all.

Therefore, it is hypothesized that the duration and magnitude of leaching would also have been different between the contemporary active layer and relict active layer. Soils in the contemporary active layer would have experienced leaching throughout the Holocene until present, whereas those in the relict active layer likely only experienced leaching during the early Holocene. The variable degree of leaching within each layer could produce the biogeochemical profiles observed in the active layer, relict active layer and below the paleo thaw unconformity. Soils in the active layer would contain the lowest concentration of soluble ions due to 10,000 years of leaching. Comparatively, soils in the relict active layer would have been exposed more intermittently to leaching resulting in slightly higher soluble ion concentrations. Soils below the paleo thaw unconformity would have never experienced leaching (or very little) and contain the highest concentration of soluble ions. It is possible that, at some sites, the paleo active layer or paleo thaw unconformity was too deep to allow for complete freeze-back during the winter months. In such instances, a residual thaw layer would have been present and the magnitude of chemical weathering within this layer (layer 2) may differ from the suggested profiles above. More precisely, in the event of a residual thaw layer being present, this layer would have been subjected to the same degree of weathering as the contemporary active layer as opposed to intermittent chemical weathering if the permafrost had re-aggraded. In fact, the presence of a residual thaw layer may explain the different leachate conductivity profiles observed in the relict active layer of these study sites: progressively increasing with depth at sites on the Peel Plateau (vertical “diagonal”) versus little variation with depth for sites in the Inuvik uplands (vertical “down”).

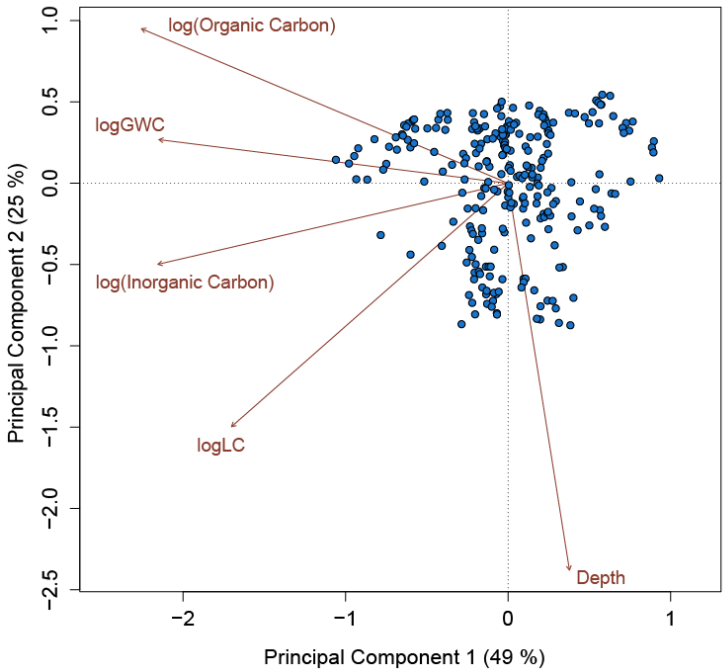

Figure 39 Principal components biplot of scores and loadings of variables at all sites across the western Canadian Arctic.

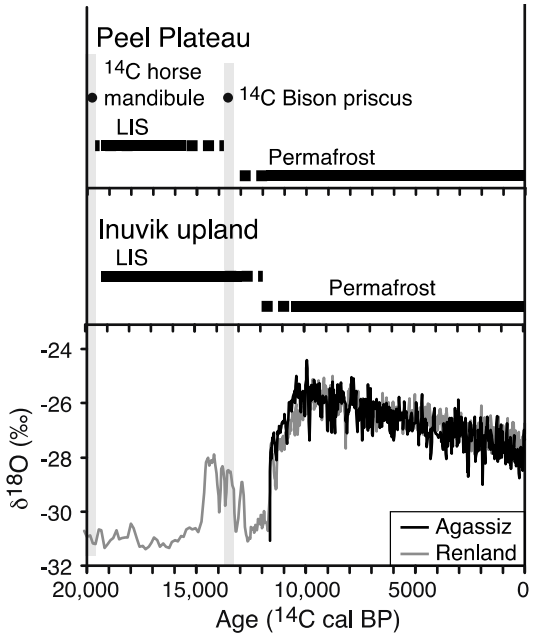

Figure 40 Timing of Laurentide Ice Sheet deglaciation events and permafrost aggradation on Peel Plateau and Inuvik upland sites, as evidenced by the change in $\delta^{18}O$ and dating of mandibule and *Bison priscus* samples. Data obtained from Lacelle et al. (2013) and Zazula et al. (2009).

6.3.1 Ground Ice and Biogeochemical Profiles and Type of Permafrost

Jorgenson et al. (2010) outlined a classification scheme for different types of permafrost based on whether it is epigenetic or syngenetic and its thermal history. Epigenetic permafrost is indicative of areas where permafrost aggrades after soil sediment has already accumulated, whereas syngenetic permafrost forms simultaneously with soil accumulation. Within their study, they used ice content depth profiles to relate to and further categorize the permafrost formation processes. The epigenetic permafrost that formed in the basal till during the LIS retreat was subjected to a period of intense thaw over the course of the early Holocene. This period of thaw was followed by subsequent rapid permafrost aggradation which led to the development of thaw unconformities that can be observed and measured through differences in GWC and the biogeochemistry between layers. Given these profiles and discontinuities as a result of the history of permafrost, it is likely that none of the types of permafrost proposed by Jorgenson et al. (2010) have been investigated in this thesis. I propose that another type of permafrost exists – one classified by epigenetic permafrost of overall very little ice content that was subjected to deep thaw during a warmer climate. The ground ice depth profile for this type of permafrost would include an ice-poor near-surface permafrost layer; ice-rich layers, however, could exist at the surface of permafrost as a result of organic matter accumulation. The geochemical and ground ice content trends discussed in this thesis are unlikely to be observed in other areas of epigenetic permafrost or of syngenetic permafrost that was not subjected to thaw.

6.4 Limitations

Limitations to this work are primarily related to the sampling methods and strategy. Ideally, sample collection methods would have been identical at all sites as opposed to via headwall sampling at slump sites and “top-down” coring at all others to ensure that no bias was introduced. In addition, lack of accessibility or research permits on territorial land claims prevented a more evenly distributed range of study sites. Having access to lands to the south, southeast and northeast of the Mackenzie Delta would have provided a better representation of the permafrost geochemistry in this region. In terms of laboratory methods, human error is always a concern when multiple people are handling samples or equipment during analysis. Furthermore, an error could have been introduced when inferring the depth of the paleo thaw unconformity if there was incomplete ionic dissolution. The proper setting of the paleo thaw unconformity depth is essential, as all subsequent data analyses rely on it. For example, in the case of NRD and Lynx 2, there is an initial peak in LC at the layer 3 boundary (Fig. 17 and 20).

If the lower value following this peak is due to incomplete dissolution, this would affect layer mean and variance results and make the relationship within layers stronger.

7. CONCLUSION

This thesis examined ground ice content and biogeochemistry in the active layer and permafrost across the western Canadian Arctic to contribute to regional baseline knowledge and understanding of this topic, and to explore the relationships with depth and thaw unconformities. The main findings were:

1. Leachate conductivity measurements provide an estimation of the total dissolved solutes within soil samples. This method should be used over the pore water extraction method, which was highly positively correlated to GWC, likely underestimating the quantity of total soluble ions.

2. Cores could be divided into three layers with statistically significant characteristics (1: active layer, 2: relict active layer, 3: permafrost below the paleo active layer) based on different parameters, though LC was the single best parameter to do so. A layer-based approach may be more applicable for future permafrost biogeochemistry studies. Not only could this allow intra and inter-site comparisons, it could also facilitate more accurate generalizations over larger regional scales. This could be instrumental in quantifying total soluble ions in permafrost and conducting risk assessments of anticipated 21st century permafrost thaw in these remote locations.

3. Continental sites on the eastern perimeter of the Mackenzie Delta had overall low GWC but it generally peaked just below both the primary and secondary thaw unconformities. Lynx 1 was the exception, with very high GWC (>500 %) in the upper 2 m of active layer and permafrost. CB slump had very low GWC throughout layer 2, but very high GWC throughout layer 3. The other thaw slump site, Wilson, had high GWC throughout permafrost.

4. LC increased with depth below the paleo thaw unconformity to reach values 2-10 times those within the active layer and relict active layer.

5. Organic carbon content was typically restricted to the surficial vegetation cover (top of layer 1), unless it had been redistributed following a fire disturbance (e.g. NRD) or incorporated into the top of permafrost at organic-rich sites (e.g. Lynx 1). Inorganic carbon contents were related to organic carbon profiles.

6. Similar to the Malone et al. (2013) study, $CaSO_4$ and $(Ca+Mg)SO_4$ dissolution was likely occurring at all sites. Halite dissolution did not appear to be occurring in layers 2 and 3, while sea salt inputs seemed likely in the active layer (layer 1).

7. PCA results indicated that the geochemical characteristics within each layer are related first to organic carbon, with GWC and LC being positively related and depth inversely related to this variable. Secondly, LC also tends to increase at greater depths.

7.1 Future Work

Vertical "diagonal" solute trends have been measured at upland sites of the Tuktoyaktuk Coastline (Kokelj, personal communication). These results would also correspond to the timing of deglaciation events and trends observed at areas deglaciated around the same time (i.e. CB and Wilson slumps). In order to further confirm this theory, sampling permafrost cores to well beyond the depth of the paleo thaw unconformity (>3 m) from both unglaciated and previously glaciated terrain at a greater number of sites following the trajectory of the LIS retreat could provide a better representation of permafrost geochemistry. This would help determine whether the geochemical profiles truly are a product of glacial retreat. For comparison purposes, sampling from areas of continuous permafrost in unglaciated terrain would provide more insight. Given that only one type of permafrost was studied within these sites, future studies could investigate the types formed under other environmental conditions brought forth by Jorgenson et al. (2010) to determine their ground ice content and biogeochemical profiles (i.e. epigenetic permafrost and syngenetic permafrost that were not subjected to thaw).

Another interesting study would be to quantify the amount of solutes present within the western Canadian Arctic. Many sites across the Arctic have been monitored for active layer thickness and the depth to the paleo-thaw unconformity is often known or inferred. If the thickness of each layer can be determined and the geochemical profiles modelled across the region based on the linear regression equations, an approximation of the total available solutes (or individual solutes) within layers could be determined. This would help to understand and prepare for the expected changes over the coming century.

8. REFERENCES

Acevedo M.F. 2013. *Data Analysis and Statistics for Geography, Environmental Science and Engineering*. Taylor and Francis Group, Boca Raton, Florida, USA.

Adam J.C., Hamlet A.F. and Lettenmaier D.P. 2009. Implications of global climate change for snowmelt hydrology in the twenty-first century. *Hydrological Processes*, 23, 962-972.

Allen C.E., Darmody R.G., Thorn C.E., Dixon J.C., and Schlyter P. 2001. Clay mineralogy, chemical weathering and landscape evolution in Arctic-Alpine Sweden. *Geoderma*, 99, 277-294.

Anderson D.M., Tice A.R., McKim H.L. 1973. The unfrozen water and the apparent specific heat capacity of frozen soils. In Permafrost: North American Contributions to the Second International Conference, Yakutsk, Siberia, USSR. National Academy of Sciences, Washington, DC. 20418, 289-295.

Anisimov O.A., Vaughan D.G., Callaghan T.V., Furgal C., Marchant H., Prowse T.D., Vilhjalmsson H., and Walsh J.E. 2007. Chapter 15: Polar Regions (Arctic and Antarctic). In Climate Change 2007: Impacts, Adaptation, Vulnerability. Contribution of Working Group II to the Fourth Assessment Report of the Intergovernmental Panel on Climate Change. [Parry M.L., Canziani O.F., Palutikof J.P., van der Linden P.J. and Hanson C.E. (edts.)]. Cambridge University Press, Cambridge, United Kingdom, 653-685.

Arnold, D. 2015. Welch's t-test. College of the Redwoods. Retrieved from: http://msemac.redwoods.edu/~darnold/math15/spring2013/R/Activities/WelchTTest.html [August 1, 2015]

Ball B.A., Barrett J.E., Gooseff M.N., Virginia R.A., and Wall. D.H. 2011. Implications of meltwater pulse events for soil biology and biogeochemical cycling in a polar desert. *Polar Research*, 30, 14555.

Beget J. 1987. Low profile of the northwest Laurentide Ice Sheet. *Arctic and Alpine Research*, 19, 81-88.

Bowden W.B., Gooseff M.N., Balser A., Green A., Peterson B.J., and Bradford J. 2008. Sediment and nutrient delivery from thermokarst features in the foothills of the North Slope, Alaska: Potential impacts on headwater stream ecosystems. *Journal of Geophysical Research*, Vol. 113, G02026. DOI: 10.1029/2007JG000470

Blum J.D., Klaue A., Nezat C.A., Driscoll C.T., Johnson C.E., Siccama T.G., Eagar C., Fahey T.J., and Likens G.E. 2002. Mycorrhizal weathering of apatite as an important calcium source in base-poor forest ecosystems. *Nature* 417:729–731.

Bockheim J.G., Walker D.A., Everett L.R., Nelson F.E. and Shiklomanov N.I. 1998. Soil development in moist non-acidic and acidic tundra in the Kuparuk watershed, arctic Alaska, U.S.A. *Arctic and Alpine Research*, 30(2), 166-174.

Boston University. 2013. Test Statistic for ANOVA. In Hypothesis Testing – Analysis of Variance (ANOVA).

Retrieved on November 29, 2015 from: http://sphweb.bumc.bu.edu/otlt/MPH-Modules/BS/BS704_HypothesisTesting-ANOVA/BS704_HypothesisTesting-Anova_print.html

Brown, J., O. Ferrians, J.A. Heginbottom, and E.S. Melnikov. 1997. Circum-Arctic Map of Permafrost and Ground-Ice Conditions. United States Geological Survey, Circum-Pacific Map Series, CP-45, scale 1:10,000,000.

Brown J., Hinkel K., and Nelson F.E. 2000. The circumpolar active layer monitoring (CALM) program: Research designs and initial results. *Polar Geography*, 24(3): 165–258.

Brown J., Hinkel K., and Nelson F.E. 2000b. The circumpolar active layer monitoring (CALM) program network. [Canada]. Boulder, Colorado USA: National Snow and Ice Data Center.

Burn C.R. 1988. The development of near-surface ground ice during the Holocene at sites near Mayo, Yukon Territory, Canada. *Journal of Quaternary Science*, 3, 31-38.

Burn C.R. 1997. Cryostratigraphy, paleogeography, and climate change during the Early Holocene warm interval, western Arctic coast, Canada. *Canadian Journal of Earth Sciences*, 34, 912-925.

Burn C.R. 1998. The response (1958-1997) of permafrost and near-surface ground temperatures to forest fire, Takhini River valley, southern Yukon Territory. Canadian *Journal for Earth Sciences*, 35, 184-199.

Burn C.R. 2011. Permafrost Distribution and Stability, in Changing Cold Environments: A Canadian Perspective (eds: H. French and O. Slaymaker), John Wiley & Sons, Ltd, Chichester, UK. DOI: 10.1002/9781119950172.ch7

Burn C.R. and Kokelj S.V. 2009. The environment and permafrost of the Mackenzie Delta area. *Permafrost and Periglacial Processes*, 20, 83-105.

Burn C.R., and Michel F.A. 1988. Evidence for recent temperature-induced water migration into permafrost from the tritium content of ground ice near Mayo, Yukon Territory, Canada. *Canadian Journal of Earth Sciences*, 25, 909-915.

Burn C.R., Michel F.A., and Smith M.W. 1986. Stratigraphic, isotopic, and mineralogical evidence for an early Holocene thaw unconformity at Mayo, Yukon Territory. *Canadian Journal of Earth Sciences*, 23, 794-891.

Callaghan T.V., Johansson M., Anisimov O., Christiansen H.H., Instanes A., Romanovsky V., and Smith S., 2011a. Chapter 5: Changing Permafrost and its Impacts. In Snow, Water, Ice and Permafrost in the Arctic (SWIPA). Oslo: Arctic Monitoring and Assessment Programme (AMAP).

Callaghan T.V., Johansson M., Prowse T.D., Olsen M.S., Reiersen L.-O. 2011b. Arctic Cryosphere: Changes and Impacts. *AMBIO: A Journal of the Human Environment*, 40(sup1), 3-5.

Catto N.R. 1996. Richardson Mountains, Yukon-Northwest Territories: The Northern portal of the postulated “ice-free corridor”. *Quaternary International*, 32, 3-19.

Cheng G. 1983. The mechanism of repeated-segregation for the formation of thick layered ground ice. *Cold Regions Science and Technology*, 8, 57-66.

Chizhov A.B., Chizhova N.I., Morkovkina I.K., and Romanov V.V. 1983. Tritium in permafrost and ground ice. Proceedings, 4th International Conference on Permafrost, National Academy of Sciences, Washington, DC, Vol. 1, pp. 147-151.

Christoffersen K.S., Amsinck S.L., Landkildehus F., Lauridsen T.L., and Jeppesen E. 2008: Lake flora and fauna in relation to ice-melt, water temperature and chemistry at Zackenberg. In: High-Arctic Ecosystem Dynamics in a Changing Climate [Meltofte H., Christensen T.R., Elberling B., Forchhammer M.C., and Rasch M. (eds.)]. Advances in Ecological Research Series, Vol. 40, Elsevier Science and Technology/Academic Press,Waltham, MA, USA, pp. 371-389.

Clark I.D., Lauriol B., Marschner M., Sabourin N., Chauret Y., and Desrochers A. 2004. Endostromatolites from permafrost karst, Yukon, Canada: paleoclimatic proxies for the Holocene hypsithermal. *Canadian Journal for Earth Sciences*, 41, 387-399.

Collins M., Knutti R., Arblaster J., Dufresne J.-L., Fichefet T., Friedlingstein P., Gao X., Gutowski W.J., Johns T., Krinner G., Shongwe M., Tebaldi C., Weaver A.J., and Wehner M. 2013: Long-term Climate Change: Projections, Commitments and Irreversibility. In: Climate Change 2013: The Physical Science Basis. Contribution of Working Group I to the Fifth Assessment Report of the Intergovernmental Panel on Climate Change [Stocker T.F., Qin D., Plattner G.-K., Tignor M., Allen S.K., Boschung J., Nauels A., Xia Y., Bex V., and Midgley P.M. (eds.)]. Cambridge University Press, Cambridge, United Kingdom and New York, NY, USA.

Conklin A. 2014. Introduction to soil chemistry: analysis and instrumentation (2nd ed.). John Wiley & Sons, Inc.: Hoboken, New Jersey, USA.

Delisle G. 2007. Near-surface permafrost degradation: How severe during the 21st century? *Geophysical Research Letters*, 34, 1-4.

Delorme L.D., Zoltai S.C., and Kalas L.L. 1977. Freshwater shelled invertebrate indicators of paleoclimate in northwestern Canada during late glacial times. *Canadian Journal for Earth Sciences*, 14, 2029-2046.

Derksen C., Smith S.L., Sharp M., Brown L., Howell S., Copland L., Mueller D.R., Gauthier Y., Fletcher C.G., Tivy A., Bernier M., Bourgeois J., Brown R., Burn C.R., Duguay C., Kushner P., Langlois A., Lewkowicz A.G., Royer A., Walker A. 2012. Variability and change in the Canadian cryosphere. *Climatic Change*, 115(1), 59-88.

Duk-Rodkin A., and Hughes O.L. 1992. Surficial geology, Fort McPherson-Bell River. Yukon-Northwest Territories. Geological Survey of Canada, Map 1745A, scale 1:250 000.

Duk-Rodkin A., and Lemmen DS. 2000. Glacial history of the Mackenzie region. In: The Physical Environment of the Mackenzie Valley, Northwest Territories: A Base Line for the Assessment of Environmental Change, Geological Survey of Canada Bulletin 547 (eds Dyke LD, Brooks, GR), pp. 41-48. Geological Survey of Canada, Ottawa, ON.

Dyke A.S., and Prest V.K. 1986. Late Wisconsinan and Holocene history of the Laurentide ice sheet. *Géographie physique et quaternaire*, 41, 237-264.

Ecosystem Classification Group. 2010. Ecological regions of the Northwest Territories – Cordillera. Department of Environment and Natural Resources, Government of the Northwest Territories, Yellowknife, NT, Canada.

Eliseev A.V., Denisov S.N., Arzhanov M.M., and Mokhov I.I. 2013. Climate-methane cycle feedback in global climate model model simulations forced by RCP scenarios. *EGU General Assembly*, 15.

Environment Canada. 1995. Ecozone and ecoregion descriptions of Canada. In Ecological Framework of Canada.
Retrieved on August 6th, 2014 from: http://ecozones.ca/english/zone/index.html

Etienne S. 2002. The role of biological weathering in Periglacial areas: a study of weathering rinds in south Iceland. *Geomorphology*, 47, 75-86.

Etzelmuller, B., Shuler T.V., Isaksen K., Christiansen H.H., Farbrot H., and Benestad R. 2011. Modeling the temperature evolution of Svalbard permafrost during the 20th and 21st century. *The Cryosphere*, 5, 67-79.

Forbes B.C., Fauria M.M., Zetterberg P. 2010. Russian Arctic warming and "greening" are closely tracked by tundra shrub willows. *Global Change Biology*, 16, 1542–54.

French H.M. 2007. *The Periglacial Environment (2nd ed.).* Edinburgh Gate: Longman Group Limited 1976.

French H., and Shur Y. 2010. The principles of cryostratigraphy. *Earth-Science Review*s, 101, 190-206.

Frey K.E. and McClelland J.W. 2009. Impacts of permafrost degradation on arctic river biogeochemistry. *Hydrological Processes*, 23(1), 169-182. DOI: 10.1002/hyp.7196

Fritz M., Wetterich S., Schirrmeister L., Meyer H., Lantuit H., Preusser F., and Pollard W.H. 2012. Eastern Beringia and beyond: Late Wisconsinian and Holocene landscape dynamics along the Yukon Coastal Plain, Canada. Palaeogeography, Palaeoclimatology, Palaeoecology, 319-320, 28-45.

Fulton R.J. 1989. Quaternary geology of the Canadian Cordillera. *In* Quaternary Geology of Canada and Greenland. Edited by R.J. Fulton. Geological Survey of Canada, Geology of Canada, no. 1, pp. 15-96.

Gajewski K. 2015. Quantitative reconstruction of Holocene temperatures across the Canadian Arctic and Greenland. *Global and Planetary Change*, 128, 14-23.

Geological Survey of Canada. 1973. Glacier Retreat. Department of Energy, Mines and Resources. Atlas of Canada, 4th Ed. Issue 031-32.

Geological Map of Canada - Map D1860A [CD-ROM]. 1997. Ottawa, Ontario: Geological Survey of Canada, Natural Resources Canada.

Hartmann, D.L., A.M.G. Klein Tank, M. Rusticucci, L.V. Alexander, S. Brönnimann, Y. Charabi, F.J. Dentener, E.J. Dlugokencky, D.R. Easterling, A. Kaplan, B.J. Soden, P.W. Thorne, M. Wild and P.M. Zhai, 2013: Observations: Atmosphere and Surface. In: Climate Change 2013: The Physical Science Basis. Contribution of Working Group I to the Fifth Assessment Report of the Intergovernmental Panel on Climate Change [Stocker, T.F., D. Qin, G.-K. Plattner, M. Tignor, S.K. Allen, J. Boschung, A. Nauels, Y. Xia, V. Bex and P.M. Midgley (eds.)]. Cambridge University Press, Cambridge, United Kingdom and New York, NY, USA.

Heino, J., R. Virkkala, and H. Toivonen, 2009: Climate change and freshwater biodiversity: detected patterns, future trends and adaptations in northern regions. Biological Reviews, 84(1), 39-54.

Heiri, O., Lotter, A. F., and G., Lemcke. 2001. Loss on ignition as a method for estimating organic and carbonate content in sediments: reproducibility and comparability of results. *Journal of paleolimnology*, *25*(1), 101-110.

Hinzman L.D., Bettez N.D., Bolton W.R., Chapin F.S., Dyurgerov M.B., Fastie C.L., Griffith B., Hollister R.D., Hope A., Huntington H.P., Jensen A.M., Jia G.J., Jorgenson T., Kane D.L., Klein D.R., Kofinas G., Lynch A.H., Lloyd A.H., McGuire A.D., Nelson F.E., Oechel W.C., Osterkamp T.E., Racine C.H., Romanovsky V.E., Stone R.S., Stow D.A., Sturm M., Tweedie C.E., Vourlitis G.L., Walker M.D., Walker D.A., Webber P.J., Welker J.M., Winker K.S., and Yoshikawa K. (2005). Evidence and implications of recent climate change in northern Alaska and other arctic regions. Climatic Change, 72(3), 251-298.

Hinzman L.D., Deal C.J., McGuire A.D., Mernild S.H., Polyakov I.V. and Walsh J.E. 2013. Trajectory of the Arctic as an integrated system. *Ecological Applications*, 23, 1837-1868. DOI: 10.1890/11-1498.1

Hubbard S.S., Gangodagamage C., Dafflon B., Wainwright H., Peterson J., Gusmeroli A., Ulrich C., Wu Y., Wilson C., Rowland J., Tweedie C., and Wullschleger S.D. 2013. Quantifying and relating land-surface and subsurface variability in permafrost environments using LiDAR and surface geophysical datasets. *Hydrogeology Journal*, 21(1), 149-169.

Jansson M., Jonsson A., Andersson A., and Karlsson J. 2010. Biomass and structure of planktonic communities along an air temperature gradient in subarctic Sweden. *Freshwater Biology*, 55(3), 691-700.

Jorgenson M.T., Romanovsky V., Harden J., Shur Y., O'Donnelle J., Shuur E.A.G., Kanevskiy M., and Marchenko S. 2010. Resilience and vulnerability of permafrost to climate change. *Canadian Journal of Forest Research*, 40, 1219-1236.

Jorgenson M.T., Shur Y.L., and Pullman E.R. 2006. Abrupt increase in permafrost degradation in Arctic Alaska. *Geophysical Research Letters*, 33, L02503. DOI: 10.1029/2005GL024960

Keene W.C., Pszenny A.P., Galloway J.N., and Hawley M.E. 1986. Sea-salt corrections and interpretation of constituent ratios in marine precipitation. *Journal of Geophysical Research: Atmospheres*, 91(D6).

Keller K., Blum J.D. and Kling G.W. 2007. Geochemistry of soils and streams on surfaces of varying ages in Arctic Alaska. *Arctic, Antarctic and Alpine Research*, 39(1), 84-98.

Keller K., Blum J.D. and Kling G.W. 2010. Stream geochemistry as an indicator of increasing permafrost thaw depth in an arctic watershed. Chemical Geology, 273, 76-81.

Kokelj S.V. and Burn C.R. 2003. Ground ice and soluble cations in near-surface permafrost, Inuvik, Northwest Territories, Canada. *Permafrost and Periglacial Processes*, 14, 275-289.

Kokelj S.V., and Burn C.R. 2005. Geochemistry of the active layer and near-surface permafrost, Mackenzie Delta region, Northwest Territories, Canada. *Canadian Journal of Earth Sciences*, 42, 37-48. DOI: 10.1139/e04-089

Kokelj S.V., and Jorgenson M.T. 2013. Advances in Thermokarst Research. *Permafrost and Periglacial Processes*, 24(2), 108-119. DOI: 10.1002/ppp.1779

Kokelj S.V., Lacelle D., Lantz T.C., Tunnicliffe J., Malone L., Clark I.D., and Chin K.S. 2013. Thawing of massive ground ice in mega slumps drives increases in stream sediment and solute flux across a range of watershed scales. *Journal of Geophysical Research: Earth Surface*, 118, 681-692.

Kokelj S.V., and Lewkowicz A.G. 1999. Salinization of permafrost terrain due to natural geomorphic disturbance, Fosheim Peninsula, Ellesmere Island. *Arctic*, 52, 372-385.

Kokelj S.V., Smith C.A.S., and Burn C.R. 2002. Physical and chemical characteristics of the active layer and permafrost, Herschel Island, western Arctic Coast, Canada. *Permafrost and Periglacial Processes*, 13, 171-185.

Kokelj S.V., Tunnicliffe J., Lacelle D., Lantz T.C., Chin K.S., and Fraser R. 2015. Increased precipitation drives mega slump development and destabilization of ice-rich permafrost terrain, northwestern Canada. *Global and Planetary Change*, 129, 56-68.

Kokelj S.V., Lantz T.C., Kanigan J., Smith S.L., and Coutts R. 2009a. Origin and polycyclic behaviour of tundra thaw slumps, Mackenzie Delta Region, Northwest Territories, Canada. *Permafrost and Periglacial Processes*, 20, 173-184. DOI: 10.1002/ppp.642

Kokelj S.V., Zajdlik B., and Thompson M.S. 2009b. The impacts of thawing permafrost on the chemistry of lakes across the subarctic boreal-tundra transition, Mackenzie Delta region, Canada. *Permafrost and Periglacial Processes*, 20(2), 185-199. DOI: 10.1002/ppp.641

Konishchev V.N., and Rogov V.V. 1993. Investigations of cryogenic weathering in Europe and Northern Asia. *Permafrost and Periglacial Processes*, 4, 49-64.

Kotler E., and Burn C.R. 2000. Cryostratigraphy of the Klondike “muck” deposits, west-central Yukon Territory. *Canadian Journal of Earth Sciences*, 37, 849-861.

Koven C.D., Riley W.J. and Stern A. 2013. Analysis of permafrost thermal dynamics and response to climate change in the CMIP5 earth system models. *Journal of Climate*, 26, 1877-1900.

Koven C.D., Ringeval B., Friedlingstein P., Clais P., Cadule P., Khvorostyanov D., Krinner G., and Tarnocai C. 2011. Permafrost carbon-climate feedbacks accelerate global warming. *Proceedings of the National Academy of Sciences*, 108(36), 14769-14774.

Lacelle, D., Bjornson, J., Lauriol, B. Clark, I.D. 2004. Segregated-intrusive ice of subglacial meltwater origin in retrogressive thaw flow headwalls, Richardson Mountains, NWT, Canada. *Quaternary Science Reviews*, 23(5-6), 681-696.

Lacelle D., Brooker A., Fraser R.H., and Kokelj S.V. 2015a. Distribution and growth of thaw slumps in the Richardson Mountains-Peel Plateau region, northwestern Canada. *Geomorphology*, 235, 40-51. DOI: 10.1016/j.geomorph.2015.01.024

Lacelle D., Fontaine M., Forest A.P., and Kokelj S.V. 2014. High-resolution stable water isotopes as tracers of thaw unconformities in permafrost: A case study from western Arctic Canada. *Chemical Geology*, 368, 85-96.

Lacelle D., Fontaine M., and Kokelj S.V. 2015b. Geochemistry of the active layer and permafrost in northwestern Canada: from measurements to Quaternary stratigraphy. Paper presented at GeoQuébec 2015: Challenges from North to South, Québec, QC, September 20-23, 2015. (pp. 1-8). Québec, QC: Canadian Geotechnical Society.

Lacelle D., Juneau V., Pellerin A., Lauriol B., and Clark I.D. 2008. Weathering regime and geochemical conditions in a polar desert environment, Haughton impact structure region, Devon Island, Canada. *Canadian Journal for Earth Sciences*, 45, 1139-1157.

Lacelle D., Lauriol B., Zazula G., Ghaleb B., Utting N., and Clark I.D. 2013. Timing of advance and basal condition of the Laurentide Ice Sheet during the last glacial maximum in the Richardson Mountains, NWT. *Quaternary Research*, 80, 274-283.

Lantz T.C., Kokelj S.V., Gergel S.E., and Henry G.H.R. 2009. Relative impacts of disturbance and temperature: persistent changes in microenvironment and vegetation in retrogressive thaw slumps. *Global Change Biology*, 15, 1664-1675.

Lantz T.C., Marsh P., and Kokelj S.V. 2013. Recent shrub profileration in the Mackenzie Delta Uplands and microclimatic implications. *Ecosystems*, 16, 47-59.

Larsen J.N., Anisimov O.A., Constable A., Hollowed A., Maynard N., Prestrud P., Prowse T., and Stone J.M.R. 2014. Chapter 28: Polar Regions. In Climate Change 2014: Impacts, Adaptation, and Vulnerability. Part B: Regional Aspects. Contribution of Working Group II to the Fifth Assessment Report of the Intergovernmental Panel on Climate Change. [Barros V.R., Field C.B., Dokken D.J., Mastrandrea M.D., Mach K.J., Bilir T.E., Chatterjee M., Ebi K.L., Estrada Y.O., Genova R.C., Girma B., Kissel E.S., Levy A.N., MacCracken S., Mastrandrea P.R., and White L.L. (edts.)]. Cambridge University Press, Cambridge, United Kingdom and New York, NY, USA, 1-71.

Lauriol B., Duguay C.R., and Riel A. 2002. Response of the Porcupine and Old Crow rivers in northern Yukon, Canada to Holocene climatic change. *The Holocene*, 12(1), 27-34.

Lauriol B., Lacelle D., Labrecque S., Duguay C.R., and Telka A. 2009. Holocene evolution of lakes in the Bluefish Basin, Northern Yukon, Canada. *Arctic*, 62(2), 212-224.

Lawrence D.M., Slater A.G., Tomas R.A., Holland M.M., Deser C. 2008. Accelerated Arctic land warming and permafrost degradation during rapid sea ice loss. *Geophysical Research Letters*, 35, L11506.

Lewis T., Lafrenière M.J., Lamoureux S.F. 2012. Hydrochemical and sedimentary responses of

paired High Arctic watersheds to unusual climate and permafrost disturbance, Cape Bounty, Melville Island, Canada. *Hydrological Processes*, 26, 2003-2018.

Lewkowicz A.G. 2001. Temperature regime of a small sandstone tor, latitude 80°N, Ellesmere Island, Nunavut, Canada. *Permafrost and Periglacial Processes*, 12, 351-366.

Lipson D.A., Jha M., Raab T.K., and Oechel W.C. 2010. Reduction of iron (III) and humic substances plays a major role in anaerobic respiration in an Arctic peat soil. *Biogeosciences*, 115(G4). DOI: 10.1029/2009JG001147

Lipson D.A., Zona D., Raab T.K., Bozzolo F., Mauritz M. and Oechel W.C. 2012. Water table height and microtopography control biogeochemical cycling in an Arctic coastal tundra ecosystem. *Biogeosciences*, 9, 577-591.

Mackay J.R. 1978. Freshwater shelled invertebrate indicators of paleoclimate in northwestern Canada during late glacial times: Discussion. *Canadian Journal of Earth Sciences*, 15, 461-462.

Mackay J.R. 1983. Downward water movement intro frozen ground, western arctic coast, Canada. *Canadian Journal of Earth Science*, 20, 120-134.

Mackay J.R. 1995. Active layer changes (1968 to 1993) following the forest-tundra fire near Inuvik, N.W.T. Canada. *Arctic and Alpine Research*, 27(4), 323-336.

Mackay J.R. and Dallimore S.R. 1992. Massive ice of Tuktoyaktuk area, western Arctic coast, Canada. *Canadian Journal of Earth Sciences*, 29, 1235-1249.

Malone L., Lacelle D., Kokelj S.V. and Clark I.D. 2013. Impacts of hillslope thaw slumps on the geochemistry of permafrost catchments (Stony Creek watershed, NWT, Canada). *Chemical Geology*, 356, 38-49.

Meyer H., Schirrmeister L., Andreev A., Wagner D., Hubberten H.-W., Yoshikawa K., Bobrov A., Wetterich S., Opel T., Kandiano E., Brown J. 2010. Lateglacial and Holocene isotopic and environmental history of northern coastal Alaska – Results from a buried ice- wedge system at Barrow. *Quaternary Science Reviews*, 29, 3720-3735.

Miller G.H., Brigham-Grette J., Alley R.B., Anderson L., Bauch H.A., Douglas M.S.V., Edwards M.E., Elias S.A., Finney B.P., Fitzpatrick J.J., Funder S.V., Herbert T.D., Hinzman L.D., Kaufman D.S., MacDonald G.M., Polyak L., Robock A., Serreze M.C., Smol J.P., Spielhagen R., White J.W.C., Wolfe A.P., Wolff E.W. 2010. Temperature and precipitation history of the Arctic. *Quaternary Science Reviews*, 29, 1679-1715.

Murton, J.B. 2001. Thermokarst sediments and sedimentary structures, Tuktoyaktuk Coastlands, western Arctic Canada. *Global and Planetary Change*, 28, 175-192.

Murton, J.B. and French, H.M. 1994. Cryostructures in permafrost, Tuktoyaktuk coastlands, western arctic Canada. *Canadian Journal of Earth Sciences*, 31, 737-747.Myers-Smith I.H., Hik D.S., Kennedy C., Cooley D., Johnstone J.F., Kenney A.J., and Krebs C.J. 2011. Expansion of canopy-forming willows over the twentieth century on Herschel Island, Yukon Territory, Canada. *AMBIO: A Journal of the Human Environment*, 40(6), 610-623.

Natural Resources Canada. 2014. National Fire Database – Fire History Data. Retrieved on July 30th, 2014 from: http://cwfis.cfs.nrcan.gc.ca/datamart

Navarro A.F., Cegarra J., Roig A., and Garcia D. 1993. Relationships between organic matter and carbon contents of organic wastes. *Bioresource Technology*, 44, 203-207.

Newman B.D., Throckmorton H.M., Graham D.E., Gu B., Hubbard S.S., Liang L., Wu Y., Heikoop J.M., Herndon E.M., Phelps T.J., Wilson C.J., Wullschleger S.D. 2015. Microtopographic and depth controls on active layer chemistry in Arctic polygonal ground. *Geophysical Research Letters*, 42, 1808-1817. DOI: 10.1002/2014GL062804

Norris, D.K. *Geology, Aklavik, District of Mackenzie*. 1:250,000. Geological Survey of Canada, 1517A. Ottawa: Energy, Mines and Resources, 1981a.

Norris, D.K. *Geology, Arctic Red River, District of Mackenzie*. 1:250,000. Geological Survey of Canada, 1521A. Ottawa: Energy, Mines and Resources, 1981b.

Norris, D.K. *Geology, Fort McPherson, District of Mackenzie*. 1:250,000. Geological Survey of Canada, 1520A. Ottawa: Energy, Mines and Resources, 1981c.

Norris, D.K. *Geology, Mackenzie Delta, District of Mackenzie*. 1:250,000. Geological Survey of Canada, 1515A. Ottawa: Energy, Mines and Resources, 1981d.

Oksanen J., Blanchet F.G., Kindt R., Legendre P., Minchin P.R., O'Hara R.B., Simpson G.L., Solymos P., Stevens M.H.H., and Wagner H. 2015. Vegan: Community Ecology Package. R package version 2.2-1. http://CRAN.r-project.org/package-vegan/

Osterkamp T.E., and Burn C.R. 2003. Permafrost, in Encyclopedia of Atmospheric Sciences, edited by J. R. Holton, pp. 1717–1729, Academic, Oxford, U. K.

O'Sullivan J.B. 1966. Geochemistry of permafrost, Barrow, Alaska. In: Proceedings, International Conference on Permafrost, National Academy of Sciences, National Research Council, Washington, DC, pp. 30-37. Publication 1287.

Overland J.E., Wang M., Walsh J.E., Christensen J.H., Kattsov V.M., and Chapman W.L. 2011. Chapter 3: Climate model projections for the Arctic. In Snow, Water, Ice and Permafrost in the Arctic (SWIPA). Oslo: Arctic Monitoring and Assessment Programme (AMAP).

Péwé T.L., and Sellmann P.V. 1973. Geochemistry of permafrost and quaternary stratigraphy. Permafrost: North American Contribution to the Second International Conference, 13–28 July, Yakutsk, Siberia. 166 – 170.

Ping C.L., Bockheim J.G., Kimble J.M., Michaelson G.J., and Walker D.A. 1998. Characteristics of cryogenic soils along a latitudinal transect in Arctic Alaska. *Journal of Geophysical Research – Atmospheres*, 103, 28917-28928.

Prick A., and Pissart A. 1993. Variations dilatométriques de cylindres de roches calcaires subissant des cycles de gel-dégel. *Permafrost and Periglacial Processes*, 4, 1-15.

R Core Team. 2013. R: A language and environment for statistical computing. R Foundation for Statistical Computing, Vienna, Austria. http://www.R-project.org/

Rampton V.N. 1988. Quaternary geology of the Tuktoyaktuk Coastlands, Northwest Territories. *Geological Survey of Canada*, Memoir 423.

Reimann C. 2008. *Statistical data analysis explained: applied environmental statistics with R*. Chichester, England; Hoboken, NJ: John Wiley & Sons. Retrieved from: http://books2.scholarsportal.info/search.html?searchTerm=Reimann%2C+Clemens&searchField=Author

Ritchie J.C. 1984. Past and present vegetation of the Far Northwest of Canada. University of Toronto Press.

Ritchie J.C., Cwynar L.C, and Spear R.W. 1983. Evidence from north-west Canada for an early Holocene Milankovitch thermal maximum. *Nature*, 305, 126-128.

Romanovsky V.E., Smith S.L., and Christiansen H.H. 2010. Permafrost thermal state in the Polar Northern Hemisphere during the International Polar Year 2007-2009: a Synthesis. *Permafrost and Periglacial Processes*, 21, 106-116.

Saito K., Kimoto M., Zhang T., Takata K. and Emori S. 2007. Evaluating a high-resolution climate model: simulated hydrothermal regimes in frozen ground regions and their change under the global warming scenario. *Journal of Geophysical Research*, 112 (F2).

Sanborn P., Smith C., Froese D. Zazula G., Westgate J. 2006. Full-glacial paleosols in perennially frozen loess sequences, Klondike goldfields, Yukon Territory, Canada. 2006. *Quaternary Research*, 66(1), 147-157.

Schumacher B.A. 2002. Methods for the determination of total organic carbon (TOC) in soils and sediments. *Ecological Risk Assessment Support Center*, 2002:1-23.

Schuur E.A.G., Bockheim J., Canadell J.G., Euskirchen E., Field C.B., Goryachkin S.V., Hagemann S., Kuhry P., Lafleur P.M., Lee H., Mazhitova G., Nelson F.E., Rinke A., Romanovsky V.E., Shiklomanov N., Tarnocai C., Venevsky S., Vogel J.G., and Zimov S.A. 2008. Vulnerability of permafrost carbon to climate change: implications for the global carbon cycle. *BioScience*, 58(8), 701-714.

Schuur E.A.G., Vogel J.G., Crummer K.G., Lee H., Sickman J.O. and Osterkamp T.E. 2009. The effect of permafrost thaw on old carbon release and net carbon exchange from tundra. *Nature*, 459, 556-559. DOI: 10.1038/nature08031

Serreze M.C., Walsh J.E., Chapin III F.S., Osterkamp T., Dyurgerov M., Romanovsky V., Oechel W.C., Morison J., Zhang T., and Barry R.G. 2000. Observational evidence of recent change in the northern high-latitude environment. *Climatic Change*, 46, 159-207.

Sheskin D.J. 2011. *Handbook of parametric and nonparametric statistical procedures (5th ed.).* Chapman and Hall/CRC, Boca Raton, FL.

Shur Y., Hinkel K.M., and Nelson F.E. 2005. The transient layer: Implications for geocryology and climate-change science. *Permafrost and Periglacial Processes*. 16, 5-17.

Shur Y.L., and Jorgenson M.T. 2007. Patterns of permafrost formation and degradation in relation to climate and ecosystems. *Permafrost and Periglacial Processes*, 18, 7-19.

Smith M.W. 1985. Observations of soils freezing and frost heaving at Inuvik, Northwest Territories, Canada. *Canadian Journal of Earth Sciences*, 22, 283-290.

Smith S.L., Burgess M.M., Riseborough D., and Nixon F.M. 2005. Recent trends from Canadian Permafrost Thermal Monitoring Network Sites. *Permafrost and Periglacial Processes*, 16(1), 19-30.

Smith S.L., Wolfe S.A., Riseborough D.W., and Nixon F.M. 2009. Active-layer characteristics and summer climatic indices, Mackenzie Valley, Northwest Territories, Canada. *Permafrost and Periglacial Processes*, 20, 201-220.

St. Jacques J.-M., and Sauchyn D.J. 2009. Increasing winter baseflow and mean annual streamflow from possible permafrost thawing in the Northwest Territories, Canada. *Geophysical Research Letters*, 36, L01401.

Tape K., Sturm M., and Racine C. 2006. The evidence for shrub expansion in Northern Alaska and the Pan-Arctic. *Global Change Biology*, 12, 686–702.

Tarnocai C., Canadell J.G., Schuur E.A.G., Kuhry P., Mazhitova G., and Zimov S. 2009. Soil organic carbon pools in the northwestern circumpolar permafrost region. *Global Biogeochemical Cycles*, 23(GB2023).

Thienpont J.R., Ruhland K.M., Pisaric M.F.J., Kokelj S.V., Kimpe L.E., Blais J.M., and Smol J.P. 2013. Biological responses to permafrost thaw slumping in Canadian Arctic lakes. *Freshwater Biology*, 58, 337-353.

van Everdingen R., ed. 1998. Revised 2005 van Everdingen, R. (Ed.), 1998. Multi-language glossary of permafrost and related ground-ice terms. National Snow and Ice Data Center / World Data Center for Glaciology, Boulder. CO.

Vardy S.R., Warner B.G., and Aravena R. 1997. Holocene climate effects on the development of a peatland on the Tuktoyaktuk Peninsular, Northwest Territories. *Quaternary Research*, 47, 90-104.

Vasavada, N. 2014. One-way ANOVA with post-hoc Tukey HSD Test Calculator for Multiple Comparison. Retrieved on November 30, 2015 from: http://statistica.mooo.com/OneWay_Anova_with_TukeyHSD_result

Vincent J.-S. 1989. Quaternary geology of the northern Canadian Interior Plains. In “Quaternary geology of Canada and Greenland” (R.J. Fulton, Ed.), pp. 100-137. No. 1, Geological Survey of Canada, Geology of Canada.

Wickland K.P., Striegl R.G., Neff J.C., and Sachs T. 2006. Effects of permafrost melting on CO_2 and CH_4 exchange of a poorly drained black spruce lowland. *Journal of Geophysical Research*, Vol. 111, G02011. DOI: 10.1029/2005JG000099

Williams P.J. and Smith M.W. 1989. The Frozen Earth, Fundamentals of Geocryology. Studies in Polar Research Series. xvi + 306 pp. Cambridge, New York, Port Chester, Melbourne, Sydney: Cambridge University Press.

Xu L., Myneni R.B., Chapin III F.S., Callaghan T.V., Pinzon J.E., Tucker C.J., Zhu Z., Bi J., Ciais P., Tommervik H., Euskirchen E.S., Forbes B.C., Piao S.L., Anderson B.T., Ganguly S.,

Nemani R.R., Goetz S.J., Beck P.S.A., Bunn A.G., Cao C., and Stroeve J.C. 2013. Temperature and vegetation seasonality diminishment over northern lands. *Nature Climate Change*, 3, 581-586.

Zazula G.D., Mackay G., Andrews T.D., Shapiro B., Letts B., and Brock F. 2009. A late Pleistocene steppe bison (*Bison priscus*) partial carcass from Tsiigehtchic, Northwest Territories, Canada. Quaternary Science Reviews, 28, 2734, 2742.

Zhuang Q., Melillo J.M., Sarofim M.C., Kicklighter D.W., McGuire A.D., Felzer B.S., Sokolov A., Prinn R.G., Steudler P.A. and Hu S. 2006. CO2 and CH4 exchanges between land ecosystems and the atmosphere in northern high latitudes over the 21st century. *Geophysical Research Letters*, 33, L17403. DOI: 10.1029/2006GL026972

Zona D., Lipson D.A., Zulueta R.C., Oberbauer S.F. and Oechel W.C. 2011. Microtopographic controls on ecosytem functioning in the Arctic Coastal Plain. *Biogeosciences*, 116(G4).

Zona D., Oechel W., Kochendorfer J., Paw U., Salyuk A., Olivas P., Oberbauer S., and Lipson D. 2009. Methane fluxes during the initiation of a large-scale water table manipulation experiment in the Alaskan Arctic tundra. *Global Biogeochemical Cycles*, 23, GB2013. DOI: 10.1029/2009GB003487

APPENDIX A: LAYER MEANS ± SD OF TRANSFORMED VARIABLES FOR EACH SITE

Table A1 Layer mean ± SD at each site in the western Canadian Arctic for the following transformed variables: GWC, PW, LC, Organic Carbon and Inorganic Carbon.

Site	Layer	logGWC	sqrtPW	logLC	log(Organic C)	log(Inorganic C)
Campbell	1	1.56 ± 0.48	-	0.02 ± 0.41	0.44 ± 0.49	-0.07 ± 0.14
	2	1.61 ± 0.16	0.47 ± 0.14	0.06 ± 0.17	0.18 ± 0.17	0.21 ± 0.17
Caribou	1	2.62 ± 0.06	-	0.89 ± 0.07	1.27 ± 0.04	1.15 ± 0.13
	2	1.63 ± 0.26	-	-0.10 ± 0.37	-0.09 ± 0.37	-0.07 ± 0.29
CB	1	1.74 ± 0.21	-	0.34 ± 0.13	0.66 ± 0.25	0.33 ± 0.09
	2	1.45 ± 0.09	-	0.56 ± 0.25	0.28 ± 0.04	0.29 ± 0.07
	3	2.18 ± 0.04	1.26 ± 0.09	0.82 ± 0.09	0.29 ± 0.02	0.42 ± 0.02
Lynx 1	1	2.66 ± 0.07	0.72 ± 0.06	0.72 ± 0.10	1.31 ± 0.03	0.45 ± 0.09
	2	2.31 ± 0.56	0.94 ± 0.53	0.43 ± 0.22	0.76 ± 0.47	0.29 ± 0.30
Lynx 2	1	1.40 ± 0.21	-	0.04 ± 0.18	0.18 ± 0.23	0.03 ± 0.27
	2	1.49 ± 0.25	0.73 ± 0.12	0.21 ± 0.08	-0.04 ± 0.16	0.15 ± 0.22
	3	1.50 ± 0.16	0.79 ± 0.11	1.11 ± 0.37	-0.07 ± 0.12	0.08 ± 0.15
NRD	1	1.63 ± 0.11	-	0.35 ± 0.06	0.53 ± 0.22	0.32 ± 0.14
	2	1.81 ± 0.29	1.43 ± 0.16	0.49 ± 0.17	0.42 ± 0.05	0.38 ± 0.04
	3	2.19 ± 0.18	1.48 ± 0.67	1.03 ± 0.28	0.62 ± 0.21	0.38 ± 0.17
NRT2	1	2.01 ± 0.28	0.72 ± 0.40	0.60 ± 0.13	0.69 ± 0.24	0.26 ± 0.05
	2	2.07 ± 0.32	0.39 ± 0.08	0.48 ± 0.12	0.57 ± 0.11	0.24 ± 0.04
R2T2	1	1.57 ± 0.24	-	0.19 ± 0.22	0.47 ± 0.29	0.12 ± 0.12
	2	1.66 ± 0.17	0.60 ± 0.15	0.14 ± 0.17	0.21 ± 0.06	0.35 ± 0.15
	3	1.51 ± 0.13	0.84 ± 0.14	1.32 ± 0.09	0.17 ± 0.01	0.38 ± 0.02
R2T3	1	1.72 ± 0.28	-	0.32 ± 0.22	0.61 ± 0.28	0.03 ± 0.03
	2	1.93 ± 0.34	0.65 ± 0.16	0.23 ± 0.18	0.42 ± 0.30	0.23 ± 0.12
	3	1.54 ± 0.14	0.91 ± 0.15	1.31 ± 0.09	0.18 ± 0.02	0.35 ± 0.05
Wilson	1	1.64 ± 0.09	-	0.39 ± 0.13	0.49 ± 0.15	0.32 ± 0.07
	2	2.08 ± 0.23	1.08 ± 0.24	0.65 ± 0.09	0.28 ± 0.01	0.40 ± 0.01
	3	1.93 ± 0.21	1.06 ± 0.23	0.80 ± 0.08	0.27 ± 0.01	0.43 ± 0.01

Table A2 Layer mean ± SD at each site in the western Canadian Arctic for the following log-transformed dissolved ions: Ca^{2+}, SO_4^{2-}, Mg^{2+}, Fe^{2+}, Na^{+}, K^{+}, Mn^{2+}, Cl^{-}.

Site	Unit	Ca^{2+}	SO_4^{2-}	Mg^{2+}	Fe^{2+}	Na^{+}	K^{+}	Mn^{2+}	Cl^{-}
CB	1	-0.27 ± 0.20	-0.56 ± 0.12	-0.39 ± 0.16	-0.49 ± 0.20	-1.24 ± 0.06	-1.00 ± 0.27	-1.20 ± 0.42	-1.68 ± 0.28
	2	0.34 ± 0.34	0.51 ± 0.37	-0.08 ± 0.28	-3.03 ± 1.03	-0.81 ± 0.16	-0.62 ± 0.17	-1.81 ± 0.30	-2.20 ± 0.12
	3	0.64 ± 0.11	0.90 ± 0.12	0.20 ± 0.10	-3.51 ± 0.41	-0.30 ± 0.05	-0.45 ± 0.03	-1.70 ± 0.14	-1.83 ± 0.12
Lynx 2	1	0.05 ± 0.15	-0.45 ± 0.16	-0.42 ± 0.17	-2.20 ± 1.20	-1.04 ± 0.07	-1.23 ± 0.16	-3.50 ± 0.89	-2.14 ± 0.37
	2	0.17 ± 0.06	-0.02 ± 0.12	-0.49 ± 0.05	-4.22 ± 0.14	-0.95 ± 0.09	-0.99 ± 0.04	-4.26 ± 0.00	-2.12 ± 0.29
	3	1.23 ± 0.43	1.38 ± 0.55	0.19 ± 0.23	-4.26 ± 0.00	-0.70 ± 0.14	-0.65 ± 0.15	-3.94 ± 0.28	-2.39 ± 0.05
NRD	1	-0.97 ± 0.32	0.11 ± 0.06	-1.01 ± 0.17	-0.33 ± 0.41	-1.06 ± 0.08	-0.95 ± 0.10	-2.48 ± 0.45	-1.97 ± 0.14
	2	0.04 ± 0.29	0.44 ± 0.24	-0.37 ± 0.14	-1.94 ± 0.05	-0.76 ± 0.16	-0.58 ± 0.09	-1.62 ± 0.49	-2.03 ± 0.09
	3	0.94 ± 0.36	1.29 ± 0.54	0.26 ± 0.25	-1.53 ± 1.12	-0.25 ± 0.17	-0.44 ± 0.13	-0.74 ± 0.31	-1.28 ± 0.23
R2T2	1	0.15 ± 0.22	-0.79 ± 0.22	-0.33 ± 0.20	-1.76 ± 0.36	-0.95 ± 0.08	-1.06 ± 0.48	-1.87 ± 0.60	-1.78 ± 0.52
	2	0.25 ± 0.14	-0.30 ± 0.37	-0.56 ± 0.12	-3.63 ± 1.02	-0.89 ± 0.07	-0.92 ± 0.19	-3.93 ± 0.65	-2.22 ± 0.24
	3	1.48 ± 0.08	1.72 ± 0.10	0.21 ± 0.12	-4.17 ± 0.19	-0.57 ± 0.09	- 0.48 ± 0.02	-3.69 ± 0.47	-2.32 ± 0.06
R2T3	1	0.15 ± 0.23	-0.57 ± 0.33	-0.21 ± 0.26	-1.29 ± 0.54	-1.03 ± 0.03	-1.16 ± 0.33	-1.69 ± 0.55	-1.52 ± 0.51
	2	0.23 ± 0.18	-0.33 ± 0.30	-0.35 ± 0.29	-2.63 ± 1.49	-1.07 ± 0.09	-1.10 ± 0.17	-3.01 ± 1.27	-1.89 ± 0.37
	3	1.44 ± 0.13	1.62 ± 0.12	0.40 ± 0.16	-4.23 ± 0.12	-0.40 ± 0.28	-0.53 ± 0.09	-3.43 ± 0.83	-2.11 ± 0.25
Wilson	1	0.07 ± 0.18	-0.16 ± 0.36	-0.19 ± 0.12	-0.88 ± 0.26	-1.00 ± 0.13	-1.16 ± 0.21	-1.26 ± 0.24	-1.75 ± 0.09
	2	0.47 ± 0.11	0.54 ± 0.16	-0.07 ± 0.10	-3.30 ± 0.69	-0.44 ± 0.09	-0.61 ± 0.05	-1.96 ± 0.17	-1.56 ± 0.13
	3	0.62 ± 0.11	0.84 ± 0.11	0.12 ± 0.06	-4.13 ± 0.22	-0.32 ± 0.04	-0.49 ± 0.02	-1.76 ± 0.11	-1.49 ± 0.18

APPENDIX B: ANOVA RESULTS

Table B The Q-critical (α=0.05), Q-statistic, and associated ρ-value from the post-hoc Tukey HSD test (H_0: $\bar{x}_i = \bar{x}_{i+1}$) of the layer X_i and layer X_{i+1} transformed gravimetric water content (GWC), pore water conductivity (PWC), leached conductivity (LC), organic carbon (Organic C), inorganic carbon (Inorganic C) and solutes (Ca, SO_4, Mg, Fe, Na, K, Mn, Cl) at all sites, when applicable. An • indicates that the null hypothesis (H_0) was rejected, and therefore, the indicated alternative hypothesis is supported.

					Between Groups			Within Groups		
	$F_{critical}$	$F_{statistic}$	ρ-value	Reject H_0	SS	df	MS	SS	df	MS
CB										
GWC	3.220	144.090	$1.56 X10^{-19}$	•	3.978	2	1.989	0.580	42	0.014
LC	3.369	35.302	$3.89 X10^{-8}$	•	1.420	2	0.710	0.523	26	0.020
Organic C	3.369	17.722	$1.39 X10^{-5}$	•	0.940	2	0.470	0.690	26	0.027
Inorganic C	3.369	8.555	0.001	•	0.077	2	0.038	0.117	26	0.004
Ca^{2+}	3.369	63.988	$9.07 X10^{-11}$	•	5.038	2	2.519	1.024	26	0.039
SO_4^{2-}	3.369	203.230	$1.34 X10^{-16}$	•	13.309	2	6.655	0.851	26	0.033
Mg^{2+}	3.369	38.292	$1.78 X10^{-8}$	•	2.097	2	1.048	0.712	26	0.027
Fe^{2+}	3.369	116.838	$1.02 X10^{-13}$	•	59.078	2	29.539	6.573	26	0.253
Na^{+}	3.369	403.244	$2.69 X10^{-20}$	•	5.406	2	2.703	0.174	26	0.007
K^{+}	3.369	24.888	$9.14 X10^{-17}$	•	1.800	2	0.900	0.940	26	0.036
Mn^{2+}	3.369	10.396	0.0005	•	2.020	2	1.010	2.526	26	0.097
Cl^{-}	3.369	11.487	0.0003	•	0.956	2	0.478	1.082	26	0.042
Wilson										
GWC	3.305	9.224	0.0007	•	0.789	2	0.394	1.325	31	0.043
PWC	4.279	0.015	0.904	NS	0.001	1	0.001	1.267	23	0.055
LC	3.555	24.376	$7.54 X10^{-6}$	•	0.456	2	0.228	0.168	18	0.009
Organic C	3.555	18.012	$5.06 X10^{-5}$	•	0.175	2	0.088	0.087	18	0.005
Inorganic C	3.555	15.587	0.0001	•	0.035	2	0.018	0.020	18	0.001
Ca^{2+}	3.555	27.201	$3.63 X10^{-6}$	•	0.878	2	0.439	0.290	18	0.016
SO_4^{2-}	3.555	32.272	$1.11 X10^{-6}$	•	2.833	2	1.416	0.790	18	0.044
Mg^{2+}	3.555	14.405	0.0002	•	0.264	2	0.132	0.165	18	0.009
Fe^{2+}	3.555	58.339	$1.36 X10^{-8}$	•	30.880	2	15.440	4.764	18	0.265
Na^{+}	3.555	88.730	$4.76 X10^{-10}$	•	1.431	2	0.716	0.145	18	0.008
K^{+}	3.555	63.500	$7.00 X10^{-9}$	•	1.366	2	0.683	0.194	18	0.011
Mn^{2+}	3.555	26.362	$4.48 X10^{-6}$	•	1.607	2	0.804	0.549	18	0.030

Cl^-	3.555	5.285	0.016	•	0.202	2	0.101	0.344	18	0.019
NRD										
GWC	3.422	20.958	$6.57 X10^{-6}$	•	1.412	2	0.706	0.775	23	0.034
PWC	5.591	0.022	0.886	NS	0.071	1	0.071	22.472	7	3.210
LC	3.592	34.080	$1.13 X10^{-6}$	•	1.392	2	0.696	0.347	17	0.020
Organic C	3.592	0.844	0.447	NS	0.070	2	0.035	0.708	17	0.042
Inorganic C	3.592	0.444	0.648	NS	0.016	2	0.008	0.314	17	0.018
Ca^{2+}	3.592	56.525	$3.08 X10^{-8}$	•	11.929	2	5.964	1.794	17	0.106
SO_4^{2-}	3.592	35.019	$9.36 X10^{-7}$	•	4.259	2	2.130	1.034	17	0.061
Mg^{2+}	3.592	78.992	$2.47 X10^{-9}$	•	5.177	2	2.589	0.557	17	0.033
Fe^{2+}	3.592	13.065	0.0004	•	8.940	2	4.470	5.816	17	0.342
Na^+	3.592	76.793	$3.07 X10^{-9}$	•	1.987	2	0.994	0.220	17	0.013
K^+	3.592	43.861	$1.94 X10^{-7}$	•	0.946	2	0.473	0.183	17	0.011
Mn^{2+}	3.592	26.438	$6.05 X10^{-6}$	•	9.823	2	4.911	3.158	17	0.186
Cl^-	3.592	32.288	$1.62 X10^{-6}$	•	1.578	2	0.789	0.416	17	0.024
NRT2										
GWC	4.139	0.211	0.649	NS	0.021	1	0.021	3.228	33	0.098
PWC	4.242	15.033	0.0007	•	0.370	1	0370	0.616	25	0.025
LC	4.381	5.418	0.031	•	0.080	1	0.080	0.279	19	0.015
Organic C	4.381	2.360	0.141	NS	0.069	1	0.069	0.553	19	0.029
Inorganic C	4.381	1.058	0.317	NS	0.002	1	0.002	0.036	19	0.002
Lynx1										
GWC	3.960	3.205	0.077	NS	0.926	1	0.926	23.115	80	0.289
PWC	3.976	1.131	0.291	NS	0.288	1	0.288	18.101	71	0.255
LC	4.067	13.776	0.0006	•	0.559	1	0.559	1.746	43	0.041
Organic C	4.067	10.834	0.002	•	2.017	1	2.017	8.004	43	0.186
Inorganic C	4.067	2.205	0.145	NS	0.169	1	0.169	3.295	43	0.077
Lynx 2										
GWC	3.238	0.839	0.440	NS	0.072	2	0.036	1.677	39	0.043
PWC	4.325	1.284	0.270	NS	0.017	1	0.017	0.285	21	0.014
LC	3.403	50.704	$2.41 X10^{-9}$	•	5.720	2	2.860	1.354	24	0.056
Organic C	3.403	5.441	0.011	•	0.371	2	0.185	0.818	24	0.034
Inorganic C	3.403	0.596	0.559	NS	0.060	2	0.030	1.207	24	0.050
Ca^{2+}	3.403	56.545	$8.29 X10^{-10}$	•	7.150	2	3.575	1.157	24	0.063
SO_4^{2-}	3.403	77.934	$3.18 X10^{-11}$	•	16.206	2	8.103	2.495	24	0.104
Mg^{2+}	3.403	42.514	$1.29 X10^{-8}$	•	2.307	2	1.154	0.651	24	0.027

Fe^{2+}	3.403	22.369	3.28 X10^{-6}	•	27.198	2	13.599	14.590	24	0.608
Na^{+}	3.403	27.638	5.93 X10^{-7}	•	0.569	2	0.284	0.247	24	0.010
K^{+}	3.403	43.382	1.07 X10^{-8}	•	1.540	2	0.770	0.426	24	0.018
Mn^{2+}	3.403	3.871	0.035	•	2.726	2	1.363	8.449	24	0.352
Cl^{-}	3.403	2.296	0.122	NS	0.374	2	0.187	1.956	24	0.082
R2T2										
GWC	3.276	2.162	0.131	NS	0.140	2	0.070	1.099	34	0.032
PWC	4.351	9.880	0.005	•	0.220	1	0.220	0.445	20	0.022
LC	3.493	69.816	9.53 X10^{-10}	•	4.429	2	2.215	0.634	20	0.032
Organic C	3.493	6.436	0.007	•	0.393	2	0.196	0.610	20	0.031
Inorganic C	3.493	9.107	0.002	•	0.292	2	0.146	0.321	20	0.016
Ca^{2+}	3.493	98.770	4.31 X10^{-11}	•	5.434	2	2.717	0.550	20	0.028
SO_4^{2-}	3.493	100.219	3.78 X10^{-11}	•	17.426	2	8.713	1.739	20	0.087
Mg^{2+}	3.493	38.146	1.49 X10^{-7}	•	1.760	2	0.880	0.461	20	0.023
Fe^{2+}	3.493	19.376	2.09 X10^{-5}	•	22.038	2	11.019	11.374	20	0.569
Na^{+}	3.493	38.169	1.49 X10^{-7}	•	0.417	2	0.208	0.109	20	0.005
K^{+}	3.493	4.583	0.023	•	0.918	2	0.459	2.002	20	0..100
Mn^{2+}	3.493	28.602	1.36 X10^{-6}	•	21.078	2	10.539	7.370	20	0.368
Cl^{-}	3.493	4.573	0.023	•	1.138	2	0.569	2.490	20	0.124
R2T3										
GWC	3.214	12.273	6.07 X10^{-5}	•	1.597	2	0.798	2.797	43	0.065
PWC	4.225	15.297	0.0006	•	0.387	1	0.387	0.657	26	0.025
LC	3.443	150.642	1.45 X10^{-13}	•	6.888	2	3.444	0.503	22	0.023
Organic C	3.443	6.447	0.006	•	0.615	2	0.308	1.050	22	0.048
Inorganic C	3.443	21.104	7.64 X10^{-6}	•	0.321	2	0.160	0.167	22	0.008
Ca^{2+}	3.443	169.180	4.39 X10^{-14}	•	9.378	2	4.689	0.610	22	0.028
SO_4^{2-}	3.443	213.964	3.82 X10^{-15}	•	25.167	2	12.583	1.294	22	0.059
Mg^{2+}	3.443	27.706	9.77 X10^{-7}	•	3.124	2	1.562	1.240	22	0.056
Fe^{2+}	3.443	15.420	6.52 X10^{-5}	•	29.344	2	14.672	20.932	22	0.951
Na^{+}	3.443	33.421	2.15 X10^{-7}	•	2.672	2	1.336	0.879	22	0.040
K^{+}	3.443	36.195	1.10 X10^{-7}	•	2.170	2	1.085	0.659	22	0.030
Mn^{2+}	3.443	4.370	0.025	•	8.864	2	4.432	22.310	22	1.014
Cl^{-}	3.443	4.425	0.024	•	1.056	2	0.528	2.625	22	0.119
Caribou										
GWC	4.062	57.441	1.64 X10^{-9}	•	3.553	1	3.553	2.722	44	0.062
LC	4.279	28.068	2.23 X10^{-5}	•	3.318	1	3.318	2.719	23	0.118

Organic C	4.279	40.680	1.65 $X10^{-6}$	•	4.741	1	4.741	2.680	23	0.117
Inorganic C	4.279	64.629	3.94 $X10^{-8}$	•	5.020	1	5.020	1.787	23	0.078
Campbell										
GWC	4.113	0.293	0.592	NS	0.015	1	0.015	1.885	36	0.052
LC	4.351	0.088	0.770	NS	0.006	1	0.006	1.290	20	0.064
Organic C	4.351	3.712	0.068	NS	0.300	1	0.300	1.618	20	0.081
Inorganic C	4.351	13.459	0.002	•	0.343	1	0.343	0.509	20	0.025

NS: Not significant

APPENDIX C: RESULTS FROM THE POST-HOC TUKEY HSD TEST

Table C The Q-critical (α=0.05), Q-statistic, and associated ρ-value from the post-hoc Tukey HSD test (H_0: $\bar{x}_i = \bar{x}_{i+1}$) of the layer X_i and layer X_{i+1} transformed gravimetric water content (GWC), pore water conductivity (PWC), leached conductivity (LC), organic carbon (Organic C), inorganic carbon (Inorganic C) and solutes (Ca, SO_4, Mg, Fe, Na, K, Mn, Cl) at all sites, when applicable. An • indicates that the null hypothesis (H_0) was rejected, and therefore, the indicated alternative hypothesis is supported.

			H_1: $\bar{x}_1 \neq \bar{x}_2$			H_1: $\bar{x}_1 \neq \bar{x}_3$			H_1: $\bar{x}_2 \neq \bar{x}_3$		
	$Q_{critical}$	v	$Q_{statistic}$	ρ-value	Reject H_0	$Q_{statistic}$	ρ-value	Reject H_0	$Q_{statistic}$	ρ -value	Reject H_0
CB											
GWC	3.436	42	7.915	0.001	•	14.925	0.001	•	22.429	0.001	•
LC	3.514	26	4.101	0.020	•	11.873	0.001	•	5.005	0.004	•
Organic C	3.514	26	6.101	0.001	•	7.699	0.001	•	0.196	0.900	•
Inorganic C	3.514	26	1.644	0.487	NS	4.555	0.009	•	5.137	0.003	•
Ca^{2+}	3.514	26	8.156	0.001	•	15.839	0.001	•	3.992	0.024	•
SO_4^{2-}	3.514	26	15.744	0.001	•	27.991	0.001	•	5.724	0.001	•
Mg^{2+}	3.514	26	4.975	0.004	•	12.374	0.001	•	4.515	0.010	•
Fe^{2+}	3.514	26	13.412	0.001	•	20.802	0.001	•	2.542	0.190	NS
Na^{+}	3.514	26	14.084	0.001	•	40.137	0.001	•	16.700	0.001	•
K^{+}	3.514	26	5.200	0.003	•	9.859	0.001	•	2.321	0.236	NS
Mn^{2+}	3.514	26	5.188	0.003	•	5.527	0.002	•	0.950	0.767	NS
Cl^{-}	3.514	26	6.778	0.001	•	2.653	0.166	NS	4.744	0.007	•
Wilson											
GWC	3.480	31	5.999	0.001	•	3.753	0.032	•	2.635	0.166	NS
PWC	2.926	23	-	-	-	-	-	-	0.172	0.900	NS
LC	3.608	18	6.852	0.001	•	9.804	0.001	•	4.228	0.020	•
Organic C	3.608	18	7.789	0.001	•	7.388	0.001	•	0.402	0.900	NS
Inorganic C	3.608	18	6.506	0.001	•	7.493	0.001	•	1.885	0.397	NS
Ca^{2+}	3.608	18	8.116	0.001	•	10.121	0.001	•	3.260	0.080	NS
SO_4^{2-}	3.608	18	8.587	0.001	•	11.113	0.001	•	3.924	0.032	•
Mg^{2+}	3.608	18	3.101	0.100	NS	7.397	0.001	•	5.385	0.003	•
Fe^{2+}	3.608	18	12.143	0.001	•	14.716	0.001	•	4.377	0.016	•
Na^{+}	3.608	18	15.978	0.001	•	17.597	0.001	•	3.687	0.044	•
K^{+}	3.608	18	13.492	0.001	•	14.903	0.001	•	3.165	0.091	NS
Mn^{2+}	3.608	18	10.250	0.001	•	6.680	0.001	•	3.038	0.108	NS
Cl^{-}	3.608	18	3.682	0.045	•	4.417	0.015	•	1.274	0.639	NS
NRD											
GWC	3.541	23	2.855	0.130	NS	9.154	0.001	•	5.181	0.004	•
PWC	3.344	7	-	-	-	-	-	-	0.157	0.900	NS
LC	3.627	17	2.145	0.308	NS	11.670	0.001	•	6.939	0.001	•

Organic C	3.627	17	1.144	0.691	NS	1.166	0.682	NS	1.836	0.418	NS
Inorganic C	3.627	17	0.987	0.753	NS	1.084	0.714	NS	0.016	0.900	NS
Ca^{2+}	3.627	17	6.881	0.001	•	14.517	0.001	•	5.097	0.006	•
SO_4^{2-}	3.627	17	2.956	0.122	NS	11.826	0.001	•	6.374	0.001	•
Mg^{2+}	3.627	17	7.794	0.001	•	17.256	0.001	•	6.382	0.001	•
Fe^{2+}	3.627	17	6.094	0.001	•	5.083	0.006	•	1.305	0.626	NS
Na^{+}	3.627	17	5.653	0.003	•	17.407	0.001	•	8.291	0.001	•
K^{+}	3.627	17	7.752	0.001	•	12.129	0.001	•	2.579	0.192	NS
Mn^{2+}	3.627	17	4.418	0.016	•	10.007	0.001	•	3.786	0.040	•
Cl^{-}	3.627	17	0.907	0.785	NS	10.885	0.001	•	8.909	0.001	•
NRT2											
GWC	2.877	33	0.65	0.660	NS	-	-	-	-	-	-
PWC	2.913	25	5.483	0.001	•	-	-	-	-	-	-
LC	2.960	19	3.292	0.031	•	-	-	-	-	-	-
Organic C	2.960	19	2.172	0.141	NS	-	-	-	-	-	-
Inorganic C	2.960	19	1.455	0.317	NS	-	-	-	-	-	-
Lynx1											
GWC	2.814	80	2.532	0.077	NS	-	-	-	-	-	-
PWC	2.820	71	1.504	0.291	NS	-	-	-	-	-	-
LC	2.852	43	5.249	0.001	•	-	-	-	-	-	-
Organic C	2.852	43	4.655	0.002	•	-	-	-	-	-	-
Inorganic C	2.852	43	2.100	0.145	NS	-	-	-	-	-	-
Lynx 2											
GWC	3.455	39	1.556	0.520	NS	1.694	0.463	NS	0.175	0.900	NS
PWC	2.941	21	-	-	-	-	-	-	1.602	0.270	NS
LC	3.531	24	2.184	0.289	NS	13.684	0.001	•	10.688	0.001	•
Organic C	3.531	24	3.693	0.039	•	4.141	0.019	•	0.416	0.900	NS
Inorganic C	3.531	24	1.544	0.528	NS	0.632	0.896	NS	0.848	0.809	NS
Ca^{2+}	3.531	24	1.452	0.565	NS	14.189	0.001	•	11.837	0.001	•
SO_4^{2-}	3.531	24	4.101	0.021	•	17.304	0.001	•	12.269	0.001	•
Mg^{2+}	3.531	24	1.303	0.626	NS	11.220	0.001	•	11.638	0.001	•
Fe^{2+}	3.531	24	7.879	0.001	•	8.065	0.001	•	0.173	0.900	NS
Na^{+}	3.531	24	2.629	0.172	NS	10.341	0.001	•	7.167	0.001	•
K^{+}	3.531	24	5.509	0.002	•	13.173	0.001	•	7.122	0.001	•
Mn^{2+}	3.531	24	3.874	0.030	•	2.257	0.267	NS	1.503	0.545	NS
Cl^{-}	3.531	24	0.256	0.900	NS	2.631	0.172	NS	2.683	0.161	NS
R2T2											
GWC	3.465	34	1.734	0.448	NS	0.854	0.803	NS	2.762	0.140	NS
PWC	2.950	20	-	-	-	-	-	-	4.445	0.005	•
LC	3.578	20	0.953	0.768	NS	14.569	0.001	•	16.039	0.001	•
Organic C	3.578	20	4.578	0.011	•	3.978	0.028	•	0.529	0.900	NS

Inorganic C	3.578	20	5.489	0.003	•	4.665	0.010	•	0.524	0.900	NS
Ca^{2+}	3.578	20	1.789	0.432	NS	18.569	0.001	•	18.052	0.001	•
SO_4^{2-}	3.578	20	5.058	0.005	•	19.625	0.001	•	16.558	0.001	•
Mg^{2+}	3.578	20	4.662	0.010	•	8.228	0.001	•	12.340	0.001	•
Fe^{2+}	3.578	20	7.551	0.001	•	7.384	0.001	•	1.735	0.453	NS
Na^{+}	3.578	20	2.477	0.211	NS	11.963	0.001	•	10.576	0.001	•
K^{+}	3.578	20	1.392	0.591	NS	4.249	0.018	•	3.349	0.069	NS
Mn^{2+}	3.578	20	10.366	0.001	•	6.921	0.001	•	0.991	0.753	NS
Cl^{-}	3.578	20	3.744	0.039	•	3.502	0.056	NS	0.693	0.873	NS
R2T3											
GWC	3.433	43	2.094	0.311	NS	1.873	0.391	NS	7.007	0.001	•
PWC	2.907	26	-	-	-	-	-	-	5.531	0.001	•
LC	3.552	22	1.697	0.588	NS	15.900	0.001	•	23.140	0.001	•
Organic C	3.552	22	2.042	0.337	NS	4.686	0.009	•	3.498	0.054	NS
Inorganic C	3.552	22	5.568	0.002	•	9.073	0.001	•	4.584	0.010	•
Ca^{2+}	3.552	22	1.070	0.720	NS	18.710	0.001	•	23.554	0.001	•
SO_4^{2-}	3.552	22	2.347	0.242	NS	21.822	0.001	•	25.982	0.001	•
Mg^{2+}	3.552	22	1.354	0.606	NS	5.899	0.001	•	9.596	0.001	•
Fe^{2+}	3.552	22	3.288	0.073	NS	7.301	0.001	•	5.305	0.003	•
Na^{+}	3.552	22	0.515	0.900	NS	7.598	0.001	•	10.851	0.001	•
K^{+}	3.552	22	0.887	0.794	NS	8.923	0.001	•	10.722	0.001	•
Mn^{2+}	3.552	22	3.128	0.091	NS	4.178	0.019	•	1.348	0.608	NS
Cl^{-}	3.552	22	2.573	0.187	NS	4.159	0.020	•	2.074	0.326	NS
Caribou											
GWC	2.850	44	10.718	0.001	•	-	-	-	-	-	-
LC	2.926	23	7.492	0.001	•	-	-	-	-	-	-
Organic C	2.926	23	9.020	0.001	•	-	-	-	-	-	-
Inorganic C	2.926	23	11.369	0.001	•	-	-	-	-	-	-
Campbell											
GWC	2.868	36	0.765	0.601	NS	-	-	-	-	-	-
LC	2.950	20	0.420	0.779	NS	-	-	-	-	-	-
Organic C	2.950	20	2.725	0.068	NS	-	-	-	-	-	-
Inorganic C	2.950	20	6.003	0.001	•	-	-	-	-	-	-

NS: Not significant

- : No data